

1996

## Synthesis and Characterization of Cyclic Arylene Ether Oligomers

David Lewis Eldridge

*College of William & Mary - Arts & Sciences*

Follow this and additional works at: <https://scholarworks.wm.edu/etd>

 Part of the [Organic Chemistry Commons](#)

---

### Recommended Citation

Eldridge, David Lewis, "Synthesis and Characterization of Cyclic Arylene Ether Oligomers" (1996). *Dissertations, Theses, and Masters Projects*. Paper 1539626044.  
<https://dx.doi.org/doi:10.21220/s2-ywv3-jq16>

This Thesis is brought to you for free and open access by the Theses, Dissertations, & Master Projects at W&M ScholarWorks. It has been accepted for inclusion in Dissertations, Theses, and Masters Projects by an authorized administrator of W&M ScholarWorks. For more information, please contact [scholarworks@wm.edu](mailto:scholarworks@wm.edu).

**SYNTHESIS AND CHARACTERIZATION OF  
CYCLIC ARYLENE ETHER OLIGOMERS**

---

**A Thesis**

**Presented to**

**The Faculty of the Department of Chemistry**

**The College of William and Mary in Virginia**

**In Partial Fulfillment**

**of the Requirements for the Degree of**

**Master of Arts**

---

**by**

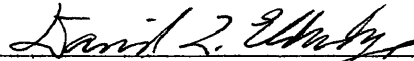
**David Lewis Eldridge**

**1996**


APPROVAL SHEET


This thesis is submitted in partial fulfillment of  
the requirements for the degree of


Master of Arts

  
David L. Eldridge

Approved, July 31, 1996

  
R.A. Orwoll

  
B.A. Siles

  
W.H. Starnes

## TABLE OF CONTENTS

Acknowledgements	v
List of Figures	vi
List of Tables	xi
Abstract	xiii
<b>INTRODUCTION</b>	<b>2</b>
<b>BACKGROUND</b>	<b>4</b>
Poly(arylene ether)s	4
Cyclization of Poly (arylene ether) oligomers	8
Calixarenes	11
<b>EXPERIMENTAL</b>	<b>13</b>
Chemicals	13
Monomers	13
Polymers	19
Gel Permeation Chromatography	26
Theory	26
Instrumentation	27
Differential Refractometer	28
Analytical Gel Permeation Chromatography	30
Preparative Gel Permeation Chromatography	32
Other Analytical Techniques and Instrumentation	34
Thin-layer chromatography	34
Infrared Spectroscopy	34
Differential Scanning Calorimetry (DSC)	34
Microscopy	35
Thermogravimetric Analysis	35
Tandem Mass Spectrometry	36
<b>RESULTS AND DISCUSSION</b>	<b>38</b>
Analytical Gel Permeation Chromatography	38
Preparative Gel Permeation Chromatography	52
Tandem Mass Spectrometry	56
Thin-layer chromatography	77
Thermal Analysis	78
Infrared Spectroscopy	96

<b>CONCLUSIONS</b>	106
<b>REFERENCES</b>	108
<b>VITA</b>	110

## ACKNOWLEDGEMENTS

I wish to sincerely thank Professor Robert A. Orwoll for all of his guidance, assistance, and criticism during the course of this investigation. It was a pleasure to work with him. I would also like to thank Professor Barbara A. Siles and Professor William H. Starnes for their careful reading and criticism of this thesis. Their time was very much appreciated.

Many other people gave me invaluable help in this endeavor. I owe special thanks to Sheeba Ahmed for all of her instruction and suggestions. Her contribution to this project was of the utmost importance. I would also like to thank Michael Glasgow for his advice and assistance. Finally, without the support of Anne Steinbach and my parents the completion of this work would have been impossible.

## LIST OF FIGURES

Figure	Page
1. Representative polymerization reaction of PAE's studied in this research.	4
2. Nucleophilic aromatic substitution.	5
3. Depiction of mechanism for the synthesis of 3-HPM.	6
4. Formation of a typical diazonium salt.	6
5. Friedel-Crafts acylation mechanism for the synthesis of 1,4-CBB.	7
6. Oligomer cyclization competing with linear polymerization of a PAE.	8
7. Examples of calixarenes.	11
8. 1,3-bis(4-fluorobenzoyl)benzene and bis(4-hydroxyphenyl)methane.	13
9. Synthesis of 1,4-bis(4-chlorobenzoyl)benzene.	13
10. Apparatus for the synthesis of 1,4-CBB and 3-HPM.	14
11. Synthesis of bis(3-hydroxyphenyl)methane.	16
12. Reaction apparatus for condensation polymerization.	20
13. PAE-MP.	22
14. PAE-PM.	23
15. PAE-MM.	24
16. PAE-PP.	25
17. A diagram of the instrumentation for GPC work in this research.	27
18. The Model 200 Differential Refractometer-Differential Viscometer.	29
19. Chart describing treatment of reaction product in order to obtain fractions of varying solubilities.	31

Figure	Page
20. General depiction of the MS-MS apparatus used in this research.	37
21. Concentration chromatogram of 1,3-FBB.	41
22. Concentration chromatogram of 1,4-CBB.	42
23. Concentration chromatogram of 3-HPM.	42
24. Concentration chromatogram of 4-HPM.	42
25. Concentration chromatogram for fraction #1 of PAE-MM.	44
26. Concentration chromatogram for fraction #2 of PAE-MM.	44
27. Concentration chromatogram for fraction #3 of PAE-MM.	44
28. Concentration chromatogram for fraction #1, PAE-MP.	46
29. Concentration chromatogram for fraction #2, PAE-MP.	46
30. Concentration chromatogram for fraction #3, PAE-MP.	46
31. Concentration chromatogram for fraction #1, PAE-PM.	48
32. Concentration chromatogram for fraction#2, PAE-PM.	48
33. Concentration chromatogram for fraction #3, PAE-PM.	48
34. Concentration chromatogram for fraction #1, PAE-PP.	50
35. Concentration chromatogram for fraction #2, PAE-PP.	50
36. Concentration chromatogram for fraction #3, PAE-PP.	50
37. Collection chromatogram for PAE-MM.	53
38. Collection chromatogram for PAE-MP.	54
39. Collection chromatogram for PAE-PM.	54
40. Precursor mass spectrum of THF/TFA mixture.	57



<b>Figure</b>	<b>Page</b>
41. Precursor ion mass spectrum of PAE-MM-A.	58
42. Product ion mass spectrum of molecular ion peak 483 (PAE-MM-A).	58
43. Fragments of molecular ion peak 483 (PAE-MM-A).	59
44. Precursor ion spectrum of PAE-MM-B.	61
45. Product ion spectrum of 966 (PAE-MM-B).	61
46. Fragments of molecular ion peak 966 (PAE-MM-B).	63
47. Precursor ion mass spectrum of PAE-MP-A.	64
48. Product ion mass spectrum of molecular ion peak 483 (PAE-MP-A).	65
49. Fragments of molecular ion peak 483 (PAE-MP-A).	66
50. Precursor ion spectrum of PAE-MP-C.	67
51. Product ion spectrum of 966 (PAE-MP-C).	68
52. Fragments of molecular ion peak 966 (PAE-MP-C).	69
53. Precursor ion mass spectrum of PAE-PM-B.	70
54. Product ion mass spectra of molecular ion peaks 485 and 483 (PAE-PM-B).	71
55. Fragments of molecular ion peak 483 and 485 (PAE-PM-B).	72
56. Precursor ion mass spectrum of PAE-PM-D.	73
57. Product ion mass spectrum of molecular ion peak 965 (PAE-PM-D).	74
58. Fragments of molecular ion peak 965 (PAE-PM-D).	75
59. DSC run of PAE-MM.	78
60. TGA of PAE-MM; heated to 400°C.	79
61. TGA run of PAE-MM; held at 125°C.	80

Figure	Page
62. PAE-MM weight gain during exposure to the atmosphere; after heating.	81
63. Two DSC heat scans and middle cooling scan of PAE-MM.	83
64. DSC run of PAE-MM-A.	84
65. DSC run of PAE-MM-B.	84
66. DSC run of PAE-PM.	86
67. TGA of PAE-PM; heated to 300°C.	86
68. TGA run of PAE-PM; first heating to 225°C.	87
69. TGA run of PAE-PM; second heating to 225°C.	87
70. DSC run of PAE-MP.	88
71. TGA of PAE-MP; heated to 350°C.	90
72. TGA of PAE-MP; first heating to 225°C.	90
73. TGA of PAE-MP; second heating to 225°C.	91
74. TGA of PAE-MP; held at 225°C for one hour.	91
75. DSC of PAE-PP.	93
76. Two DSC heat scans and middle cooling scan of PAE-PP.	94
77. TGA run of PAE-PP; held at 125°C.	95
78. IR spectrum of mineral oil.	97
79. IR spectrum of chloroform.	97
80. IR spectrum of 1,3-FBB.	99
81. IR spectrum of 3-HPM.	99
82. IR spectrum of 1,4-CBB.	100

Figure	Page
83. IR spectrum of 4-HPM.	100
84. IR spectrum of PAE-MM product mixture.	102
85. IR spectrum of PAE-MP product mixture.	102
86. IR spectrum of PAE-PM product mixture.	103
87. IR spectrum of PAE-PP product mixture.	103
88. IR spectrum of PAE-MM-A.	105
89. IR spectrum of PAE-MM-B.	105

## LIST OF TABLES

Table	Page
1. Table of reagents for the synthesis of 1,4-CBB.	15
2. Results of elemental analysis of 1,4-CBB.	16
3. Table of reagents for the synthesis of 3-HPM.	17
4. Results of elemental analysis of 3-HPM.	18
5. Poly(arylene ether)s synthesized.	19
6. Table of reagents for the synthesis of poly(arylene ether)s.	21
7. Analytical GPC data for monomers.	41
8. Analytical GPC data for PAE-MM.	43
9. Analytical GPC data for PAE-MP.	45
10. Analytical GPC data for PAE-PM.	47
11. Analytical GPC data for PAE-PP.	49
12. Peaks collected with preparative GPC.	55
13. Unknown and solvent ion peaks from mass spectra of PAE-MM-A.	59
14. Unknown and solvent peak ions from mass spectra of PAE-MM-B.	62
15. Unknown and solvent ion peaks from mass spectra of PAE-MP-A.	65
16. Unknown and solvent peak ions from mass spectra of PAE-MP-C.	68
17. Unknown and solvent ion peaks from the mass spectra of PAE-PM-B.	71
18. Unknown and solvent ion peaks from the mass spectra of PAE-MM-A.	74
19. Summary of structures determined by mass spectroscopy.	76

<b>Table</b>	<b>Page</b>
20. Summary of thermal analysis data gathered from DSC.	95
21. Characteristic IR frequencies of monomers.	98
22. Characteristic IR frequencies of PAE product mixtures.	100

## **ABSTRACT**

In the condensation reaction leading to several poly(arylene ether) (PAE) product mixtures, a considerable fraction of oligomer species in addition to the expected polymer products was detected by using gel permeation chromatography (GPC). It was surmised that these oligomers were cyclic structures. These studies give confirmation to this hypothesis.

The first part of this research involved running this reaction under such conditions as to encourage the production of cyclic oligomers. The original PAE and three of its structural isomers were synthesized by using dilute concentrations of monomers and long reaction times. Once these product mixtures were in hand, oligomeric species in each mixture were separated by using analytical GPC. Likely cyclic oligomers were then separated from the reaction mixture by using preparative GPC. Tandem mass spectrometry was used to discern which oligomeric species were cyclic. Infrared spectroscopy was also used to this end in some cases. Based on this evidence, cyclic tetramers and dimers were found in three of these isomeric PAE systems.

The last part of this research involved characterizing and comparing the thermal properties of the PAE mixtures by using differential scanning calorimetry (DSC), thermogravimetric analysis (TGA), and cross-polarizing microscopy. The TGA runs of all PAE mixtures indicated that most of the reaction products synthesized were hygroscopic.

**Synthesis and Characterization of  
Cyclic Arylene Ether Oligomers**

## INTRODUCTION

While polymerizing several combinations of bisphenols and dihalides in an effort to form poly(arylene ether)s (PAEs), Hergenrother, Jensen and Havens made an interesting discovery.<sup>1</sup> One polymer series was synthesized from the polymerization of 1,3-bis(4-chlorobenzoyl)benzene (1,3-CBB) and bis(3-hydroxyphenyl)methane (3-HPM). During analysis of the reaction product with gel permeation (*i.e.*, size-exclusion) chromatography (GPC), the researchers discovered that this polymer contained an unexpectedly large fraction of low-molecular weight species.

Further synthesis was carried out in which the aromatic linkages were varied (*i.e.*, 1,4-CBB/3-HPM, 1,3-CBB/4-HPM, and 1,4-CBB/4-HPM). These polymerizations did not produce as much of the low molecular-weight product.

Without additional study, the investigators drew the conclusion that these oligomers were cyclic. The *meta* linkages found in the benzene rings of the 1,3-CBB/3-HPM polymer system were thought to make it possible for a strain-free cyclic dimer of the polymer repeat unit to be made. The other systems with their different linkage variations did not seem as favorable to ring formation.

The focus of our research has been to isolate and collect the oligomers from the four isomeric PAE systems and then to attempt to determine which of these oligomers are cyclic. Some work had already been done towards this end before this segment of the research was begun.<sup>2</sup> A system analogous to 1,3-CBB/3-HPM, 1,3-bis(4-fluorobenzoyl)benzene (1,3-FBB)/3-HPM, had been synthesized. Similar low molecular-weight peaks were discovered when this polymer system was analyzed with GPC.



Reaction conditions were found which encouraged the production of a large amount of these oligomers. These conditions included low concentrations of monomers (reactants) and long reaction times. Samples of the isolated oligomers were collected, but conclusive evidence that any were cyclic was not discovered with GPC alone.

The purpose of this portion of our research was to determine whether the oligomers collected from the four structurally isomeric PAE systems were cyclic. We utilized tandem mass spectroscopy (MS-MS) and infrared spectroscopy (IR) in this determination. Afterwards, all data collected from these methods were used to compare the PAE systems to each other. We also conducted differential scanning calorimetry and thermogravimetric analysis on each of these systems.

## BACKGROUND

### Poly(arylene ether)s

Poly (arylene ethers)s are a class of polymers known for their use as high performance engineering thermoplastics. In this respect, PAEs can be used as coatings, adhesives, composites, molded components, toughening agents, and ultrafiltration membranes.<sup>1</sup>

The PAEs in this research are formed from the polymerization of various dihalides and bisphenols. Figure 1 shows the general reaction between these two monomers. This research utilizes dihalides where Y represents a carbonyl group.

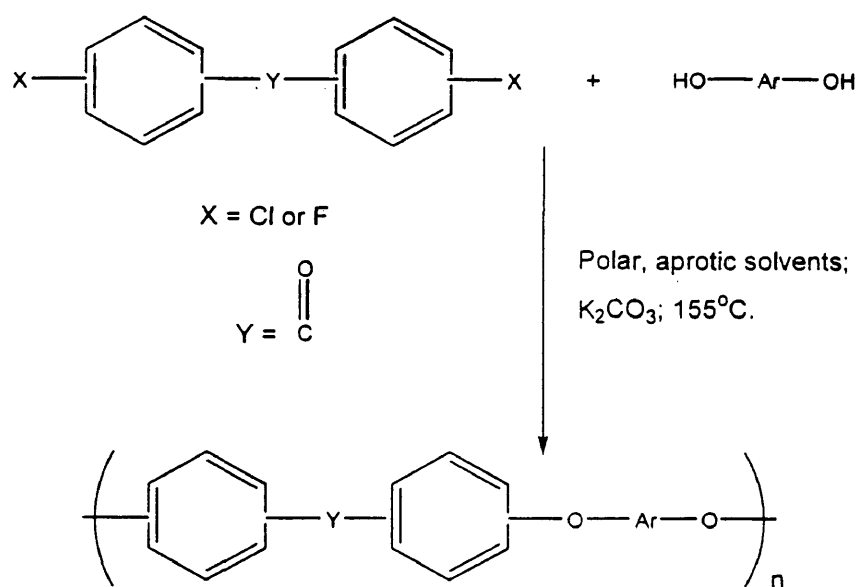


**Figure 1.** Representative polymerization reaction of PAE's studied in this research.

Poly(arylene ether)s form by condensation reactions. This polymerization reaction is a nucleophilic aromatic substitution. The mechanistic scheme for this process is shown below in Figure 2, depicting a phenol reacting with a phenol halide.<sup>3</sup>

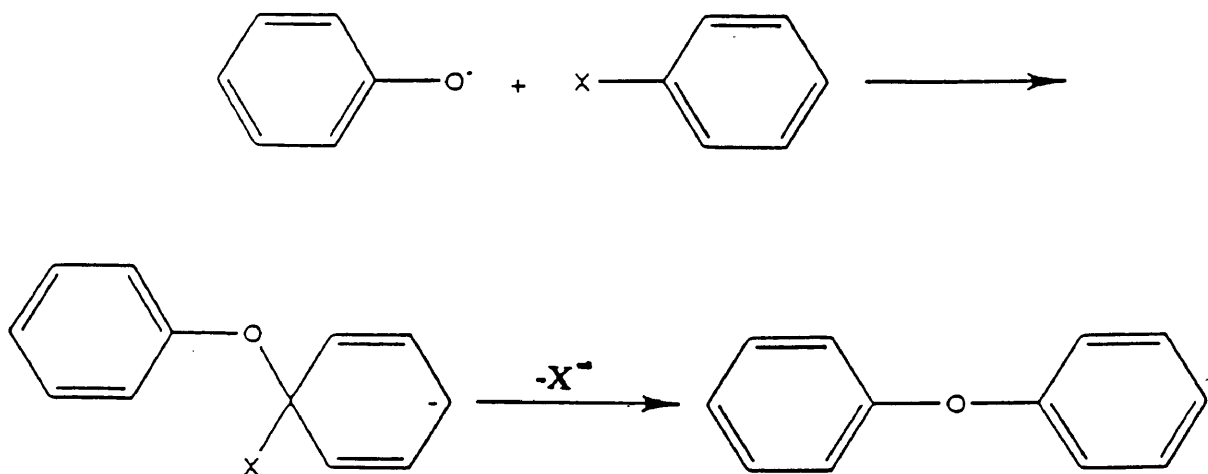
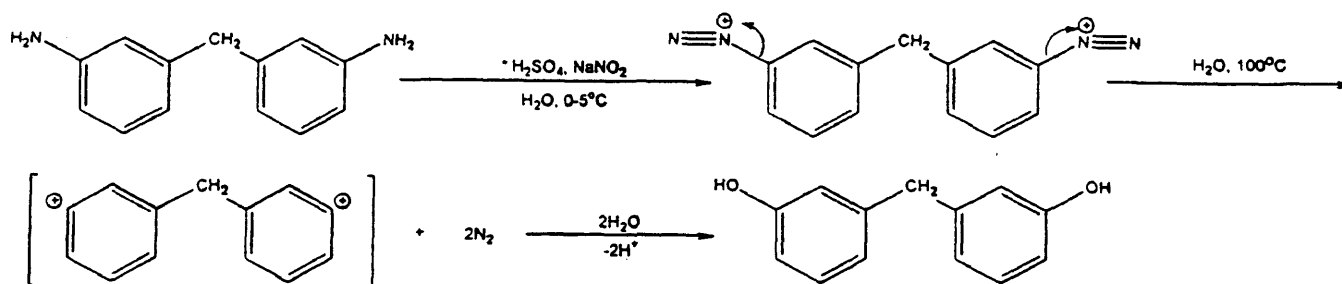


**Figure 2.** Nucleophilic aromatic substitution.

Some of the bisphenol used in the polymerization (Figure 1), bis(3-hydroxyphenyl)methane (3-HPM), was already available at the beginning of this research. However, there was not enough for our purposes; so it had to be synthesized. It is formed through a diazonium salt intermediate.<sup>4</sup> The mechanism for this reaction is depicted below in Figures 3 and 4. The other monomer, 1,4-bis(4-chlorobenzoyl)benzene (1,4-CBB), also had to be synthesized. Synthesis of this monomer follows a Friedel-Crafts acylation mechanism (Figure 5).<sup>5</sup> Both the 1,3-FBB and the 4-HPM were both provided from NASA Langley Research Center.

The depiction of the reactions in Figures 3 and 5 is not meant to suggest mechanisms in which both ends of the molecule react simultaneously.



\*See Figure 4.

**Figure 3.** Depiction of mechanism for the synthesis of 3-HPM.

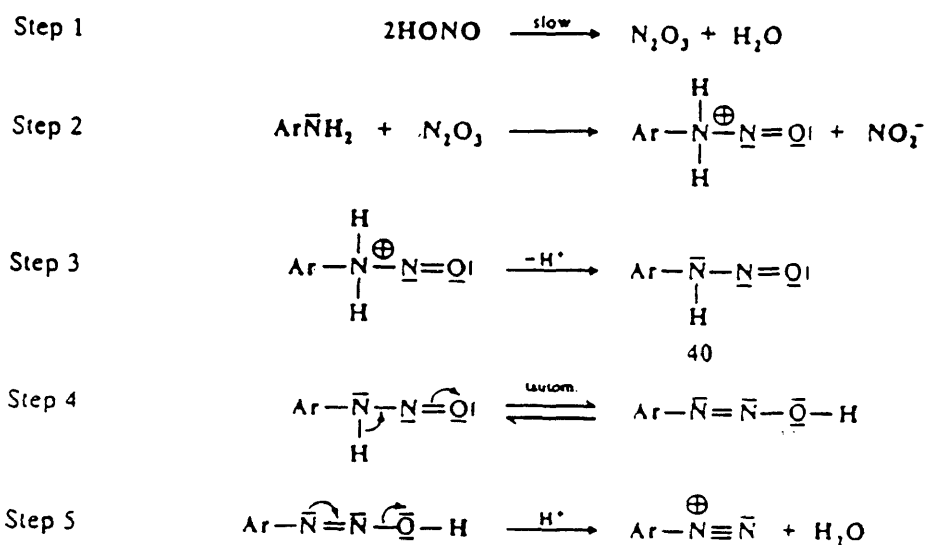


**Figure 4.** Formation of a typical diazonium salt.<sup>6</sup>

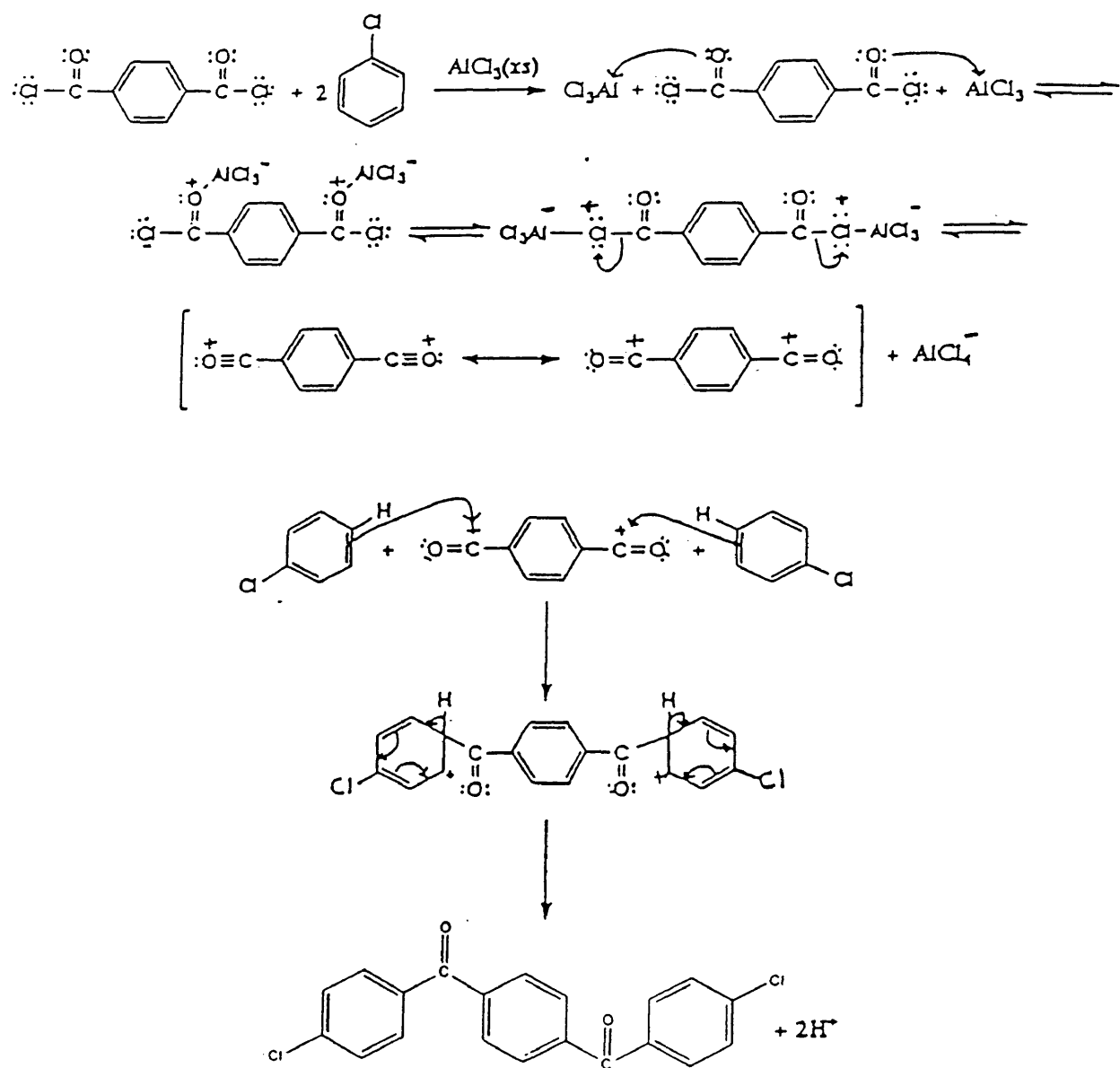


**Figure 5.** Friedel-Crafts acylation mechanism for the synthesis of 1,4-CBB.

### Cyclization of Poly(arylene ether) Oligomers

In any step (condensation) polymerization reaction there is the possibility of cyclic species forming at the expense of linear chain growth.<sup>7</sup> These cyclic compounds usually form after a given set of monomers has reacted to yield a linear oligomer such as a dimer or a tetramer. After this initial product formation, two paths can be followed by the system. Monomer can continue to add to these linear oligomers, making an increasingly longer chain, or the two functional ends of the oligomer can interact with each other and form small, cyclic compounds (Figure 6). Large cyclic structures are also possible; however, it must be kept in mind that, as the polymer chain gets longer, it is more difficult for the two functional ends to find one another and form a ring.

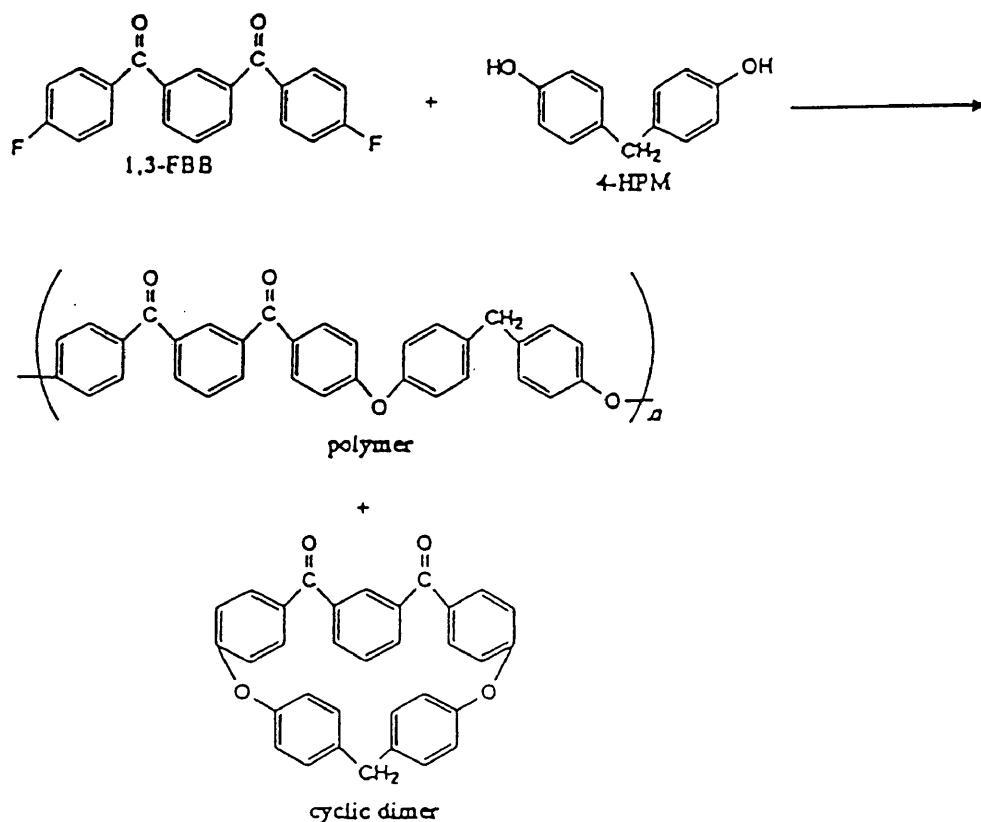


**Figure 6.** Oligomer cyclization competing with linear polymerization of a PAE.

Whether or not these cyclic compounds will form depends on both thermodynamic and kinetic factors.<sup>7,8</sup>

For a particular ring to form, its thermodynamic stability must be taken into account. Specifically, the strain in various ring structures must be considered. A cyclic structure with high ring strain possesses a low thermodynamic stability and has a lower probability of forming. In general, ring strain in smaller cyclic compounds is due to angle strain. These usually planar rings contain angles that are extremely distorted from their normal values. Larger cyclic compounds are often puckered and normally do not suffer from this type of ring strain. Most of the strain in larger rings is due to the conformational strain caused by repulsive interactions between side groups.

Kinetic factors must also be considered. The possibility of cyclization is dependent on the probability that the two functional ends on a given chain find one another. An important trend to consider is that as the potential ring size (the length of the linear chain) increases, the chain separating the functional ends may have many different conformations. Relatively few of these conformations allow the functional ends to be close enough to interact.

It is important to design reaction conditions appropriately if ring formation is to be encouraged in step polymerizations.<sup>8,9</sup> One reaction condition that can be manipulated to encourage cyclization is the concentration of reactants. Linear polymerization is a bimolecular reaction. The rate of linear polymerization, therefore, increases with higher concentrations of reactants. By lowering reactant concentration, one increases the likelihood that ring formation (a unimolecular reaction) will be the preferred pathway.

The functional ends of an oligomer chain are more likely to come in contact with each other than with another monomer or oligomer.

To encourage further these cyclizations, lengthening the reaction time is also necessary to give each oligomer time to discover its other end. Otherwise, small linear oligomers and monomers will be the major products.

Therefore, two easily adjustable reaction parameters, monomer concentration and reaction time, can be manipulated in order to encourage cyclic oligomers to form. For this reason, all polymer synthesis for this research was done with reactants at a concentration of 0.0025 M and a reaction time of 168 hours (one week), conditions previously shown to encourage the production of cyclic species.<sup>2</sup>



## Calixarenes

These poly(arylene ether) rings may have some practical value. They have some structural similarities to calixarenes. Calixarenes (*calix*, Greek for chalice; *arene*, indicating the presence of aromatic rings) are cyclic compounds containing aromatic rings bridged by aliphatic groups. These aromatic rings have functional groups which point toward the inside of the ring.<sup>10, 11</sup> Examples of these compounds are shown below in Figure 7. The hydroxyl groups of these structures form a basket-like crater. Derivatization of these hydroxyl groups allows calixarenes to be made with a variety of cavity functionalities and ring sizes.<sup>10-12</sup> These often highly specialized compounds have a tendency to bind smaller molecules (like metal ions) in their craters and have been used as complexing agents and even enzyme mimics.<sup>10,13,14</sup>

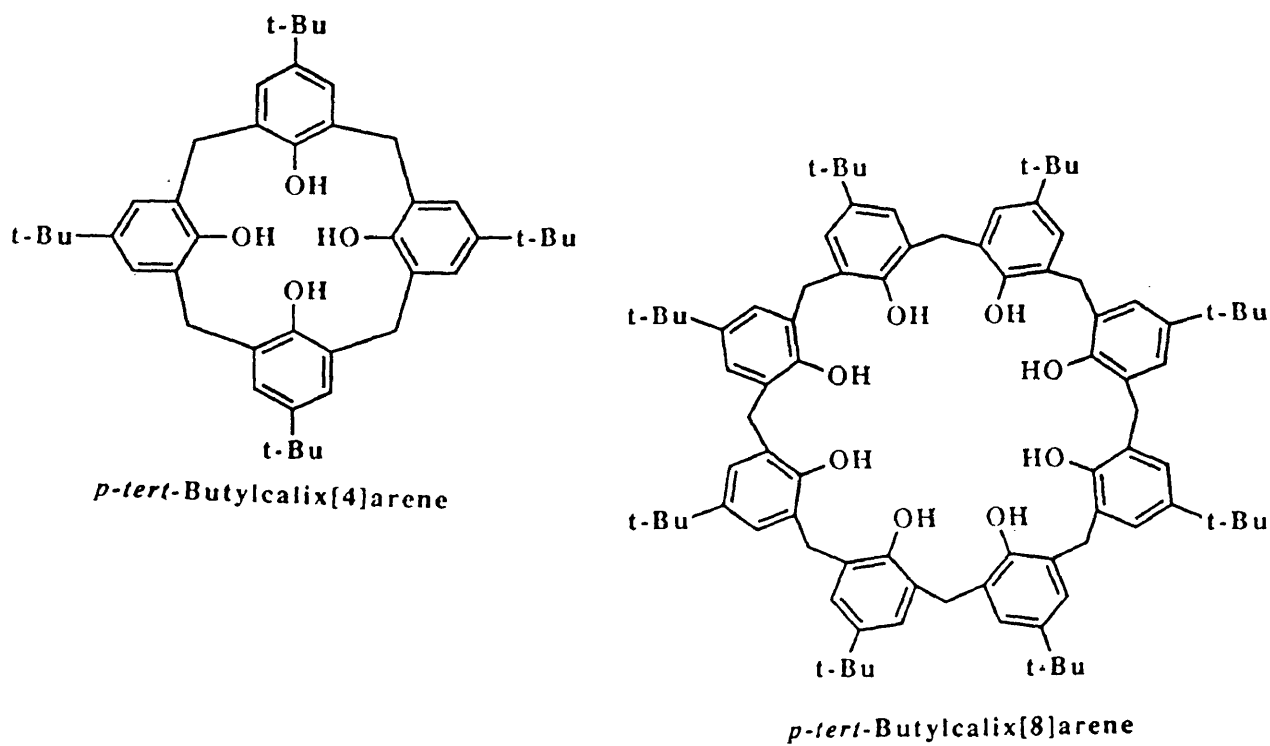


Figure 7. Examples of calixarenes.<sup>11</sup>

It is perhaps possible that the cyclic PAE oligomers that are the subject of this research could be utilized in a similar fashion. The center of the PAE rings may have an ability to form complexes with small molecules. The ether bonds and carbonyl groups could provide these rings with such an ability. Furthermore, the carbonyl groups might also be derivatized in much the same way as the hydroxyl groups of the calixarenes in Figure 7. Such possibilities could bestow these cyclic PAE oligomers with many practical uses.

## EXPERIMENTAL

### Chemicals

#### Monomers

##### *1,3-FBB and 4-HPM:*

These monomers, 1,3-bis(4-fluorobenzoyl)benzene (1,3-FBB) and bis(4-hydroxyphenyl)methane (4-HPM), were made at NASA Langley Research Center and given for use in this research project (Figure 8).<sup>1</sup>

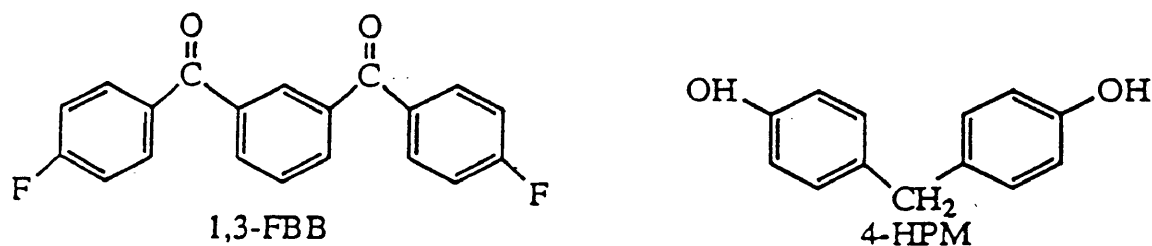


**Figure 8.** 1,3-bis(4-fluorobenzoyl)benzene and bis(4-hydroxyphenyl)methane.

##### *1,4-CBB:*

The monomer 1,4-bis(4-chlorobenzoyl)benzene (1,4-CBB) was synthesized by using the instructions of Hergenrother, Jensen and Havens.<sup>1</sup> This reaction is shown in Figure 9.

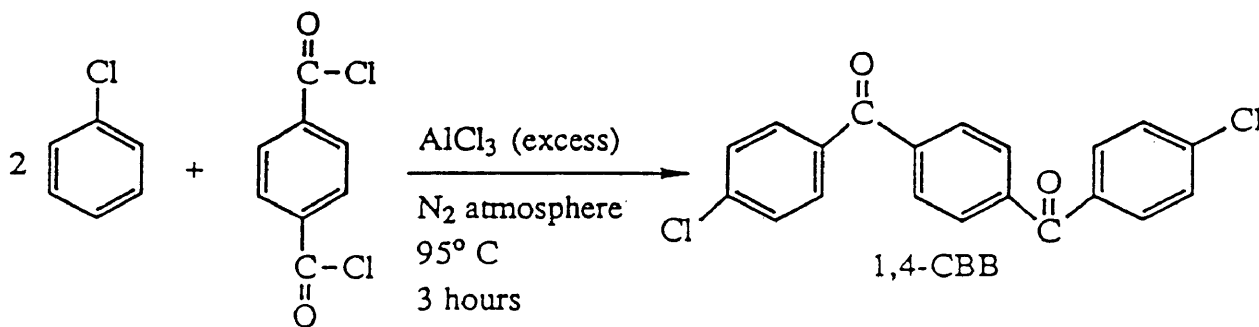


**Figure 9.** Synthesis of 1,4-bis(4-chlorobenzoyl)benzene.

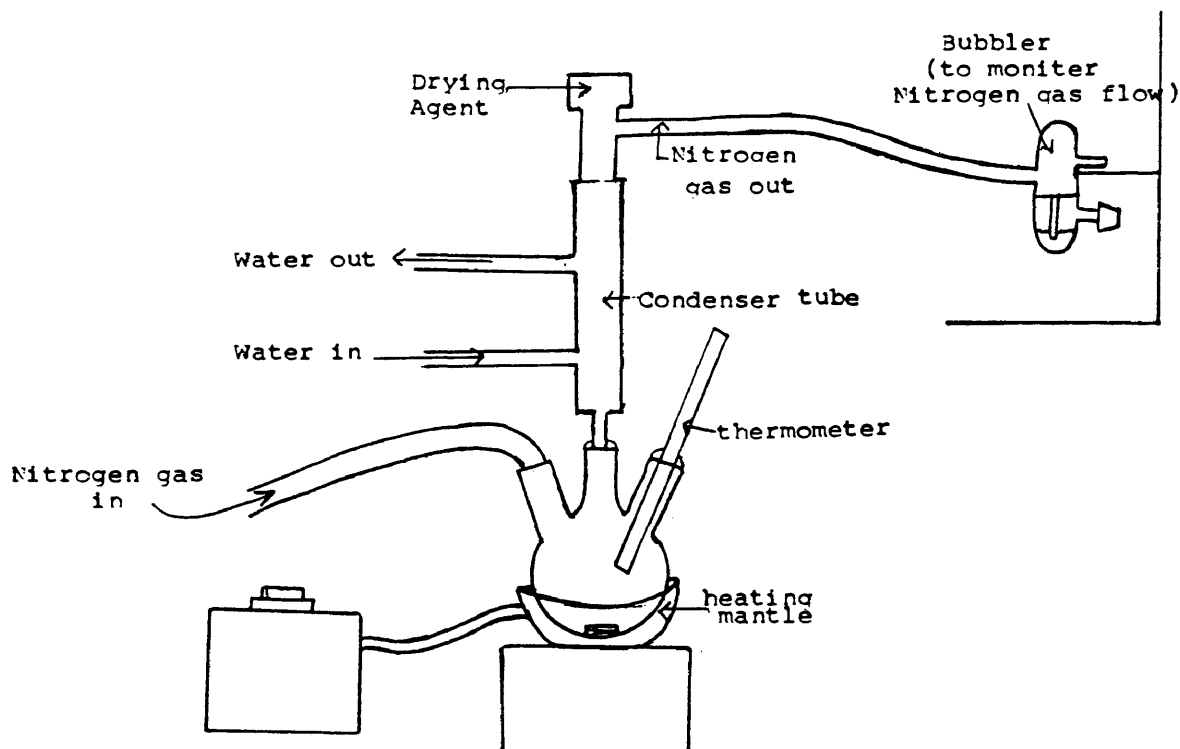


**Figure 10.** Apparatus for the synthesis of 1,4-CBB and 3-HPM.

Once the apparatus was assembled (Figure 10), the reagents in amounts shown in Table 1 were combined and allowed to react in the following manner. The terephthaloyl chloride was added to about half of the total chlorobenzene (already present in the reaction vessel). Next the anhydrous  $\text{AlCl}_3$  was added. Small portions of the remaining chlorobenzene were used to completely rinse in all of the terephthaloyl chloride and anhydrous  $\text{AlCl}_3$ . Significant clumping often prevented constant magnetic stirring. Mechanical stirring probably would have been a better choice for mixing.

**Table 1.** Table of reagents for the synthesis of 1,4-CBB.

Reagents	# of moles	Mass (g)
AlCl <sub>3</sub>	1.20	160
terephthaloyl chloride	0.50	101
chlorobenzene	6.57	739

The reaction was exothermic, and the temperature reached 30°C before being allowed to fall to room temperature. Then the reaction mixture was heated to 95°C and held at this temperature under a nitrogen atmosphere. Again, stirring magnetically was difficult. After five hours, the heat was removed and the reaction mixture was cooled to 30°C.

The product was precipitated by using 3 L of chilled 1.0 M aqueous HCl. The HCl and portions of the reaction mixture were added incrementally into a 4 L beaker. A mushy, beige precipitate formed, quickly ending all magnetic stirring. Stirring was done manually from this point.

The now cream-colored solid was thoroughly suction-filtered with a sintered glass funnel and washed on the filter with methanol. All of the solid was dried in an oven at 100°C overnight. Recrystallization from *N,N*-dimethylacetamide (DMAc) yielded white crystals.

These white crystals proved insoluble in many solvents and only partially soluble in THF. The purified product had a melting range (256-257°C) very close to the one reported in the literature (257-258°C).<sup>1</sup> Elemental analysis<sup>15</sup> (Table 2) and infrared

spectroscopy (Figure 82) also indicated that the desired product probably had been synthesized.

**Table 2.** Results of elemental analysis of 1,4-CBB.

Element	% theoretical	% actual
C	67.62	67.19
H	3.40	3.21
Cl	19.96	19.84

### 3-HPM:

The monomer bis(3-hydroxyphenyl)methane (3-HPM) was synthesized also by using the instructions of Hergenrother *et al.*<sup>1</sup> The reaction is shown below in Figure 11 and proceeds through a diazonium salt intermediate.

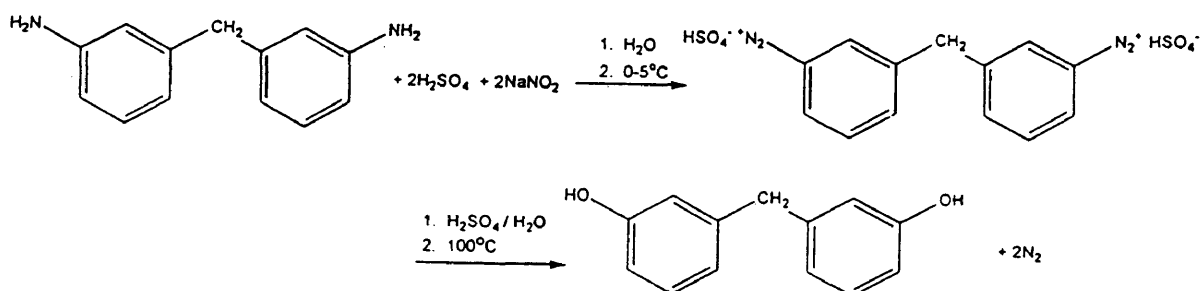


**Figure 11.** Synthesis of bis(3-hydroxyphenyl)methane.

The reagents for this synthesis are shown in Table 3 and were caused to react as follows. In an ice bath, 3,3'-methylenedianiline was mixed with about half of the sulfuric acid and water (both cold). To this mixture, the sodium nitrite was added. This mixture was magnetically stirred for 45 minutes at a temperature range between 0 and 5°C.

**Table 3.** Table of reagents for the synthesis of 3-HPM.

Reagents	# of moles	Amount
3,3'-methylenedianiline	0.0250	4.9568 g
H <sub>2</sub> O	-----	83.5 ml
H <sub>2</sub> SO <sub>4</sub>	0.8264	44.5 ml
NaNO <sub>2</sub>	0.5060	3.4900 g

The remainder of the water and sulfuric acid was brought to a boil in the reaction vessel of an apparatus identical to that pictured in Figure 10. At this point, the cold mixture was added slowly to the boiling one. The combination was then allowed to reflux for one hour.

After cooling, the reaction mixture separated into a black oil and a green aqueous layer. The aqueous layer was decanted. An extraction was then carried out on the oil with methylene chloride (110 mL). This extract was washed with deionized water (225 mL), dried with magnesium sulfate, and filtered. Use of a "Rotavapor" apparatus to remove all methylene chloride left a yellow-brown slurry. Sublimation of this slurry at 150°C yielded long, yellow needles.

The pure product had a melting point range of 102-103 °C. This range matched that of the literature.<sup>1</sup> Results of an elemental analysis (Table 4) and infrared spectroscopy (Figure 81) also substantiate the product's identity as 3-HPM.

Table 4. Results of elemental analysis of 3-HPM.

Element	% theoretical	% actual
C	77.97	77.24
H	6.04	5.72



## Polymers

The synthesis of the poly(arylene ether)s was accomplished through condensation polymerizations of the monomers previously discussed. Four structural isomers were created from different combinations of these monomers. Each isomeric polymer system was given a code designation (Table 5). After “PAE,” two letters follow. The first of these stands for the distinguishing aromatic connectivity of the dihalide (*M* = *meta* and *P* = *para*); the second letter names the linkages of the bisphenol.

**Table 5.** Poly(arylene ether)s synthesized.

Polymer System	Monomers	Description
PAE-MP	1,3-FBB/4-HPM	Light brown powder
PAE-PM	1,4-CBB/3-HPM	Clumpy, dark brown powder
PAE-MM	1,3-FBB/3-HPM	Beige powder
PAE-PP	1,4-CBB/4-HPM	Orange-brown powder

These polymerization reactions utilized the apparatus depicted below in Figure 12. All glassware was thoroughly dried to maximize yield. Again, low concentrations of these reactants were used in these reactions to increase the production of cyclic oligomers. A long reaction time (168 hours) was used for the same reason. An inert, nitrogen atmosphere was maintained at all times. The reactants were mixed through magnetic stirring.

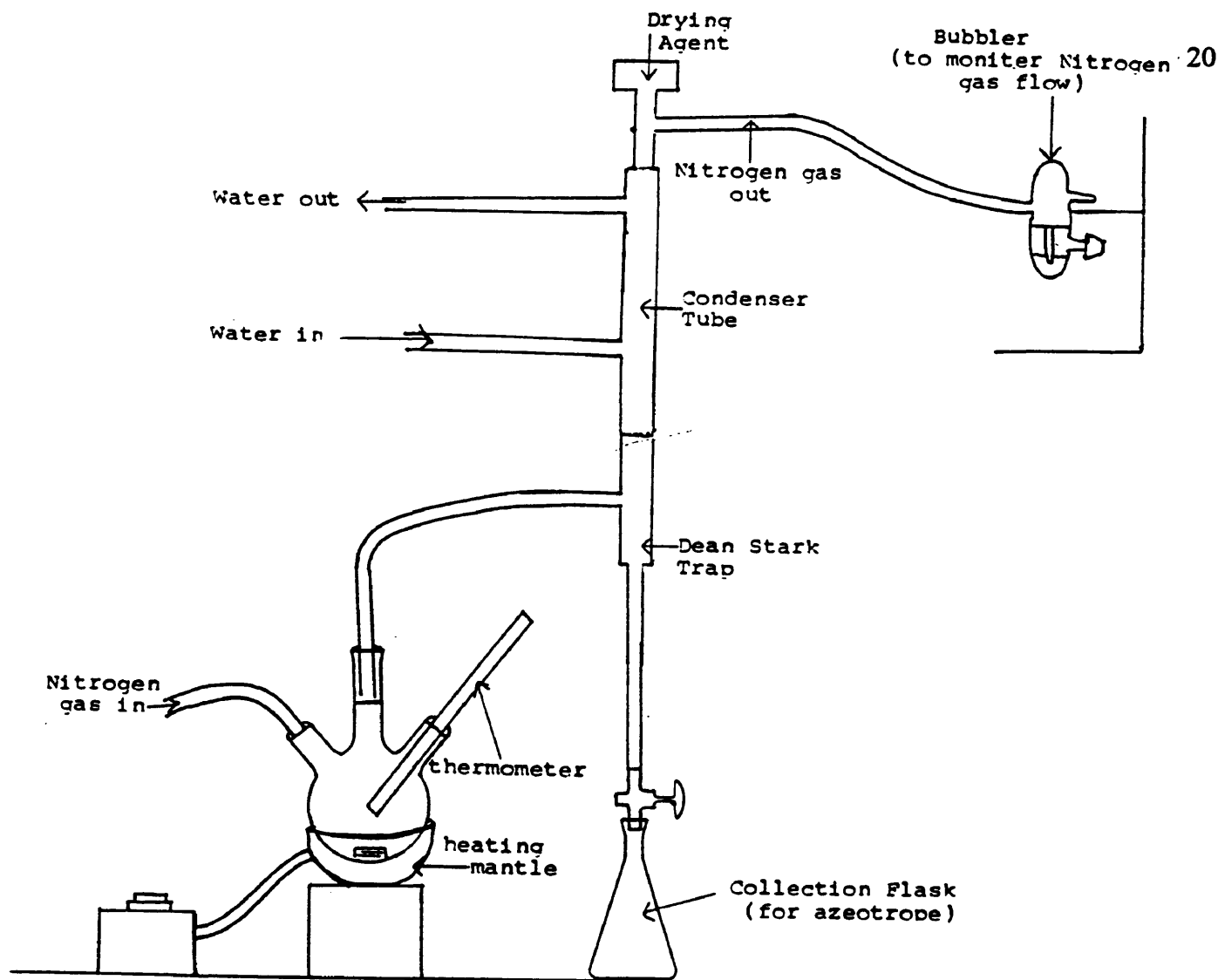


Figure 12. Reaction apparatus for condensation polymerization.

The reagents for a typical poly(arylene ether) synthesis are listed in Table 6. First, the dihalide and bisphenol were added to the round bottom flask. Potassium carbonate was then added to neutralize the acid evolved during the reaction. A 70:30 (v/v) mixture of *N,N*-dimethylacetamide (DMAc) and toluene was the final ingredient and was used to wash all of the solid reactants into the reaction vessel (and maintain the stoichiometric ratio). Additional toluene was added into the volumetric stem of the Dean Stark trap so that the level of the toluene was equal to that of the trap's shoulder.

**Table 6.** Table of reagents for the synthesis of poly (arylene ether)s.

Reagent	# of moles	Amount
dihalide	0.0025	0.8058 g
bisphenol	0.0025	0.5006 g
K <sub>2</sub> CO <sub>3</sub>	0.0026	0.3595 g
toluene	-----	12.5 mL
DMAc	-----	30.1 mL

The reaction mixture was slowly heated to 155°C and held at this temperature for seven days (168 hours). Water, which forms an azeotrope with toluene, was removed through the Dean Stark trap.

Upon completion of the reaction, the mixture was cooled and then poured into 150 mL of 1 M aqueous KOH. After efficient stirring of the mixture in base overnight, a solid had precipitated. The basic solution and solid were then separated by filtration. All of the solid was dried in an oven at 100°C for four hours. Both the solid and filtrate were saved for later examination.

All polymer reactions in Table 5 were carried out in this manner. Each of the four reactions, including depictions of some of the desired cyclic oligomers, is pictured below in Figures 13-16.

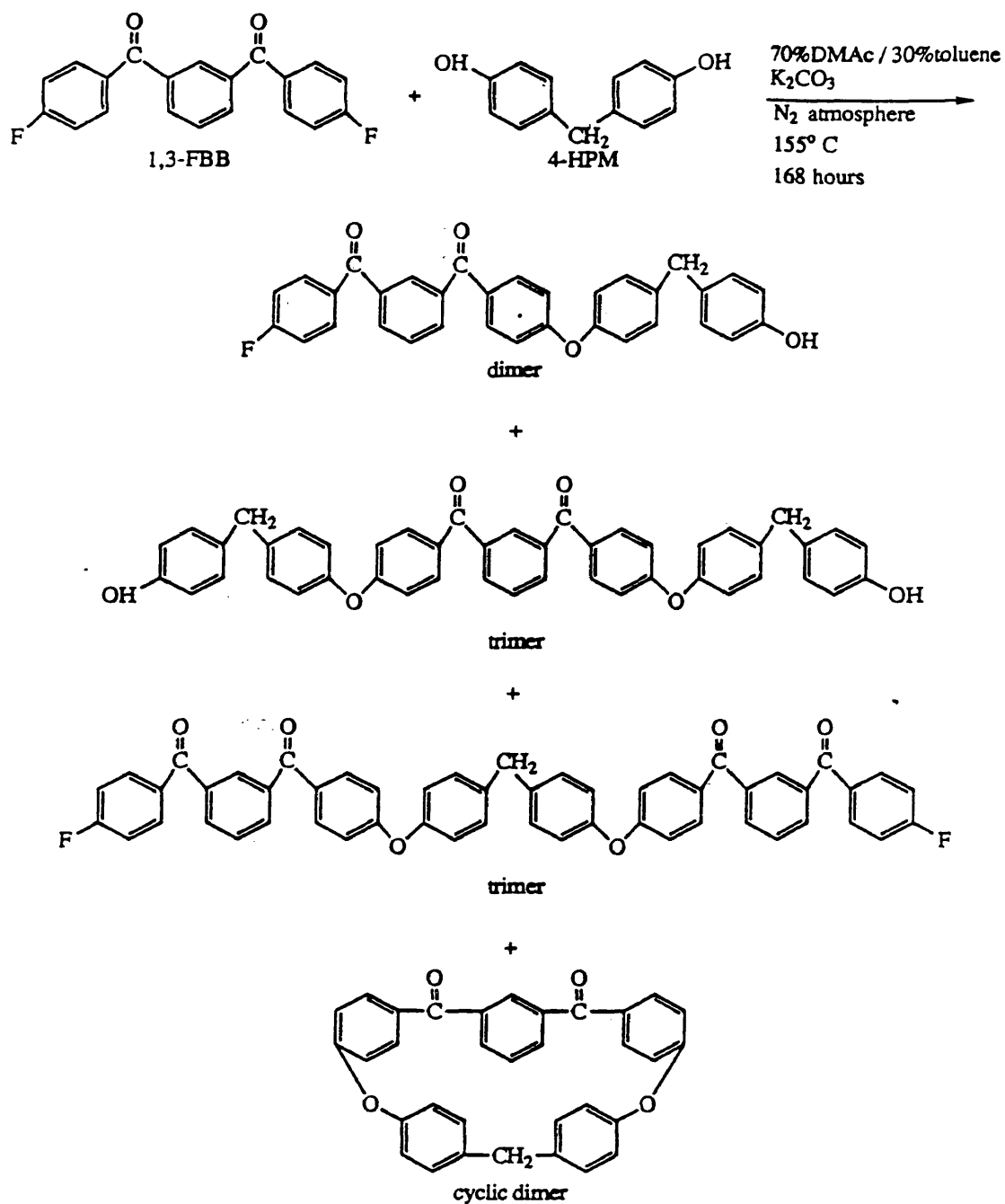


Figure 13. PAE-MP.

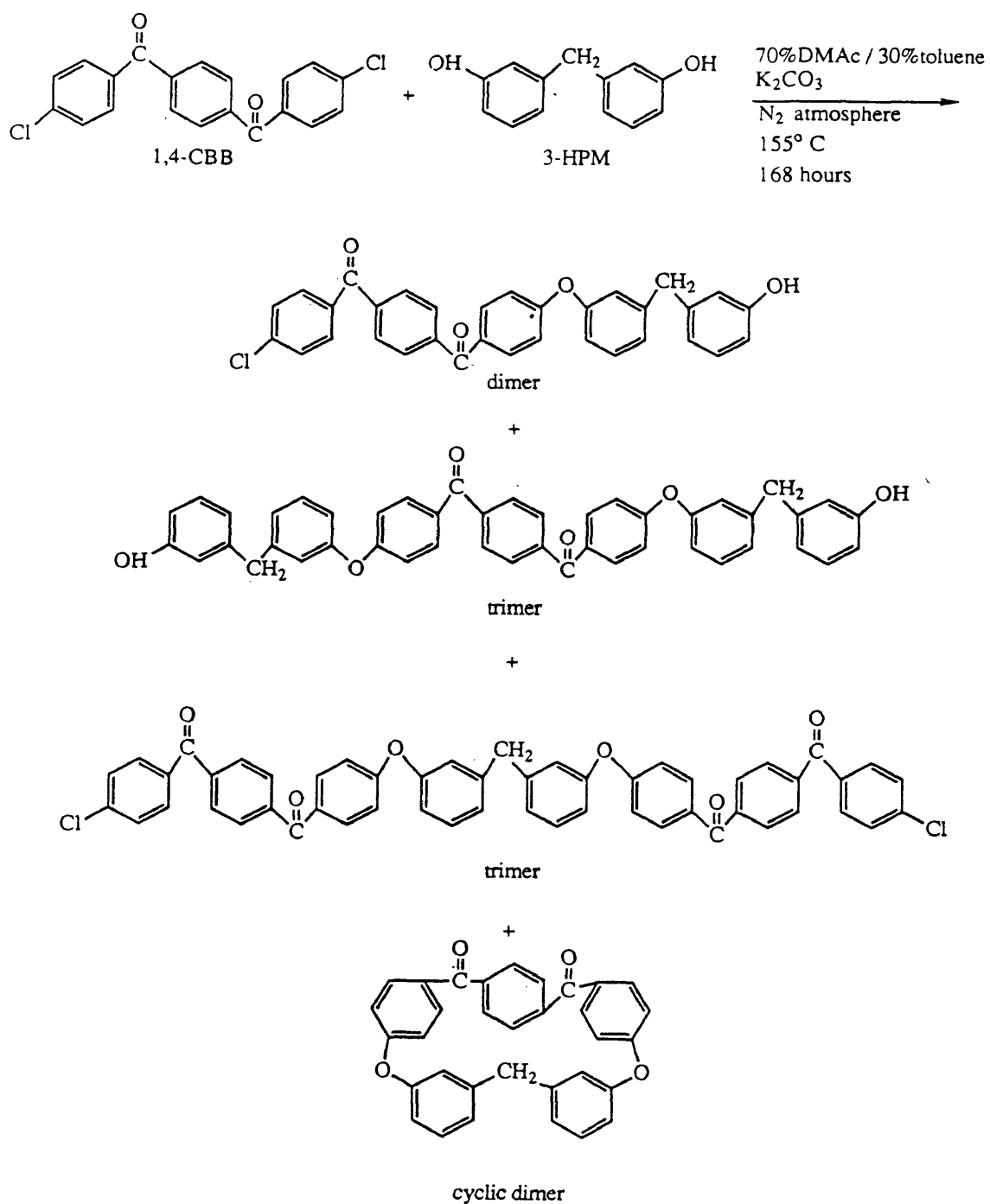


Figure 14. PAE-PM.

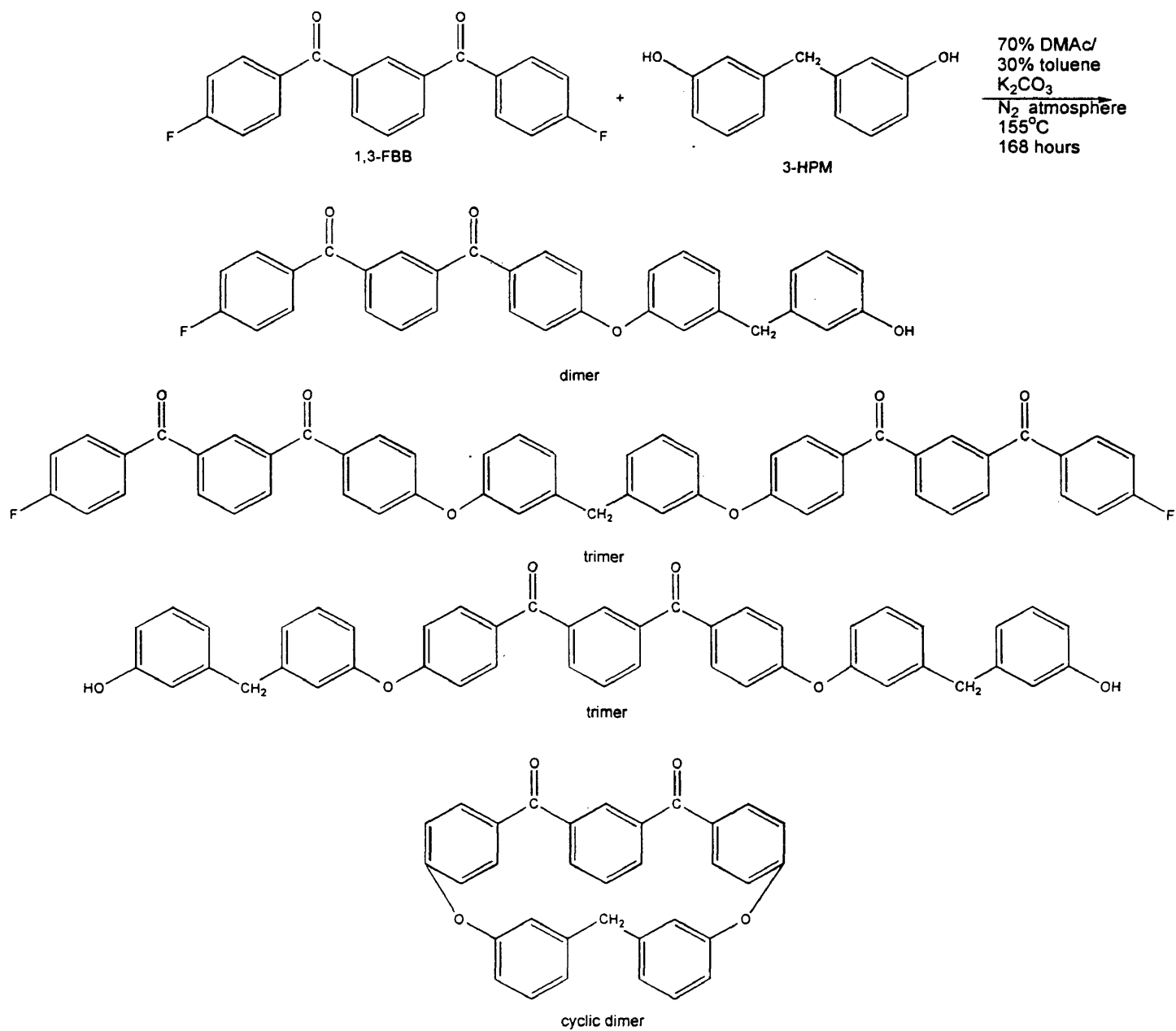


Figure 15. PAE-MM.

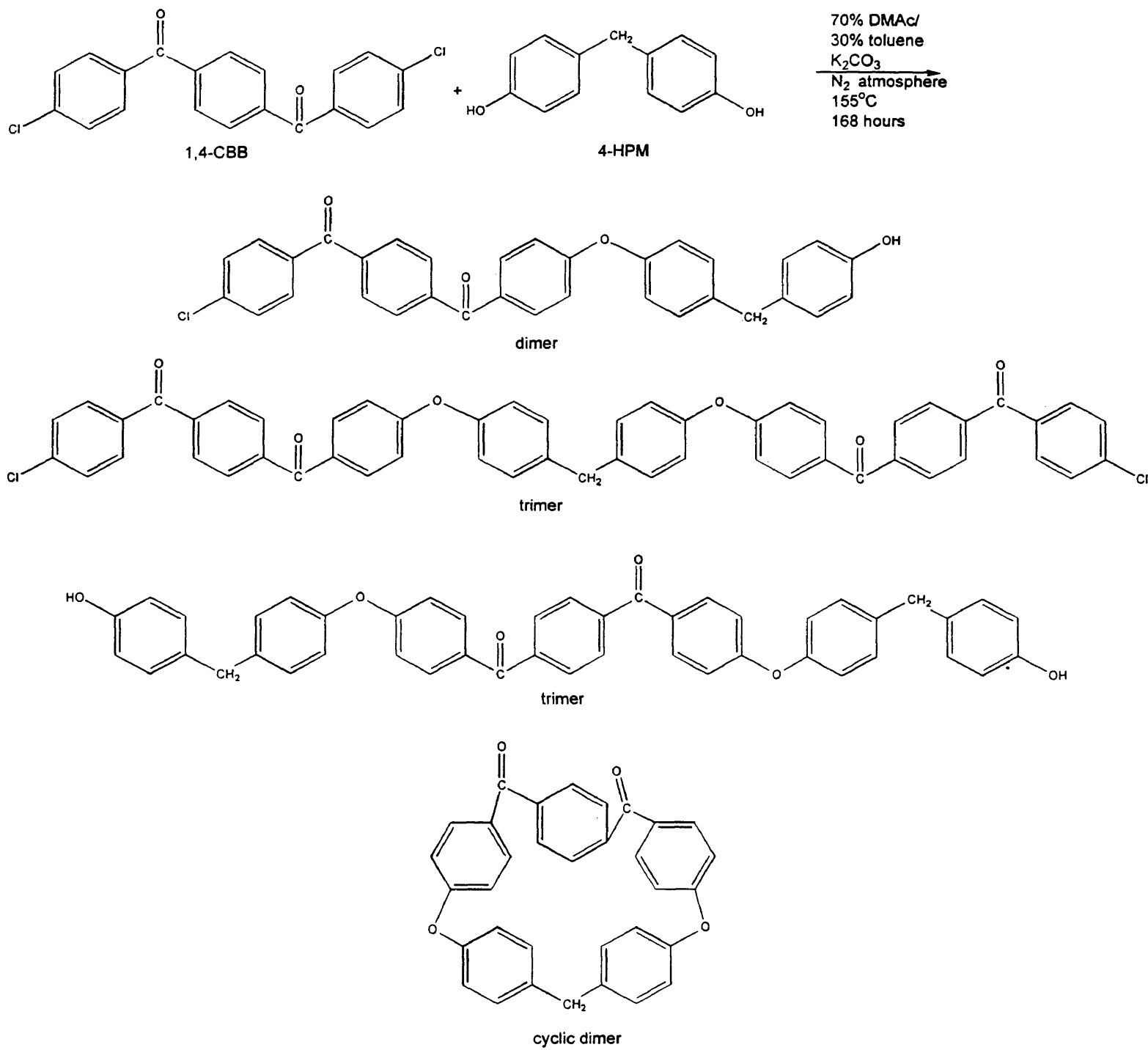


Figure 16. PAE-PP.

## **Gel Permeation Chromatography**

### **Theory**

When synthesizing a condensation polymer system, a single species of product usually is not produced. Rather, one obtains a mixture of many different sizes - long polymer chains, oligomers, and monomers. In order to analyze any one of these species, it must be separated from the others. Gel permeation (*i.e.*, size exclusion) chromatography (GPC) serves such a purpose. It allows separation of these polymer species according to their hydrodynamic volumes (roughly by size).<sup>16</sup>

The principle of GPC is straightforward.<sup>16</sup> The chromatographic column contains a packing of finely divided solid particles with each of the particles perforated by pores (stationary phase). A polymer solution is then pumped through the column.

As the solution flows past the pores of the column, the species in the sample that have diameters smaller than that of the pore size are trapped temporarily in these pores and have to work their way out before they can elute with the solvent. On the other hand, molecules which are too large to enter the pores of the column simply flow with the solvent and emerge well before the smaller molecules. In this way the size distribution of the molecules in a given polymer sample is found. The largest molecules are eluted from the column first, and the smaller molecules are eluted last.



## Instrumentation

The gel permeation chromatography instrumentation for this research (Figure 17) consisted of a Scientific Systems Model 222C HPLC pump, a Viscotek® Model 200 differential refractometer-differential viscometer (Figure 18), and one column. For both analytical and preparative work the column was a 500 mm × 22 mm Alltech® column with a polystyrene-divinylbenzene gel, 5- $\mu$  porosity, 100-Å pores, and a molecular weight range of 100 to 5,000 grams/mol. The data from the differential refractometer-differential viscometer were recorded by a computer using Viscotek® Unical GPC Software, Version 4.04.

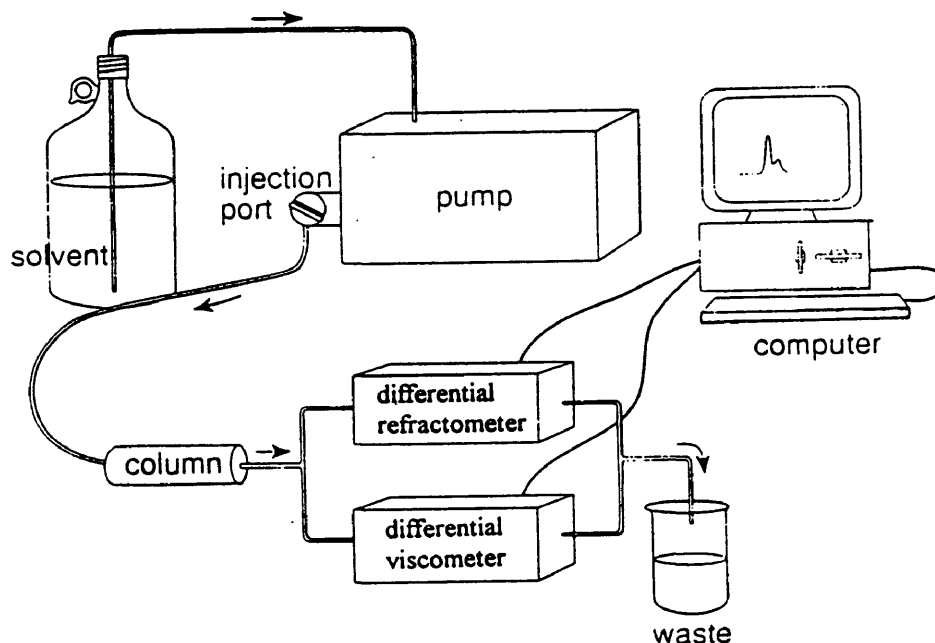


**Figure 17.** A diagram of the instrumentation for GPC work in this research.

The flow rate was set at 3.2 mL/min, and the size of the injection loop was 1 mL. All samples were dissolved in tetrahydrofuran (THF), which was used as the mobile phase. To prevent solute from going out of solution during its passage through the column, the concentration of each injected sample was kept to a maximum of 3 mg/mL.

Data from the differential refractometer and the differential viscometer were read by the computer and could be observed on the screen as the run progressed. When each run was complete, the Viscotek® software processed the data from the detector and plotted a concentration chromatogram. For the purposes of this research, the only chromatograms utilized were those from the differential refractometer.

### **Differential Refractometer**

The refractometer in the detector (Figure 18) works on the deflection principle and evaluates a given sample in the following manner. Light of wavelength 950 nm from a light emitting diode (LED) refracts through a double refractive index (RI) cell which contains the sample (from the column) in one side and the reference solvent (THF) in the other. Next, the beam is deflected in proportion to the difference in refractive indices of the solvent and solution. This deflection is then measured by directing the refracted beam onto a prism beam splitter. The light from the prism is collected with two silicon photodiodes (SiPD). The ratio of the signals of these two SiPDs is a direct measure of the deflection, and therefore the refractive index difference, between the reference solvent and

the injected sample. These signals are transmitted to an analog-to-digital converter which in turn sends a signal (in millivolts) to the computer.

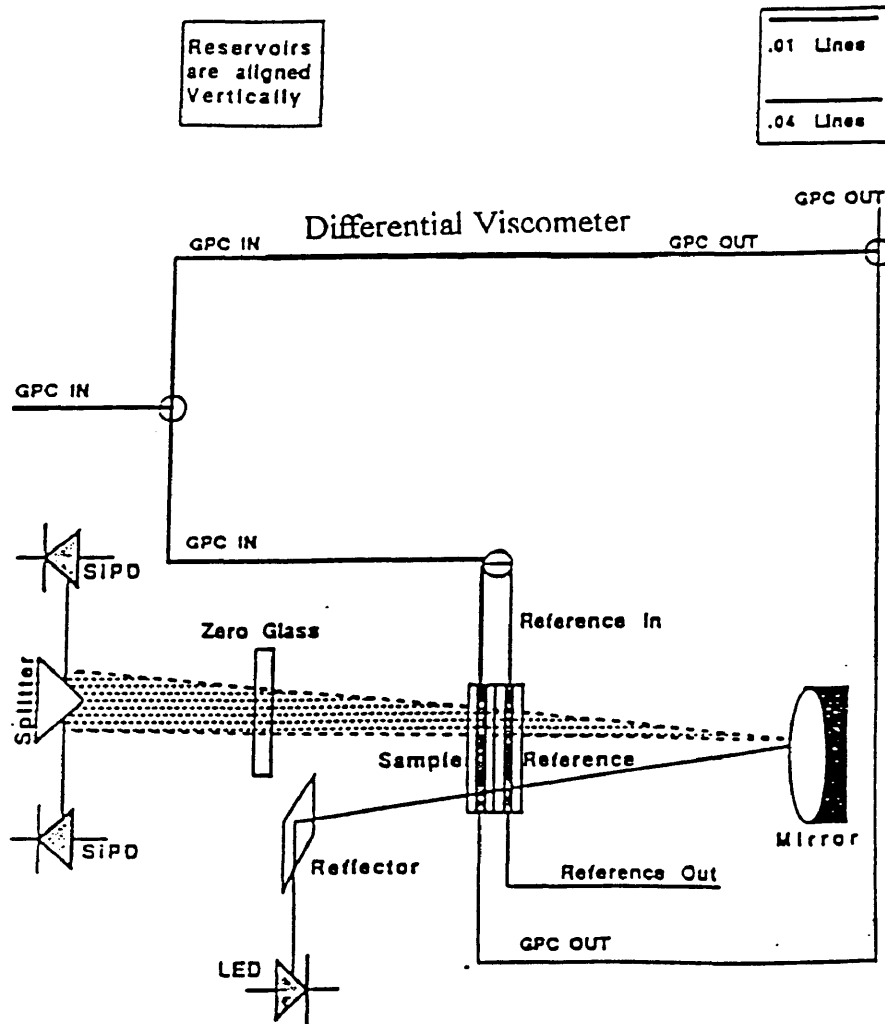


**Figure 18.** The Model 200 Differential Refractometer-Differential Viscometer.<sup>17</sup>

These millivolt signals are plotted against the volume of solvent that has been eluted at the time of the signal (the retention time). The peak area of an RI chromatogram is proportional to the mass concentration of the species eluted from the column at a given retention volume. These concentration chromatograms give a qualitative measurement of

the concentration of each species found in a given sample. More importantly for this research, however, they reveal two pieces of information. First, the number of peaks shows the minimum number of different species to be found in a given sample. Also, through the relative retention volumes of these peaks, one can estimate the relative size of each species in a given chromatogram.

### **Analytical Gel Permeation Chromatography**

As described earlier, the reaction mixtures of all four polymer systems were filtered through a sintered glass funnel, keeping both the KOH filtrate and the solid. As shown below in Figure 19, this filtrate and solid were treated to isolate fractions of the polymer reaction product. Each fraction had a different solubility.

The first of these fractions (#1) was the dried, solid material which contained all products that had precipitated during work-up and had not dissolved in the 1.0-M KOH.

A small amount of fraction #1 was added to toluene and this mixture was then filtered through a sintered glass funnel. All the toluene-soluble filtrate from this procedure was saved. The toluene was then removed with a "Rotavapor" to leave a residue. Thus, this fraction of the polymer system (#2) was both base-insoluble and toluene-soluble.

The base-soluble filtrate from the reaction product was poured into a small separatory funnel and extracted with toluene. The organic layer was saved, and the toluene was removed with a "Rotavapor" to obtain another residue. This residue, fraction #3, was soluble, then, in both base and toluene.

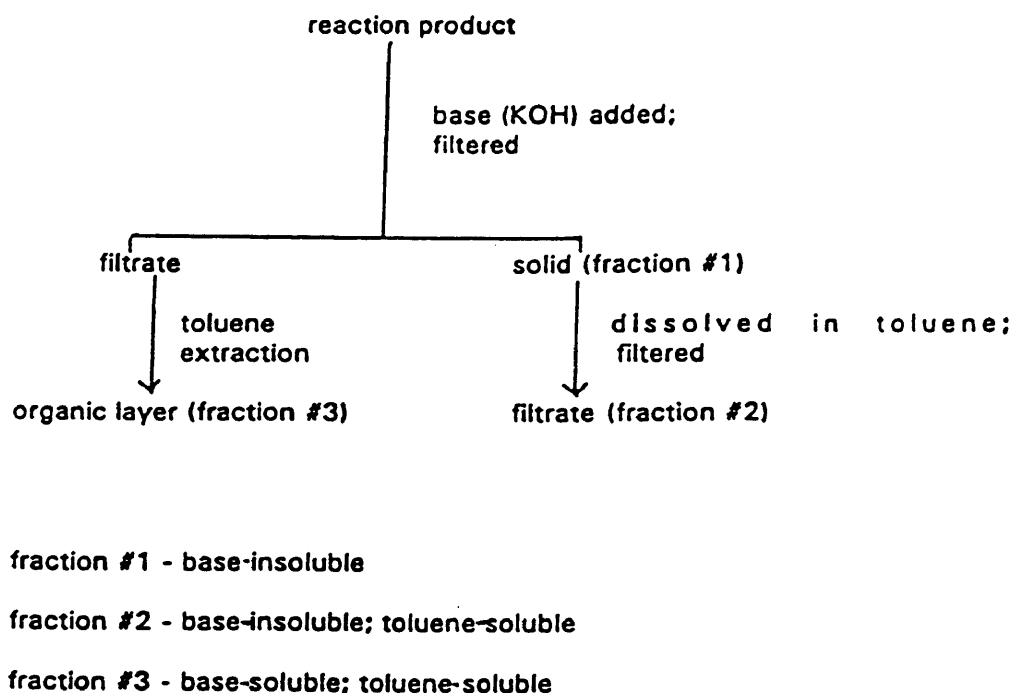


**Figure 19.** Chart describing treatment of reaction product in order to obtain fractions of varying solubilities.

Each of these fractions was dissolved in THF. A solution of each monomer was also prepared. These solutions were carefully filtered twice by using 0.5- $\mu\text{m}$  disposable filters in order to remove any dust or other insoluble particles that could clog the column. All analytical samples were stored in glass vials. Before use, these vials were thoroughly cleaned with soapy water, rinsed with acetone, and dried in an oven at approximately 110°C. A visual inspection was then made of every sample to make sure no dust was present. Finally, each sample was analyzed with GPC by using the parameters and instrumentation already discussed.

### **Preparative Gel Permeation Chromatography**

After using analytical GPC to help identify the position and number of the low-molecular-weight peaks in each polymer system, the next step was to collect each low-molecular-weight species. During the actual collection, the detector was removed, and sample was collected directly from the column.

The solid of each polymer system (fraction #1 according to Figure 19) was dissolved in THF, and the solution was injected into the loop. The conditions for the first preparative chromatography run were identical to those of the previous analytical runs. The differential refractometer was used as a detector to produce concentration chromatograms on the computer display. However, when the injection trigger was activated, a digital timer was started simultaneously. The time was noted at which each chromatogram peak began and ended (judged by both the computer display and fluctuations in the refractometer reading). In this way, it was possible to find the time when each oligomer species was eluted through the preparative column. These were the observed collection times. The actual collection times were calculated by subtracting three seconds from each end of the range to account for the time required for solution to reach the detector from the end of the column.

With collection times known, the detector was disconnected from the exit end of the preparative column so that fractions from the column could be collected. In this procedure, sample was injected onto the column with simultaneous activation of the timer. Solution was collected during the actual collection times and stored in glass vials.

After the first collection run (from which the first set of isolated oligomeric species was collected) had been completed, each oligomer sample was run again on the column with the detector in place. By examining the resulting chromatograms, it could be confirmed that each oligomer sample contained only the single, desired collection peak. After these verifications, collection runs continued (minus the detector). With each successive collection run, the eluted samples having the same collection time were stored together in the same vial. In this way, larger amounts of each oligomer sample were accumulated for later analysis.

Each isolated oligomeric species was then covered with a Kimwipe<sup>®</sup> and left in a hood to allow evaporation of THF. After most of the THF was gone, the sample was heated in a vacuum oven to remove any remaining THF. At this point, an attempt was made to weigh the collected sample of each species of interest.

## **Other Analytical Techniques and Instrumentation**

### **Thin-layer Chromatography**

All thin-layer chromatography (TLC) that was done in the course of this research used silica backed with glass as the stationary phase. Toluene and ethanol were the mobile phases.

Samples for analysis were taken directly from the GPC apparatus and dotted (3-5 dots), in as small a radius as possible, at the bottom of the silica plates. After allowing the THF to evaporate, the mobile phase was applied to the plate. Movement of the sample dots was monitored with an ultraviolet light ( $\lambda = 254/366$  nm).

### **Infrared Spectroscopy**

Two media were used in preparing samples for infrared spectroscopy (IR): chloroform (stabilized with ethanol) as a solvent and mineral oil for mulls. In both cases, NaCl plates were used to hold the sample. The instrument utilized was a Nicolet• 20XB-FTIR spectrometer. This instrument was single-beam and employed OMNIC• Version 1.2 software to read and plot the spectra. We compared our infrared spectra with well-known characteristic group absorptions.<sup>18</sup>

### **Differential Scanning Calorimetry (DSC)**

A Perkin-Elmer• DSC-7 instrument was used to detect any phase transitions to be found in our compounds. Aluminum pans were used to hold all compounds examined.



About 4-6 mg of each PAE product mixture and about 2 mg of each oligomer were utilized in each DSC run. An empty aluminum pan was used as a reference. All DSC data are expressed as heat flow (mW) versus temperature ( $^{\circ}\text{C}$ ). Endotherms are displayed as maxima and exotherms as minima. All cooling and heating rates were  $5^{\circ}\text{C}/\text{min}$ . Perkin-Elmer<sup>®</sup> Thermal Analysis Software, Version 3.00, was used to plot the data and also allowed the calculation of the change in enthalpy ( $\Delta H$ ) associated with a given phase transition.

### **Microscopy**

Product mixtures were examined under a Leica<sup>®</sup> ATC (Advanced Teaching Compound) 2000 microscope. This instrument, combined with a heat stage, was used to try to visualize transitions seen with DSC. The heating rate was hard to control, so approximate temperatures were noted with regard to any observations. The instrument also was equipped with a cross-polarizer.

### **Thermogravimetric Analysis (TGA)**

All TGA analyses were done by using a Shimadzu<sup>®</sup> TGA-50H apparatus with dry air flow (20ml/min). All samples were heated at a rate of  $5^{\circ}\text{C}/\text{min}$ . The main instrument was linked to a computer with a Shimadzu<sup>®</sup> Thermal Analyzer TA-501 apparatus. Initial data processing was done using TASystem<sup>®</sup> software. Final graphs were completed using Quattro<sup>®</sup> Pro, Version 6.01.

## **Tandem Mass Spectrometry**

Samples were analyzed by Sheeba Ahmed at Merck Research Laboratories in West Point, Pennsylvania, using a Sciex• Model API III Plus Triple Quadrupole Mass Spectrometer.<sup>19</sup> This instrument was interfaced with a liquid chromatograph (LC). The mobile phase consisted of a mixture of acetonitrile, methanol, and water. Although we did not utilize the LC, our samples were mixed with this mobile phase mixture as they were injected onto the mass spectrometer.

All samples were first dissolved in THF and then mixed with trifluoroacetic acid (TFA) before injection. The electron multiplier (detector) was set to recognize only positive ions. The TFA was used in an attempt to protonate (and add a positive charge to) our samples. Ionization of samples was accomplished via an electrospray device. A basic illustration of the instrumentation involved in this technique is depicted below (Figure 20). Utilization of the three quadrupoles and an inert collision gas provides this instrument with tandem capabilities. Initial, precursor, ions are selected at the first Quadrupole (Q1). Precursor ions selected from the first quadrupole mass filter are sent on to the second quadrupole (Q2) where they are collided with an inert gas. This fragments the chosen precursor ions into product ions which are selected at the third quadrupole mass filter (Q3).

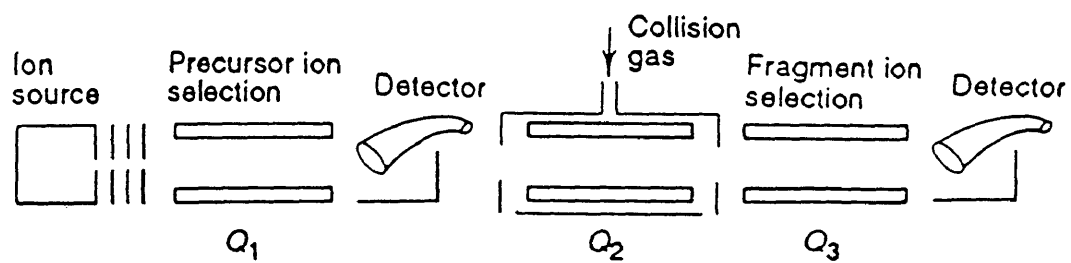


**Figure 20.** General depiction of the MS-MS apparatus used in this research.<sup>20</sup>

## RESULTS AND DISCUSSION

### Analytical Gel Permeation Chromatography

The purpose of this chromatographic study was to determine (qualitatively) the distribution of the reaction products from each combination of isomeric reactants. By using the solubility preparations done earlier, we hoped to obtain preliminary identification of peaks corresponding to cyclic oligomers.

First, chromatograms were taken of the four monomers. All are soluble in THF, although 1,4-CBB is only slightly soluble. Each of these chromatograms had more than one peak (maximum or minimum). It is believed that the minimum peak in each was produced by water. Water has a lower refractive index than THF and should produce such a signal. This peak serves as a very handy reference point for predicting the size of the other molecules which exit the column before it. In addition to the water, there were two other peaks in each monomer chromatogram: a strong peak at approximately 115 mL and another, seen only as a shoulder, at about 111 mL. The 1,4-CBB chromatogram does not clearly possess this peak, although there seems to be a slight trace. It is believed that both of these peaks correspond to impurities related to the THF mobile phase. In order for this choice of mobile phase to be useful with a differential refractometer, uninhibited, HPLC-grade THF must be used so that it will be transparent. Unfortunately, uninhibited THF also forms peroxides with time and exposure to oxygen. Although the solvent reservoir was degassed often, it still had frequent contact with atmosphere. It is also possible that these peaks are from traces of solvents from the synthesis that, despite

attempts at thorough drying, still remained with the reaction products. The only peaks which differed from one monomer to the next were therefore identified. These different peaks served as a useful size comparison when examining the polymer chromatograms. It is also interesting to note that both of the dihalide monomers eluted after the bisphenols, despite the fact that both dihalides are larger molecules. This tendency might be due to hydrogen bonding of the hydroxy ends of the bisphenol to the THF. Such increased affinity of these monomers to the mobile phase might cause them to elute first from the column. Chromatograms for the monomers are shown below in Figures 21-24. The data are summarized in Table 7.

For further reference, a sample of toluene was loaded onto the column. A large, broad peak that centered on about 124.7 mL was observed.

Next, chromatograms were obtained for each solubility fraction of each PAE system. Before beginning, several hypotheses were held about these solubility fractions. First, it was thought that the toluene extract of the base layer (fraction #3) of the reaction mixtures might contain the linear species which possessed at least one hydroxy end and had some affinity for aqueous solution. This assumption was probably premature, as end groups often have small effects on the solubilities of large molecules. Along the same line, it was presumed that the desired small, cyclic compounds might be found in the base-insoluble fractions as these portions would probably contain either cyclic oligomers or structures possessing two dihalide ends. With these ideas in mind, each system's solubility

fractions were examined using GPC. The chromatograms for all PAE systems are shown below in Figures 25-36. Relevant data of each are summarized in Tables 8-11.

Using the information gained from examining the monomer chromatograms, the polymer systems were examined. All retention volumes in each of the three fractions of each system were listed together and then sorted in descending order. Any peaks occurring after the highest retention volume found for a monomer (109.7 mL for 1,4-CBB) were considered, at this time, to belong to unidentified impurities. The minimum corresponding to water has already been discussed. However, in some cases, multiple minima were found. These were also designated as unknown impurities. Any peaks before and including 109.7 mL were designated with letters. Peaks with very close retention times were given the same letter. This allowed comparison of peaks between the fractions of a given system.

Table 7. Analytical GPC data for monomers.

Chromatogram	Retention Volume (mL)	**Intensity	Peak I.D.
1,3-FBB	*122.7	S	water
	115.6	S	impurity
	111.4	W	impurity
	108.6	S	3-HPM
1,4-CBB	*122.5	VS	water
	115.3	VS	impurity
	109.7	M	1,4-CBB
3-HPM	*122.5	VS	water
	115.8	VS	impurity
	111.0	W	impurity
	107.5	S	3-HPM
4-HPM	*122.7	S	water
	115.9	S	impurity
	110.8	W	impurity
	107.0	VS	4-HPM

\*indicates a minimum

\*\*VS = very strong; S = strong; M = medium; W = weak

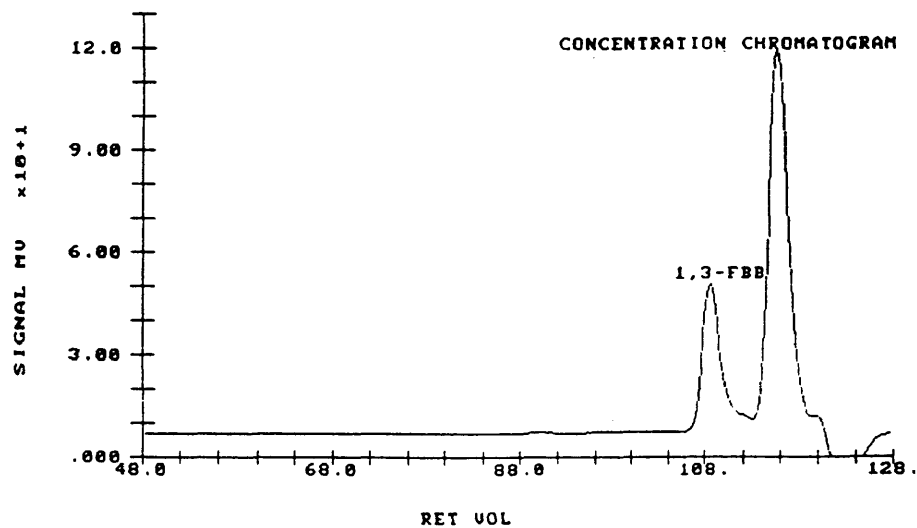


Figure 21. Concentration chromatogram of 1,3-FBB.

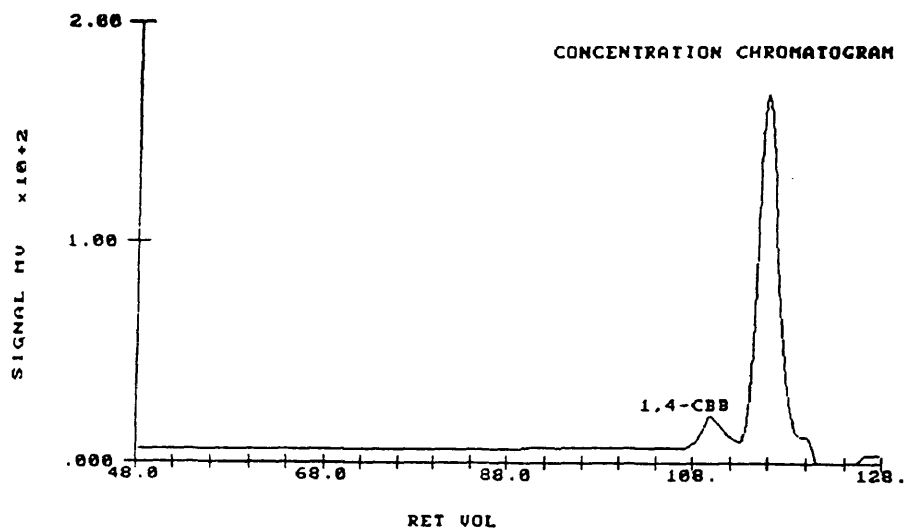


Figure 22. Concentration chromatogram of 1,4-CBB.

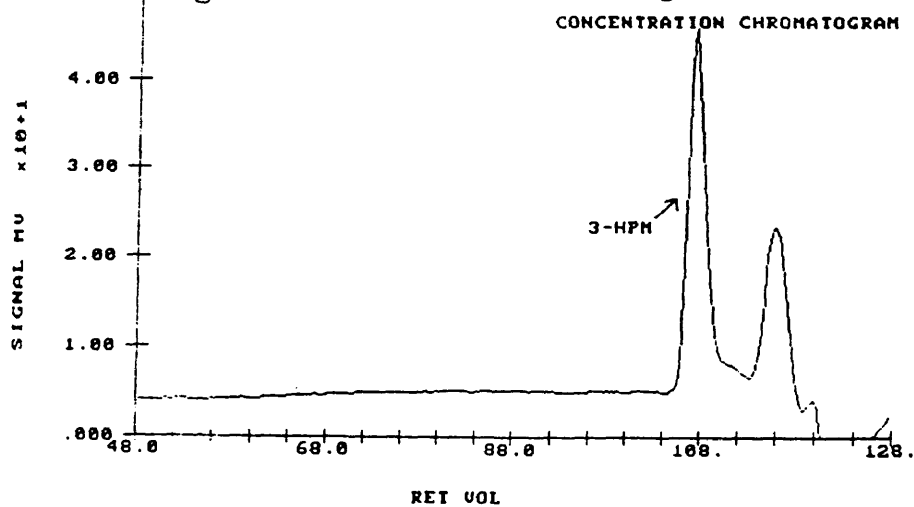


Figure 23. Concentration chromatogram of 3-HPM.

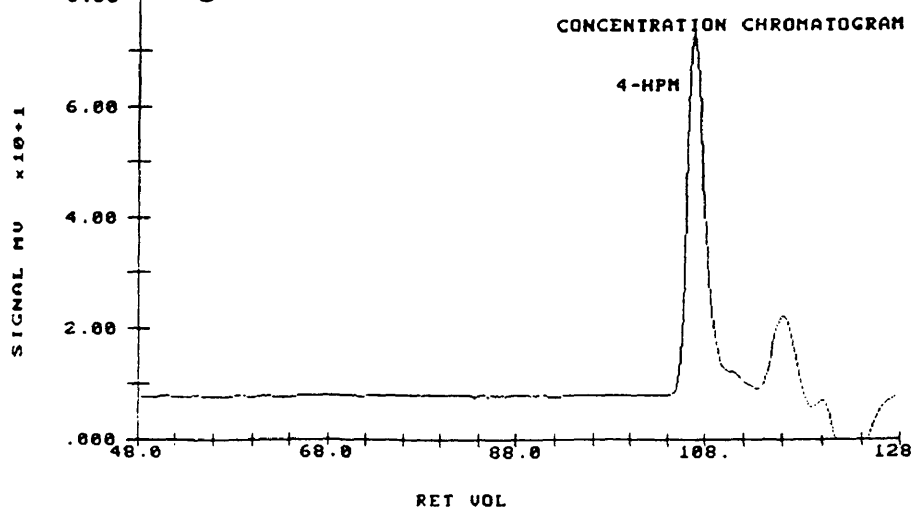


Figure 24. Concentration chromatogram of 4-HPM.



**Table 8.** Analytical GPC data for PAE-MM.

Chromatogram	Retention Volume (mL)	**Intensity	Peak I.D.
Fraction #1 -base insoluble	124.2	S	toluene
	119.0	S	impurity
	*115.9	S	water
	*111.6	S	impurity
	108.1	VS	A
	100.1	S	B
	94.9	M	C
	91.4	W	D
88.5	W	E	
86.5	W	F	
Fraction #2 -base insoluble -toluene soluble	125.6	M	toluene
	119.4	S	impurity
	*116.1	VS	water
	108.5	VS	A
	100.2	S	B
	95.2	M	C
	91.6	W	D
88.8	W	E	
Fraction #3 -base soluble -toluene soluble	124.9	VS	toluene
	118.7	S	impurity
	*115.8	VS	water
	*108.9	S	impurity
99.4	W	B	

\*indicates a minimum

\*\*VS = very strong; S = strong; M = medium; W = weak

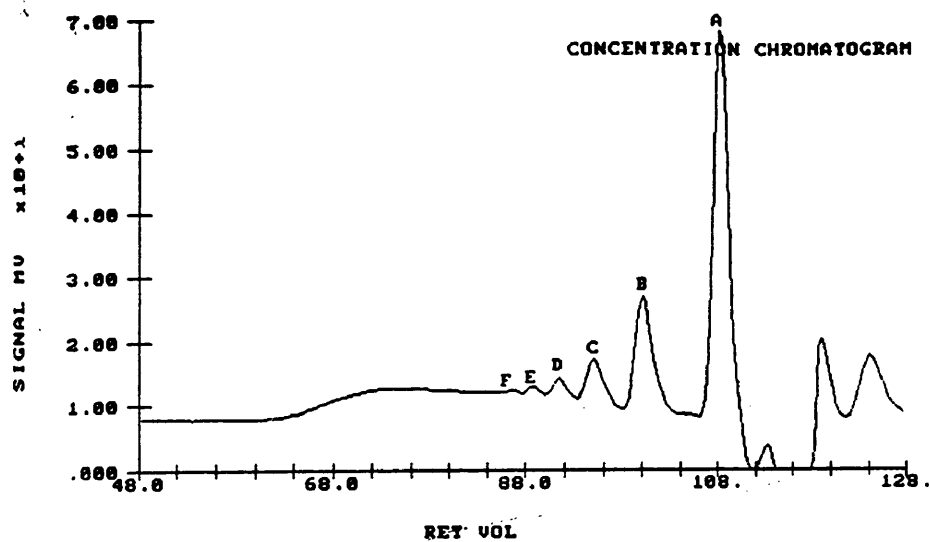


Figure 25. Concentration chromatogram for fraction #1 of PAE-MM.

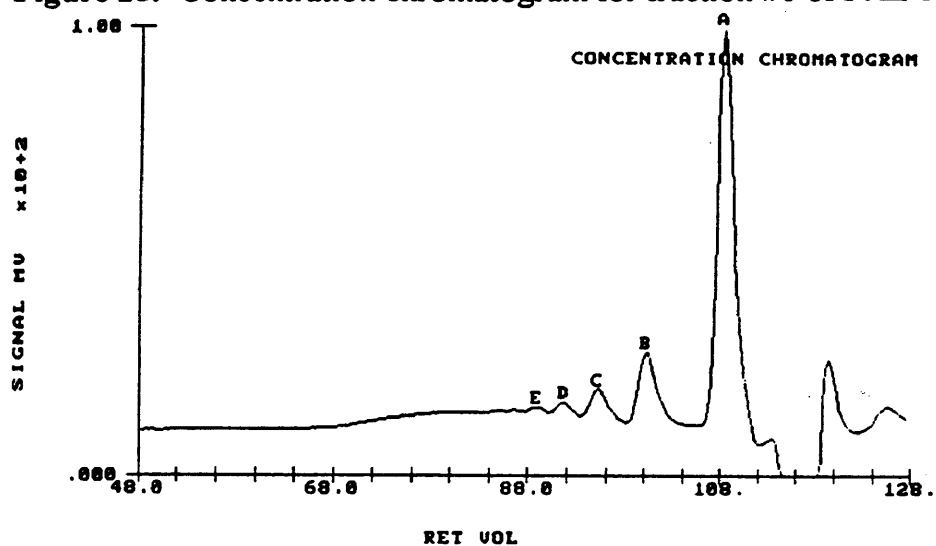


Figure 26. Concentration chromatogram for fraction #2 of PAE-MM.

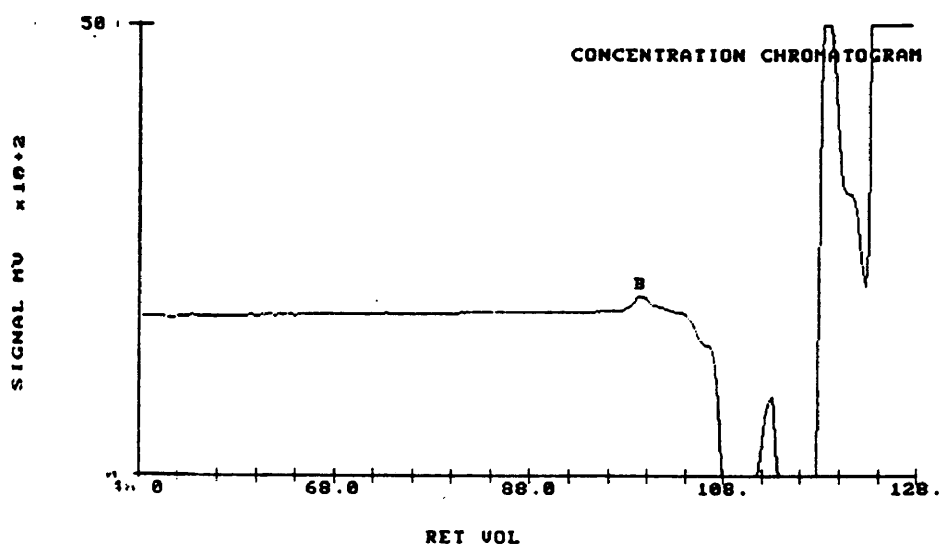


Figure 27. Concentration chromatogram for fraction #3 of PAE-MM.

Table 9. Analytical GPC data for PAE-MP.

Chromatogram	Retention Volume (mL)	**Intensity	Peak I.D.
Fraction #1 -base insoluble	*123.0	S	water
	115.8	VS	impurity
	108.1	W	A
	102.5	M	B
	99.4	S	C
	95.9	M	D
	93.8	M	E
	90.6	M	F
87.2	M	G	
Fraction #2 -base insoluble -toluene soluble	125.6	VS	toluene
	117.0	VS	impurity
	111.3	S	impurity
	109.3	S	A
	103.0	S	B
	99.7	S	C
	96.2	M	D
	94.2	M	E
	90.9	M	F
87.5	W	G	
Fraction #3 -base soluble -toluene soluble	*122.7	S	water
	115.5	VS	impurity
	102.1	W	B
	99.7	M	C
	93.5	M	E

\*indicates a minimum

\*\*VS = very strong; S = strong; M = medium; W = weak

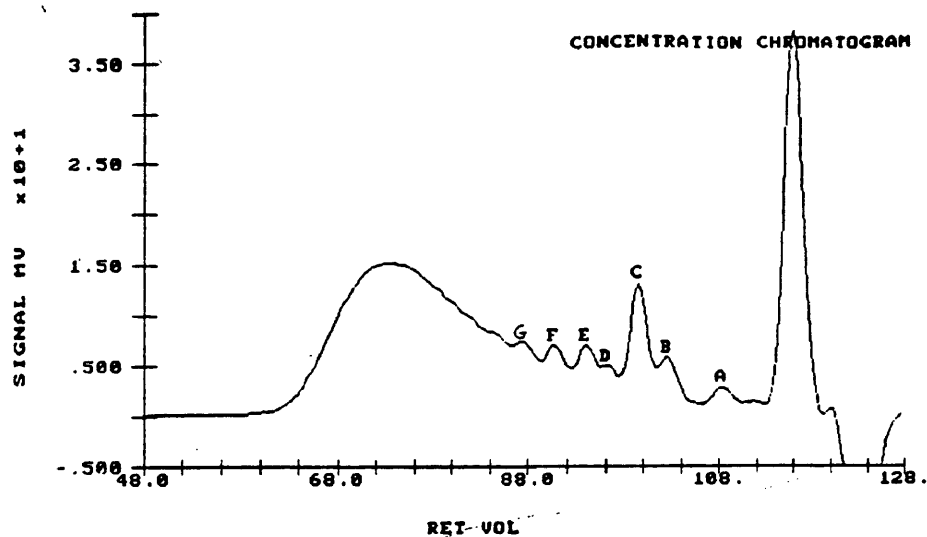


Figure 28. Concentration chromatogram for fraction #1, PAE-MP.

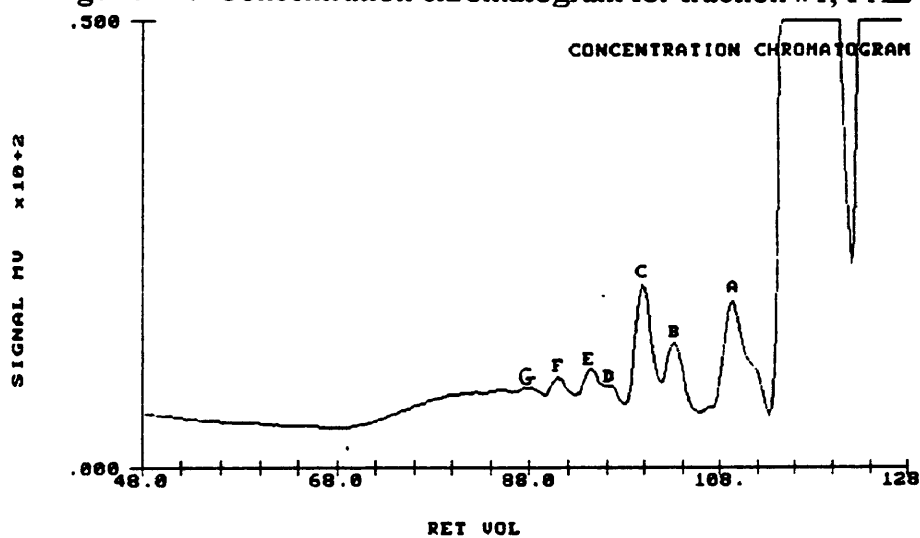


Figure 29. Concentration chromatogram for fraction #2, PAE-MP.

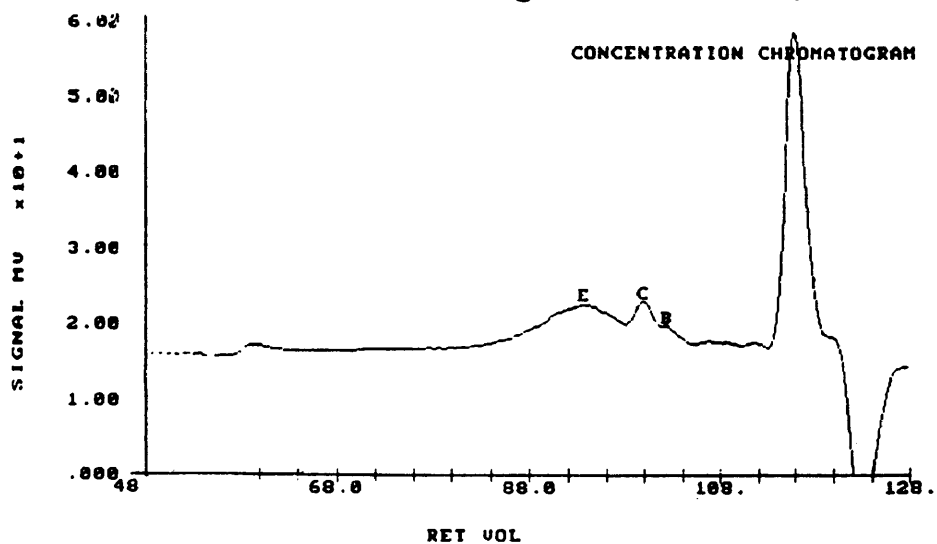


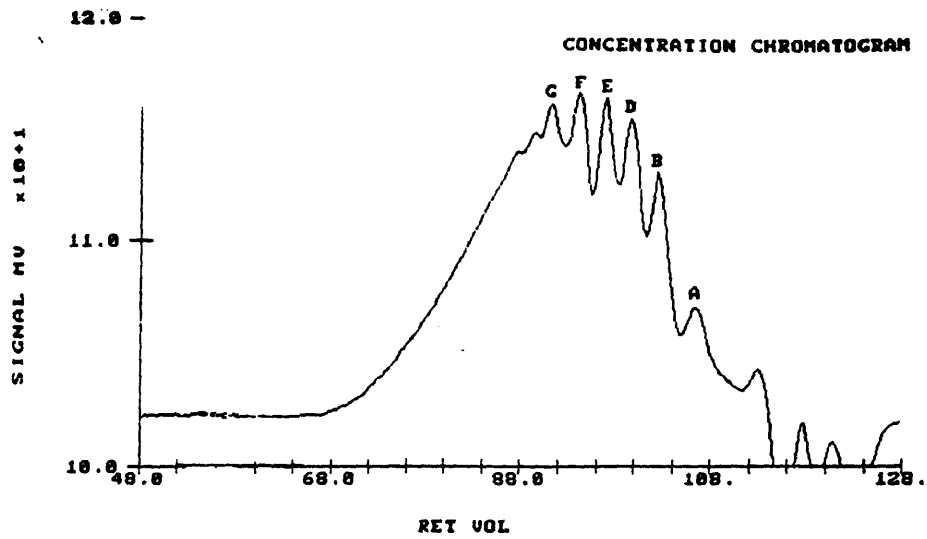
Figure 30. Concentration chromatogram for fraction #3, PAE-MP.

Table 10. Analytical GPC data for PAE-PM.

Chromatogram	Retention Volume (mL)	**Intensity	Peak I.D.
Fraction #1 -base insoluble	*123.4	S	water
	*118.9	M	impurity
	*115.5	S	impurity
	112.9	S	impurity
	106.3	S	A
	102.4	VS	B
	99.4	VS	D
	96.8	VS	E
	93.8	VS	F
90.9	VS	G	
Fraction #2 -base insoluble -toluene soluble	125.0	VS	toluene
	*122.4	S	water
	115.7	S	impurity
	111.9	W	impurity
	106.3	W	A
	102.4	M	B
	99.6	M	D
	96.7	M	E
94.0	M	F	
Fraction #3 -base soluble -toluene soluble	*122.7	S	water
	115.6	VS	impurity
	106.5	M	A
	101.7	M	C
	99.7	S	D
	96.6	M	E
93.7	W	F	

\*indicates a minimum

\*\*VS = very strong; S = strong; M = medium; W = weak



**Figure 31.** Concentration chromatogram for fraction #1, PAE-PM

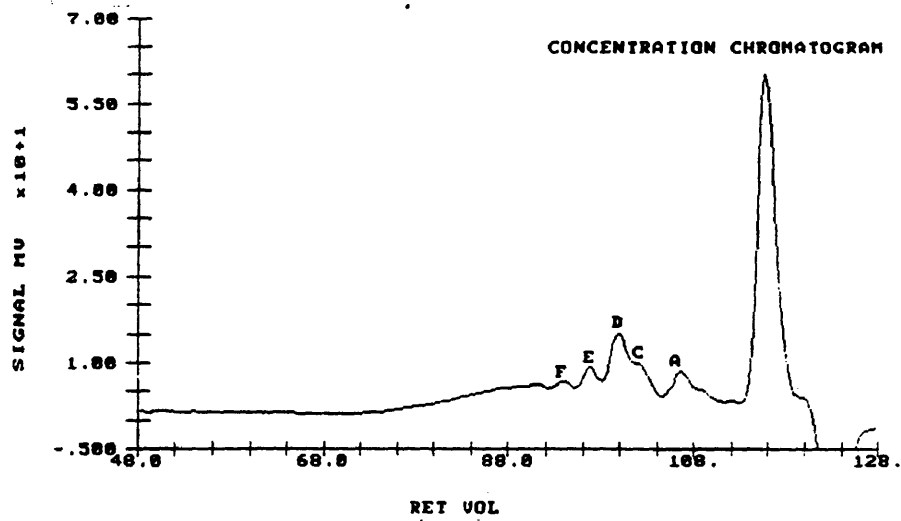


**Figure 32.** Concentration chromatogram for fraction #2, PAE-PM.

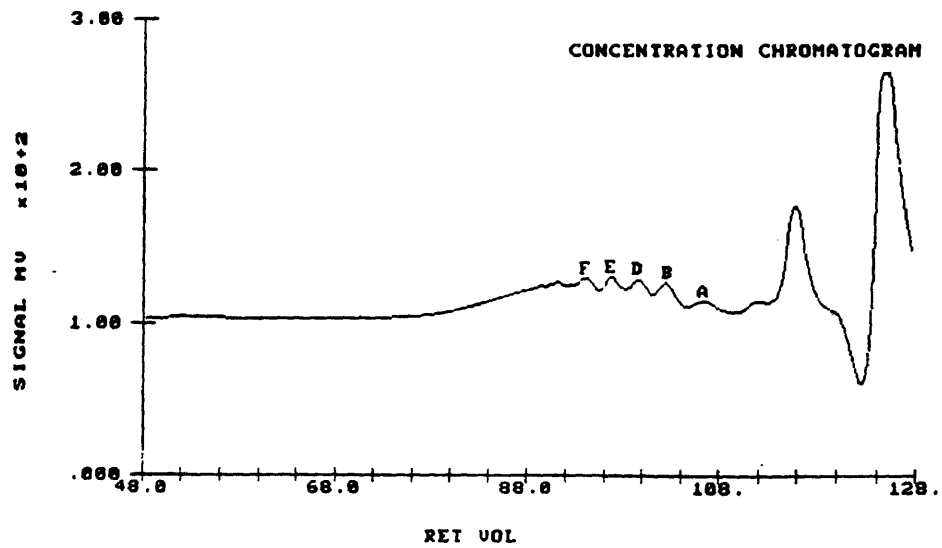


**Figure 33.** Concentration chromatogram for fraction #3, PAE-PM.

Table 11. Analytical GPC data for PAE-PP.

Chromatogram	Retention Volume (mL)	**Intensity	Peak I.D.
Fraction #1 -base insoluble	*123.7	S	toluene
	*116.6	VS	water
	102.2	W	B
	99.6	M	C
	96.9	M	D
	94.0	M	E
	90.5	M	F
60.2	S	G	
Fraction #2 -base insoluble -toluene soluble	124.7	VS	toluene
	*122.2	S	water
	116.5	VS	impurity
109.7	S	A	
Fraction #3 -base soluble -toluene soluble	124.7	VS	toluene
	116.8	VS	impurity
	109.9	S	A

\*indicates a minimum

\*\*VS = very strong; S = strong; M = medium; W = weak

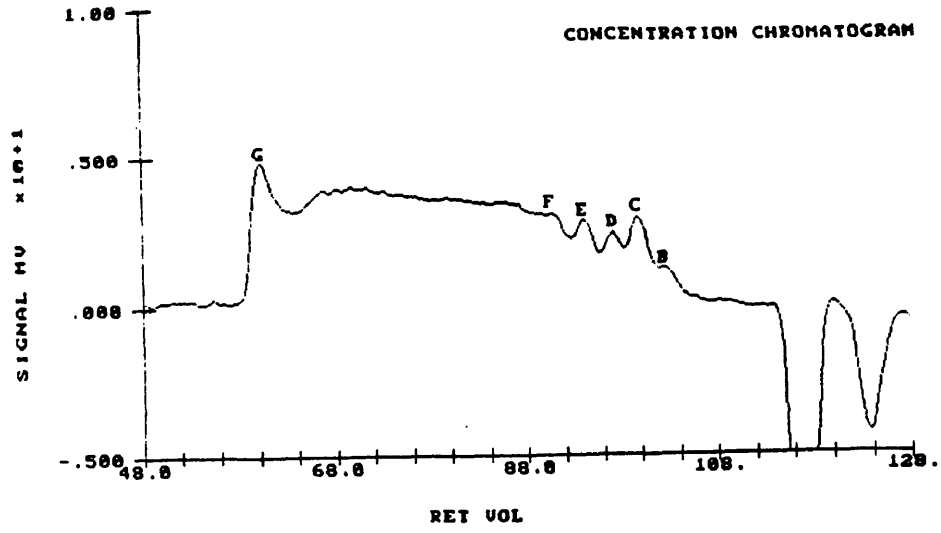


Figure 34. Concentration chromatogram for fraction #1, PAE-PP

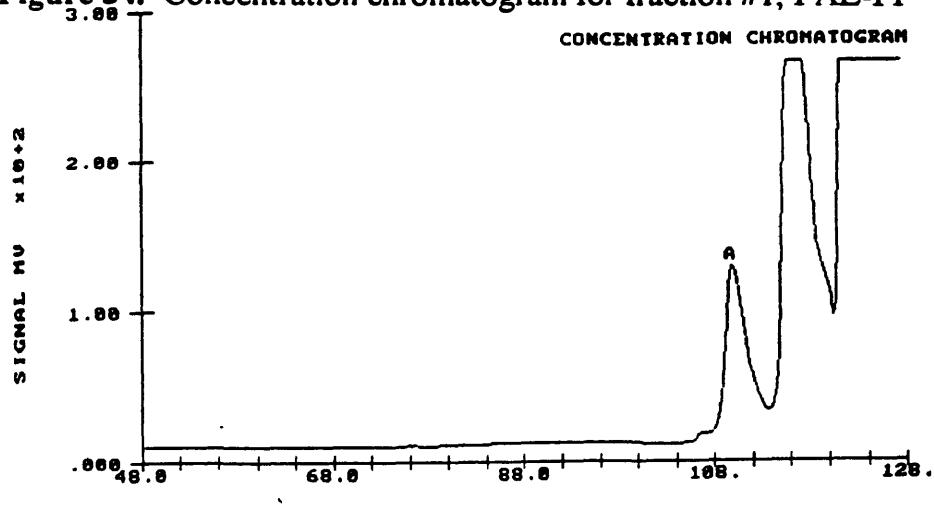


Figure 35. Concentration chromatogram for fraction #2, PAE-PP.

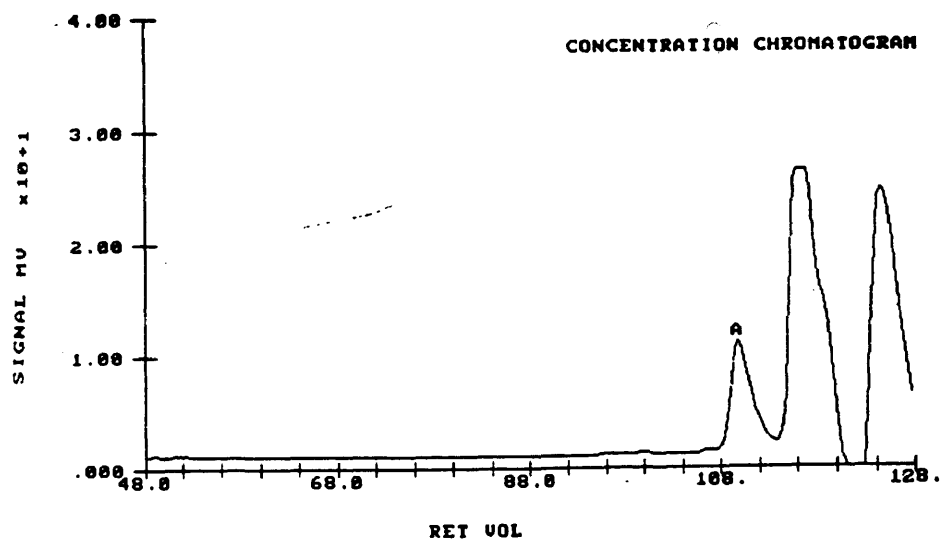


Figure 36. Concentration chromatogram for fraction #3, PAE-PP.



The information obtained from this exercise was useful with respect to revealing the presence of small species. However, fractionation based on solubility did not reveal which peaks corresponded to cyclic or linear compounds.

The PAE-MM's fractions #1 and #2 both showed a very clear distribution pattern of products. If products are eluting from the column roughly according to their molecular weight (which does not strictly occur), the lower-MW species (PAE-MM-A) have the highest concentration, and the higher-MW species possess smaller concentrations. This relatively higher concentration of smaller products is expected, considering the reaction conditions of this synthesis. All compounds in the base-insoluble fraction were soluble in toluene (except the barely visible F). Only B was seen in the base-soluble toluene extract. If all assumptions about solubility were true, it would appear that all PAE-MM species (except possibly B) are potentially cyclic. This seems unlikely.

Both the PAE-MP and the PAE-PM have more irregular distributions of product species. Again, in both of these systems, most species were found in both fractions #1 and #2. The PAE-MP-A was not found in fraction #3, so it seems a likely candidate for a cyclic species; while B, C, and E of this system were found in fraction #3 and probably have at least one hydroxy group. The peaks in the chromatogram for PAE-PM were compressed and overlapped one another. Therefore, even though its peaks were very intense, only when the tips of these peaks were visible would collection be possible using the differential refractometer as a guide. Of all the systems, the PAE-PM had the most

species which potentially had hydroxy ends. Species A, B, D, E, and F of the PAE-PM were all found in fraction #3.

The PAE-PP also had a very irregular distribution of product species with a large proportion of species in the higher-molecular-weight side. Its smallest species (A) was found only in #2 and #3. It is especially odd to find a peak in #2 and not in #1 (as #2 is extracted from #1). However, in PAE-PP #1, there does seem to be some faint activity in this region. Perhaps toluene dissolves and concentrates this species very well, causing it to show up strongly in #2 and #3. Alternatively, PAE-PP-A could also be another unknown impurity.

With these four systems, any peaks found in the base-soluble fractions were also found in either fraction #1 and #2. In most cases, it seems the functional ends on a linear species of these systems have little definite effect. It proved nearly impossible to differentiate conclusively between a cyclic and linear species strictly from this solubility method. More analysis of these species was needed.

### **Preparative Gel Permeation Chromatography**

The peaks of most interest were those of the highest retention volumes. These signals would likely result from the presence of oligomers of some kind and were collected. We set the requirement that in order to collect a peak, a distinct rise and fall in the differential refractometer reading had to be seen. This requirement limited which peaks could be collected. Analytical chromatograms of fraction #1 of each system were

taken again. During the acquisition of these chromatograms, however, the rising and falling of the differential refractometer was timed accordingly. These collection chromatograms (Figures 37-39) should be identical to the previous fraction #1 chromatograms of each system (Figures 25, 28, and 31), but this was not always the case, and that is why these collection chromatograms are displayed below. The same letter designations used in the analytical work were used here. Table 12 summarizes which peaks were collected. Individual species of PAE-PP were not collected (See Mass Spectrometry section).

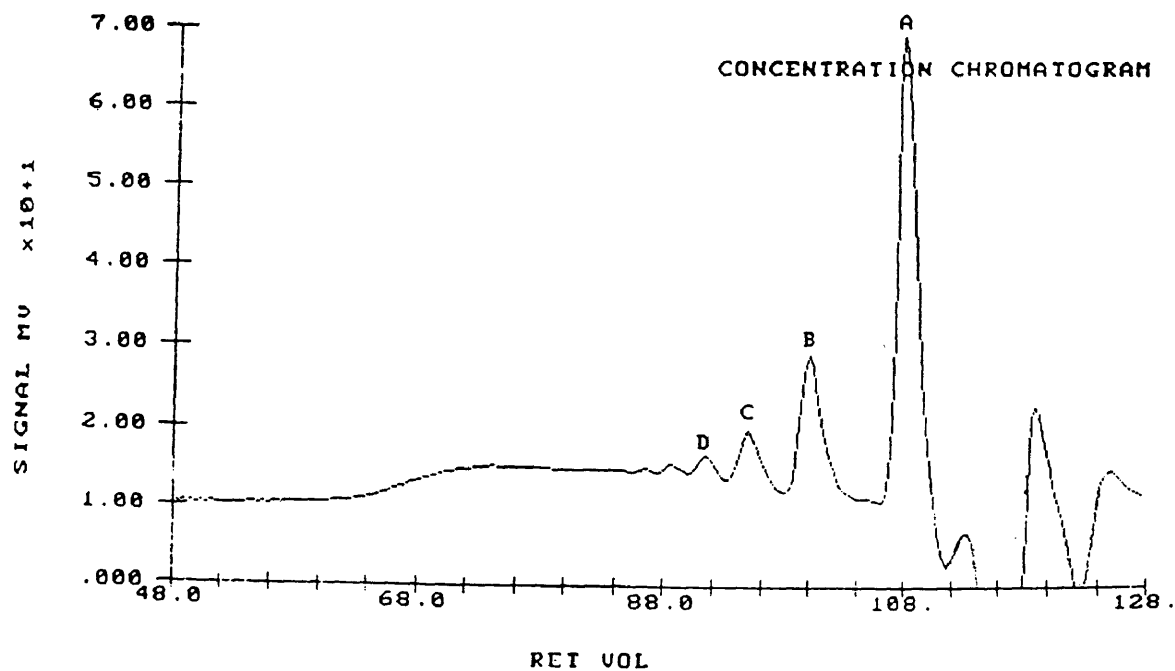


Figure 37. Collection chromatogram for PAE-MM.

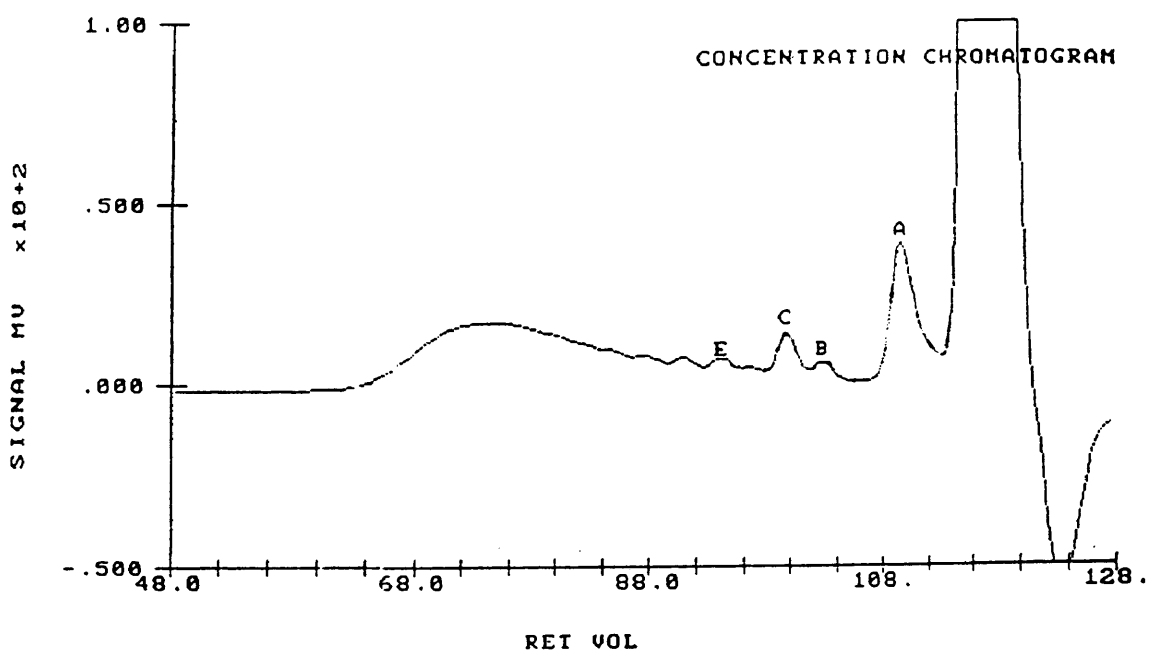


Figure 38. Collection chromatogram for PAE-MP.

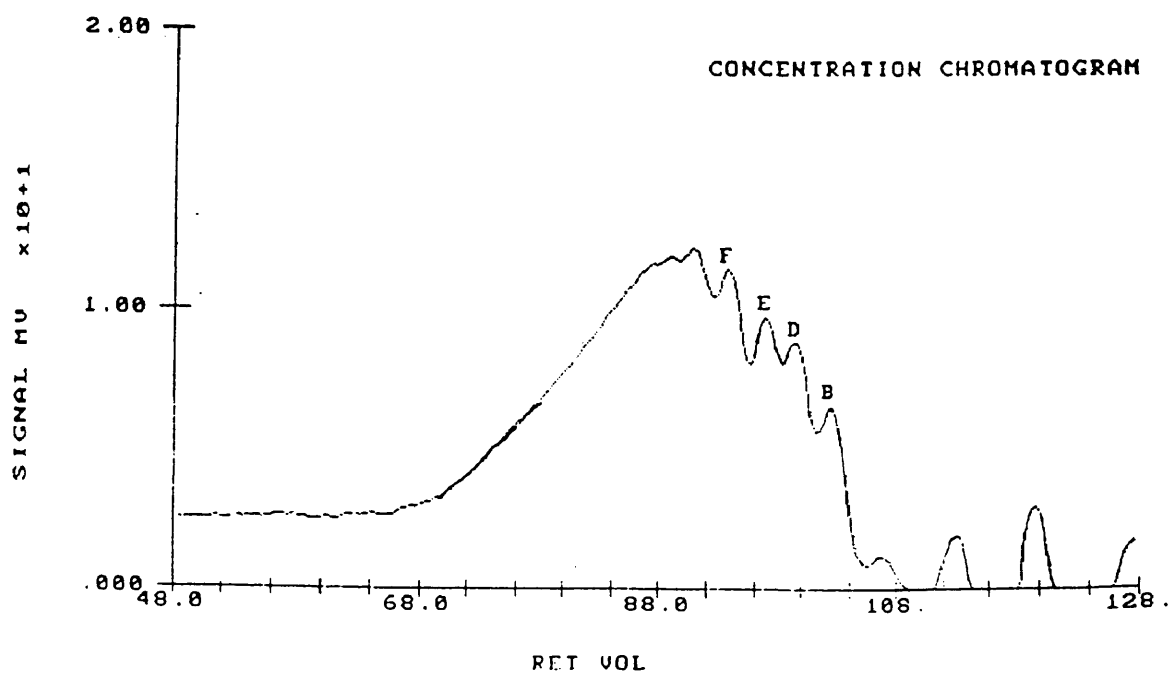


Figure 39. Collection chromatogram for PAE-PM.

**Table 12.** Peaks collected with preparative GPC.

Polymer System	Species
PAE-MM	A B C D
PAE-MP	A B C E
PAE-PM	B D E F

Once the THF was evaporated from each collected sample, it was evident that one GPC run yielded much less than one mg of each species. Attempts to weigh these species were successful only with PAE-MM-A and PAE-MM-B. For each run of PAE-MM-A about 1.9 mg was recovered, and for PAE-MM-B the yield was 0.83 mg. However, even these values seem a little high upon visual inspection of the collected samples. It proved to be extremely difficult to gather any of the other species listed in Table 12 in any manageable quantity. The analysis described in this paper, therefore, focuses on the PAE-MM mixture before separation, PAE-MM-A, and PAE-MM-B. One occasional exception to this problem was mass spectrometry. The instrument required only nanogram quantities, so more sample analysis was possible.

## Tandem Mass Spectrometry

An attempt was made to analyze each species collected with preparative GPC by using tandem mass spectroscopy. This analysis was an integral part of the entire study of these PAE compounds. It proved to be the only technique which gave a strong indication that cyclic oligomers existed in the product mixtures. Unfortunately, we were not able to ionize each of these collected species. The identities of those species for which a mass spectrum was obtained are summarized in Table 19 at the end of this section.

In addition to the various PAE species, a sample of THF combined with TFA (the solution that all species were dissolved in) also was analyzed with the MS-MS system. The precursor ion spectrum of this TFA/THF mixture is shown below in Figure 40. The solvent mass spectrum simplified the examination of the spectra of PAE samples by allowing us to eliminate many peaks from consideration. Some of these solvent peaks may be the result of the polymerization of THF which can occur in the presence of a strong acid (like TFA).<sup>21</sup> In this spectrum, the expected molecular ion peak for THF ( $m/z = 73$ ) is off scale. All precursor ion scans possess  $m/z$  values that are uncertain by  $\pm 0.6$  due to the nature of the mass spectrometer's calibration.

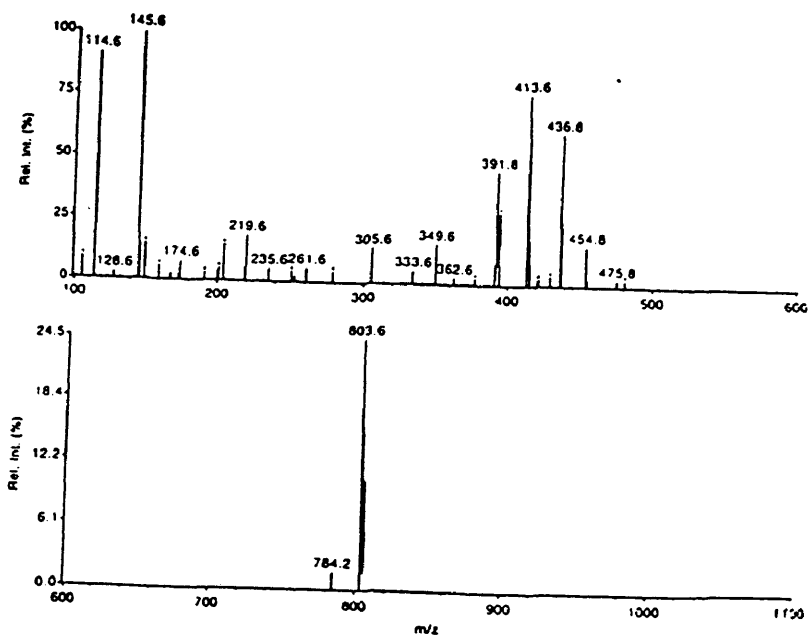


**Figure 40.** Precursor mass spectrum of THF/TFA mixture.

#### *PAE-MM:*

From the PAE-MM reaction mixture, mass spectra could only be obtained for PAE-MM-A and PAE-MM-B. No spectra were obtained for species C and D.

The precursor ion spectrum of PAE-MM-A displayed a peak at 483. This mass was expected for the cyclic dimer plus one hydrogen from protonation ( $[M + H]^+$ ). Other peaks were found in this first precursor scan. These peaks were hypothesized to come from three possible sources: fragments of the 483 molecular ion peak, the TFA/THF mixture (“solvent”), or rearrangements of these first two (“unknown”). The precursor ion spectrum of PAE-MM-A is shown below (Figure 41). A product ion spectrum was then taken of the 483 peak (Figure 42). Peaks thought to originate from the solvent and prominent unknown peaks are listed in Table 13. The ion peaks we believe to represent fragments of 483 are pictured in Figure 43.

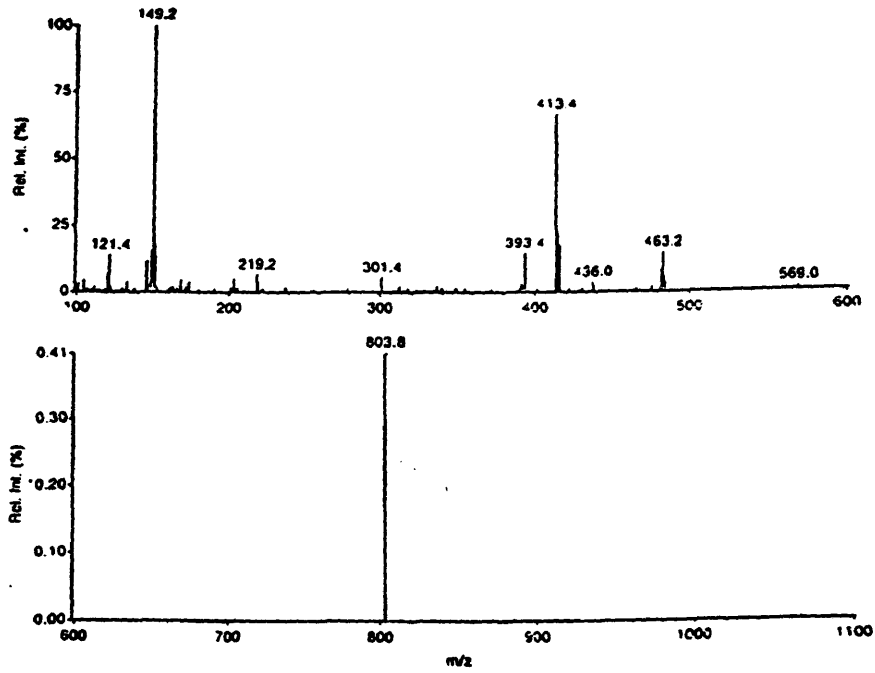


Figure 41. Precursor ion mass spectrum of PAE-MM-A.

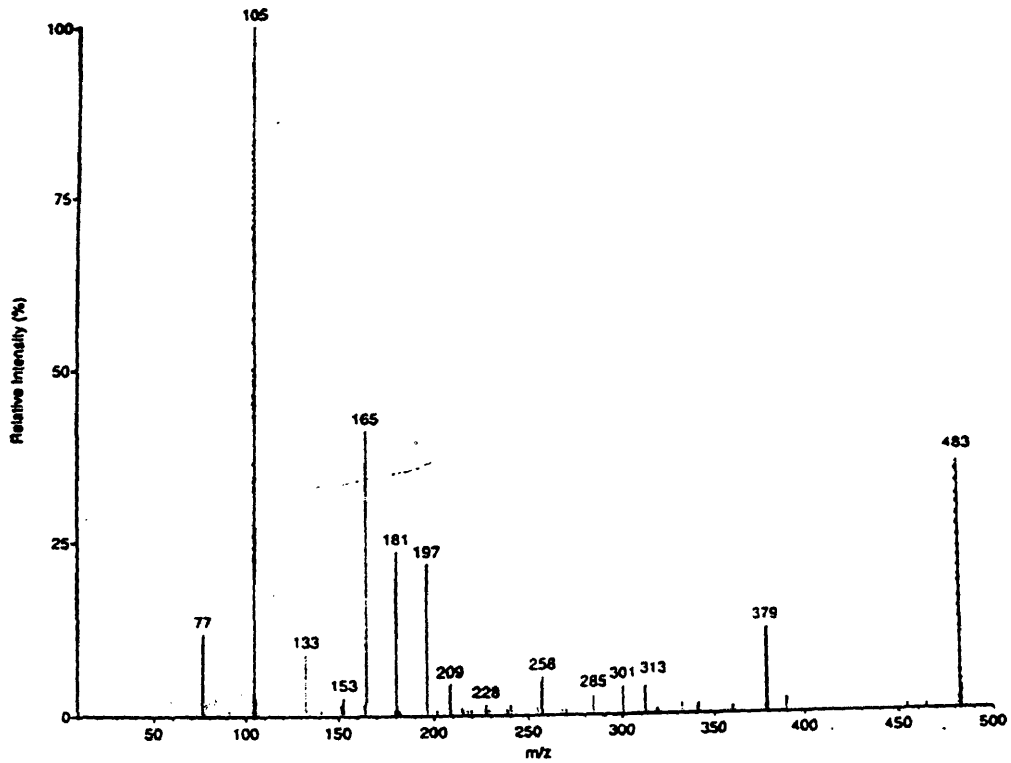


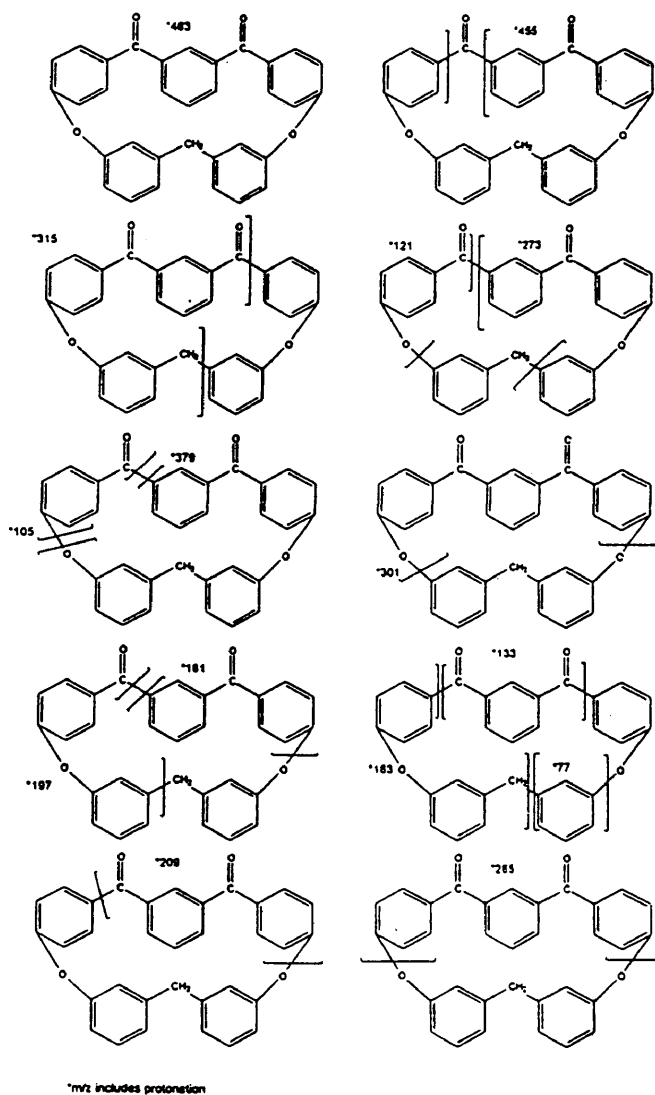
Figure 42. Product ion mass spectrum of molecular ion peak 483 (PAE-MM-A).



**Table 13.** Unknown and solvent ion peaks from mass spectra of PAE-MM-A.

Solvent	Unknown
149.2	569.0
219.2	*313
393.4	*258
413.4	*228
436.0	*165
569.0	*153
803.8	

\*from product ion spectrum

**Figure 43.** Fragments of molecular ion peak 483 (PAE-MM-A).

The fragments found in the precursor and product mass spectra pieced together rather well. Although in some cases in Figure 43 there are complementary fragments missing, it is believed that PAE-MM-A is a cyclic dimer. It is suspected either that the missing fragments were not protonated, had no positive charge and were not recognized by the instrument's detector, or were rearranged and changed into one of the unknown peaks listed in Table 13.

The precursor ion spectrum of PAE-MM-B (Figure 44) showed a peak slightly greater than 965 (965.6), a value expected for the singly protonated tetramer ( $[M + H]^+$ ). A product ion spectrum was then taken of this suspected molecular ion peak (shown in the product ion spectrum as 966). This spectrum is displayed below (Figure 45). As with PAE-MM-A, there were peaks in each spectrum that appeared to be fragments of the molecular ion peak (Figure 46). Also, there were some peaks hypothesized to be either unknown or originating from the solvent (Table 14).

The pieces in Figure 46 also fit together well, and it is hypothesized that PAE-MM-B is a cyclic tetramer. The absence of any complementary fragments can be explained in the same way as those from the examination of PAE-MM-B. Peak 484 is of particular interest. It is probably the dimer (483) or perhaps a doubly protonated tetramer. Such a peak appears for the other cyclic tetramers found in this research (see below).

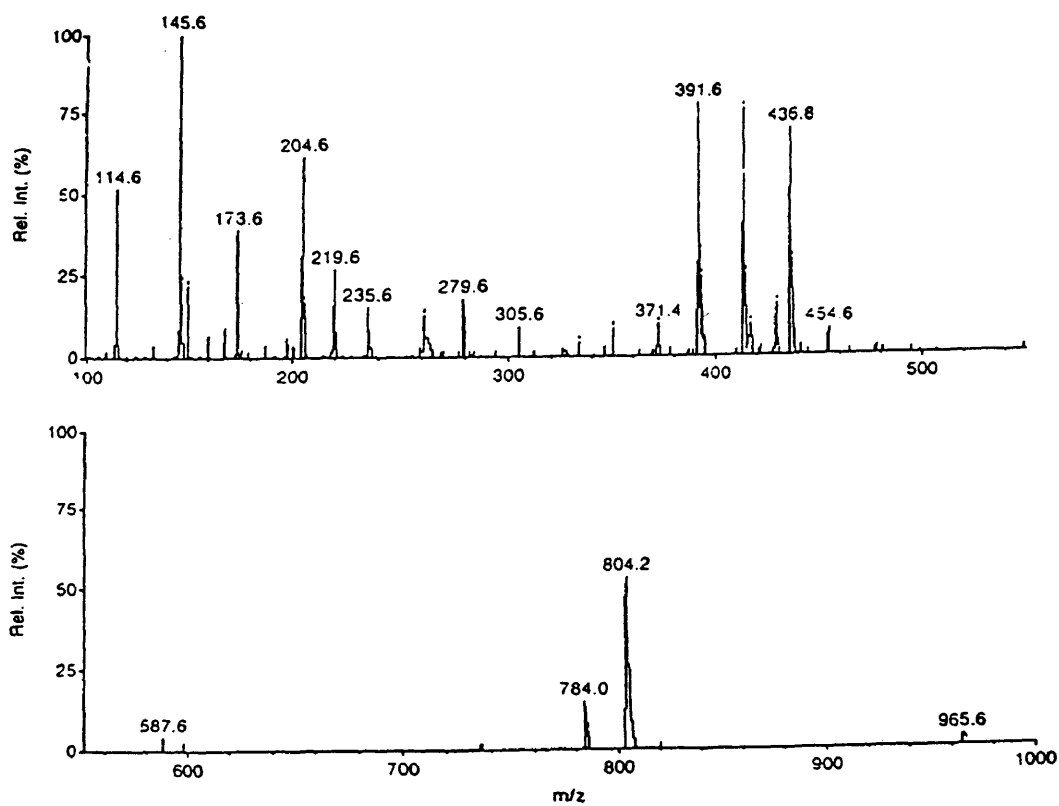


Figure 44. Precursor ion spectrum of PAE-MM-B.

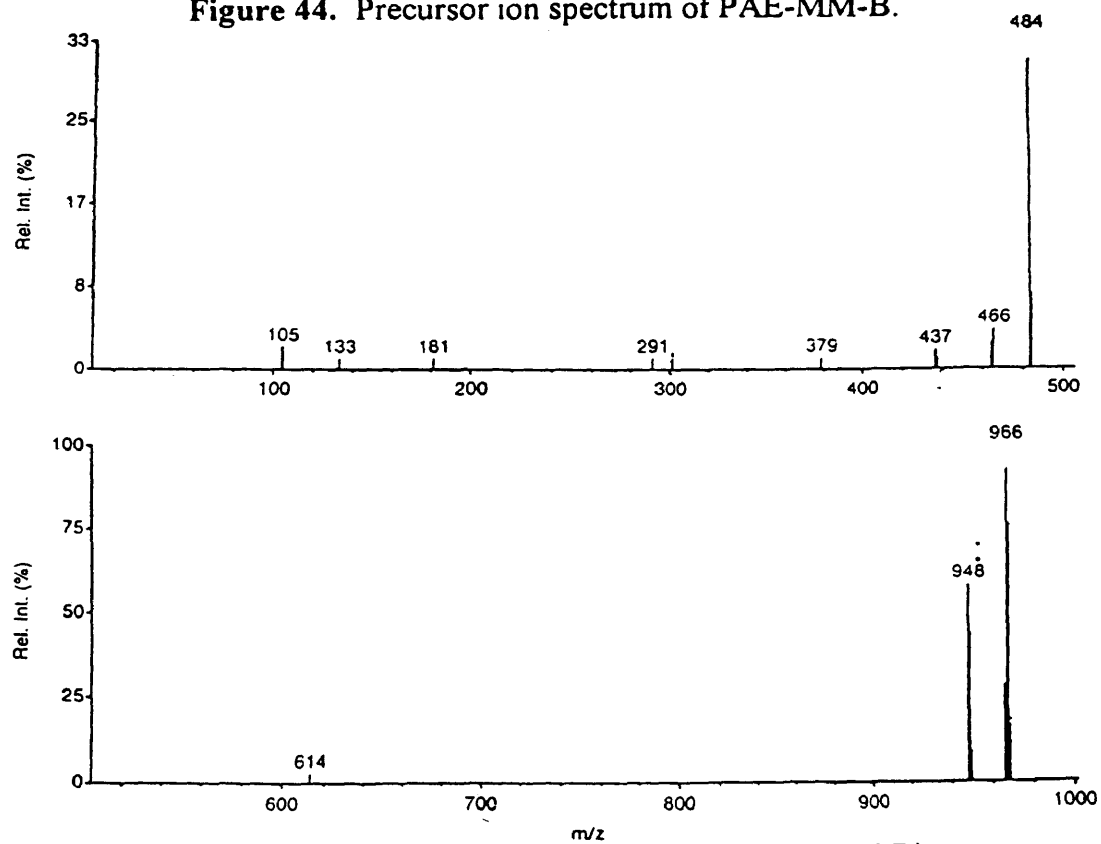


Figure 45. Product ion spectrum of 966 (PAE-MM-B).

**Table 14.** Unknown and solvent peak ions from mass spectra of PAE-MM-B.

Solvent	Unknown
114.6	371.4
145.6	*291
173.6	*437
204.6	*466
219.6	*614
235.6	*484
279.6	*948
305.6	
371.4	
391.6	
436.8	
454.6	
784.0	
804.2	

\*from product ion spectrum

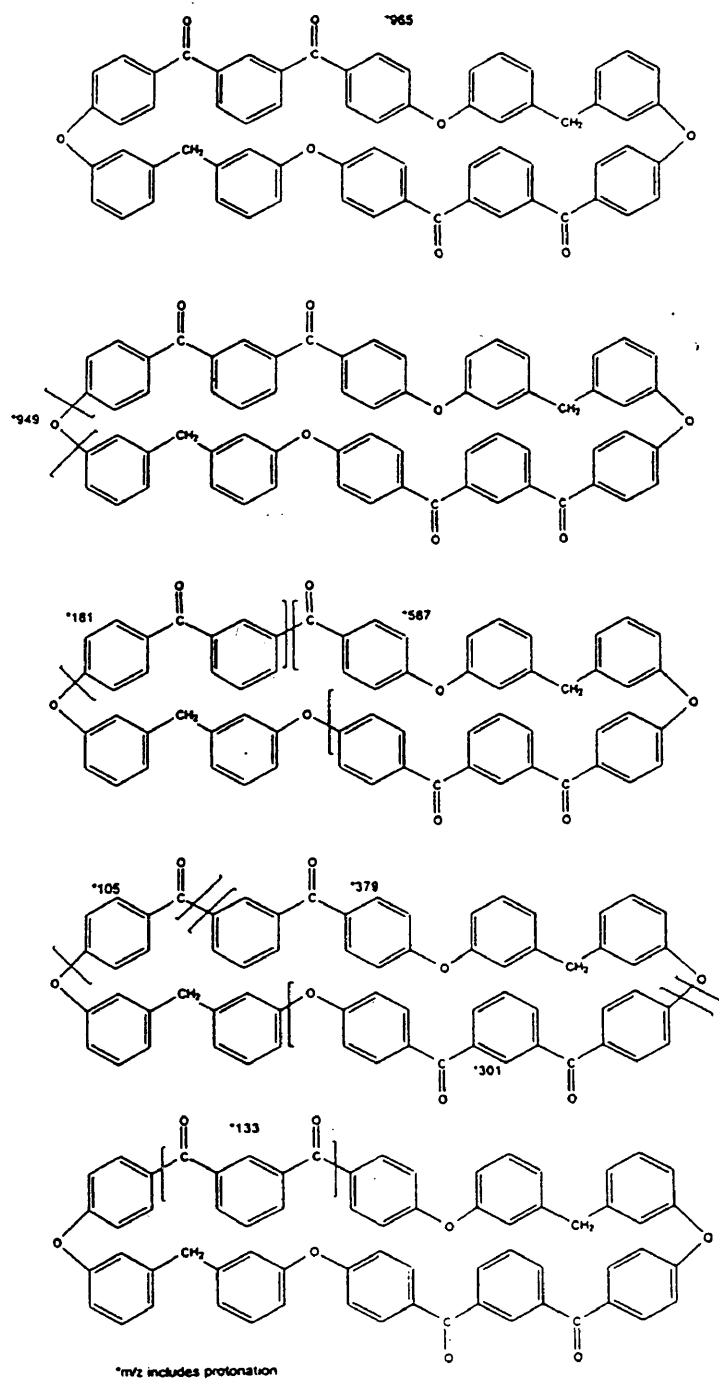


Figure 46. Fragments of molecular ion peak 966 (PAE-MM-B).

*PAE-MP:*

With the PAE-MP system, mass spectra were obtained for PAE-MP-A and PAE-MP-C. No spectra could be obtained for species B and E.

After viewing the mass spectrum of PAE-MP-A, we believed this compound, like PAE-MM-A, was a cyclic dimer. Its precursor spectrum (Figure 47) contained a 483 peak along with possible fragments of this ion peak. Again, solvent and various unknown ion peaks were identified (Table 15). Once a product ion mass spectrum was taken of the 483 ion peak (Figure 48), more evidence pointed to this compound being a cyclic dimer. Many of the fragments evident (Figure 49) are very likely to be pieces of a cyclic dimer. Some of these same fragments were also discovered in the PAE-MM-A mass spectrum.

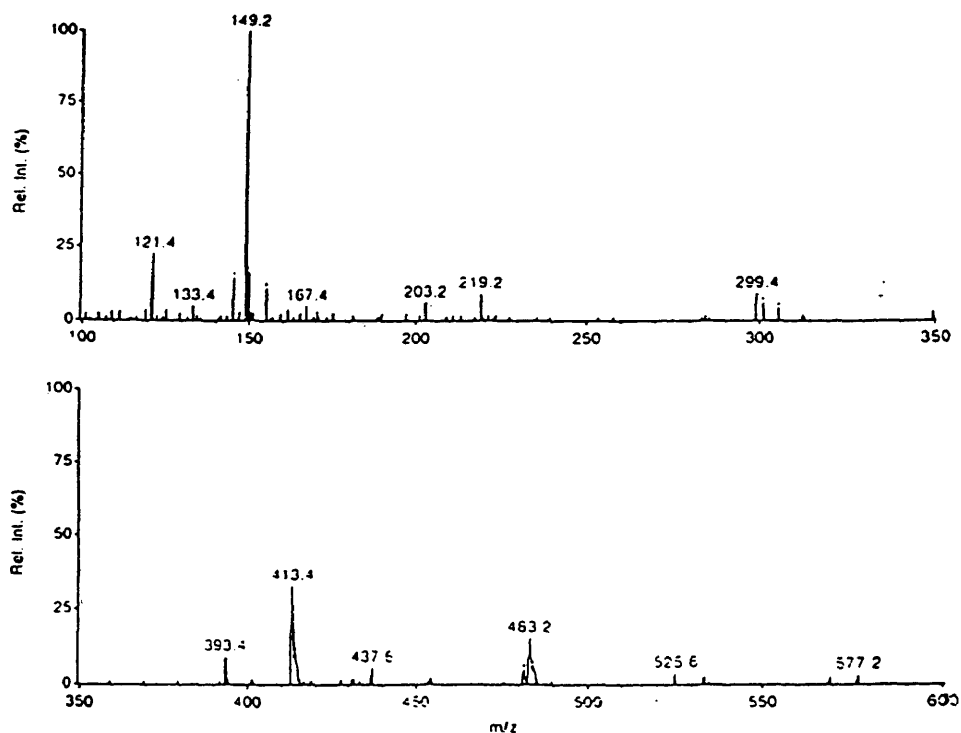
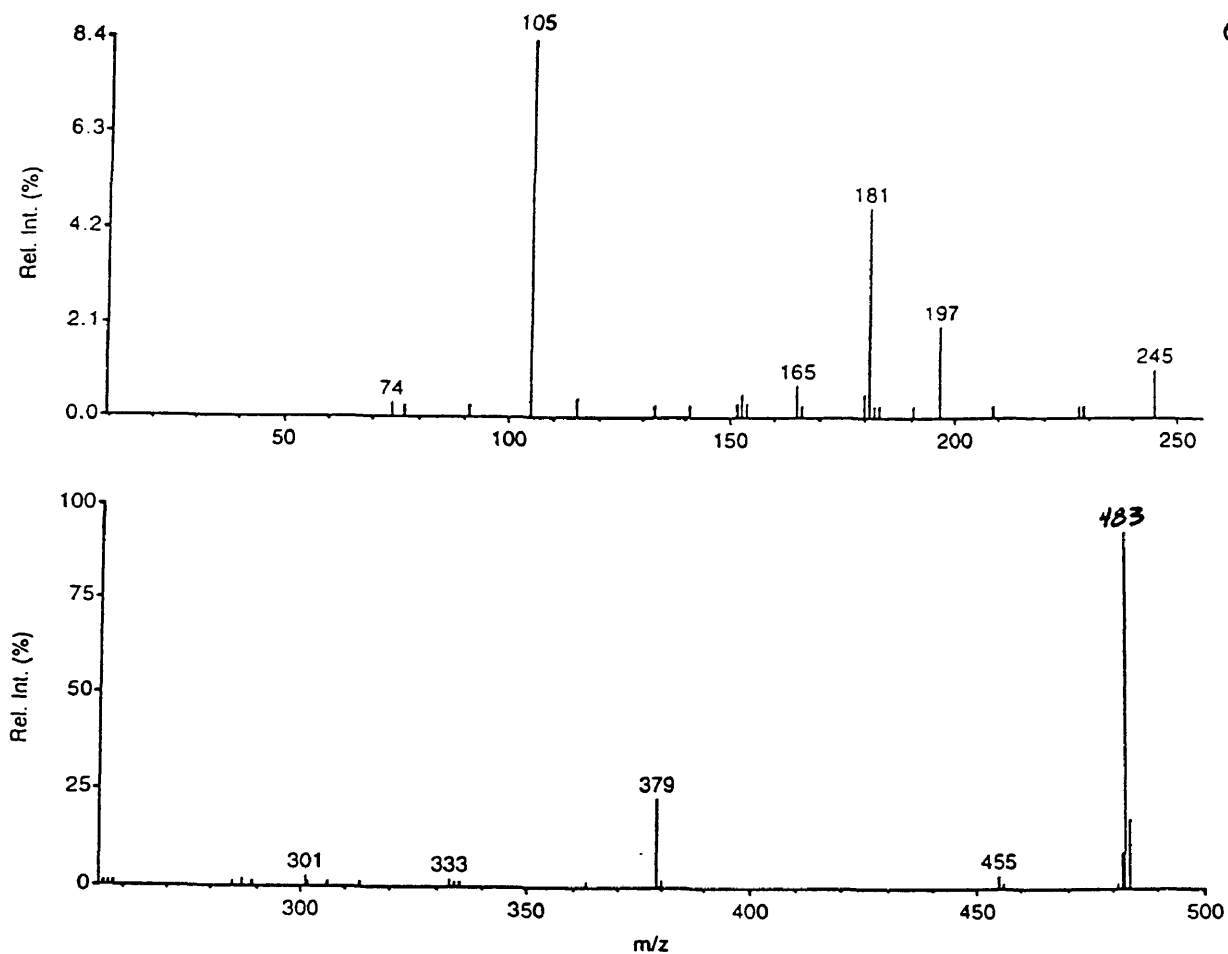


Figure 47. Precursor ion mass spectrum of PAE-MP-A.



**Figure 48.** Product ion mass spectrum of molecular ion peak 483 (PAE-MP-A).

**Table 15.** Unknown and solvent ion peaks from mass spectra of PAE-MP-A.

Solvent	Unknown
149.2	299.4
203.2	525.6
219.2	577.2
393.4	*245
413.4	*165
437.6	*74
*455	
*333	

\*from product ion spectrum

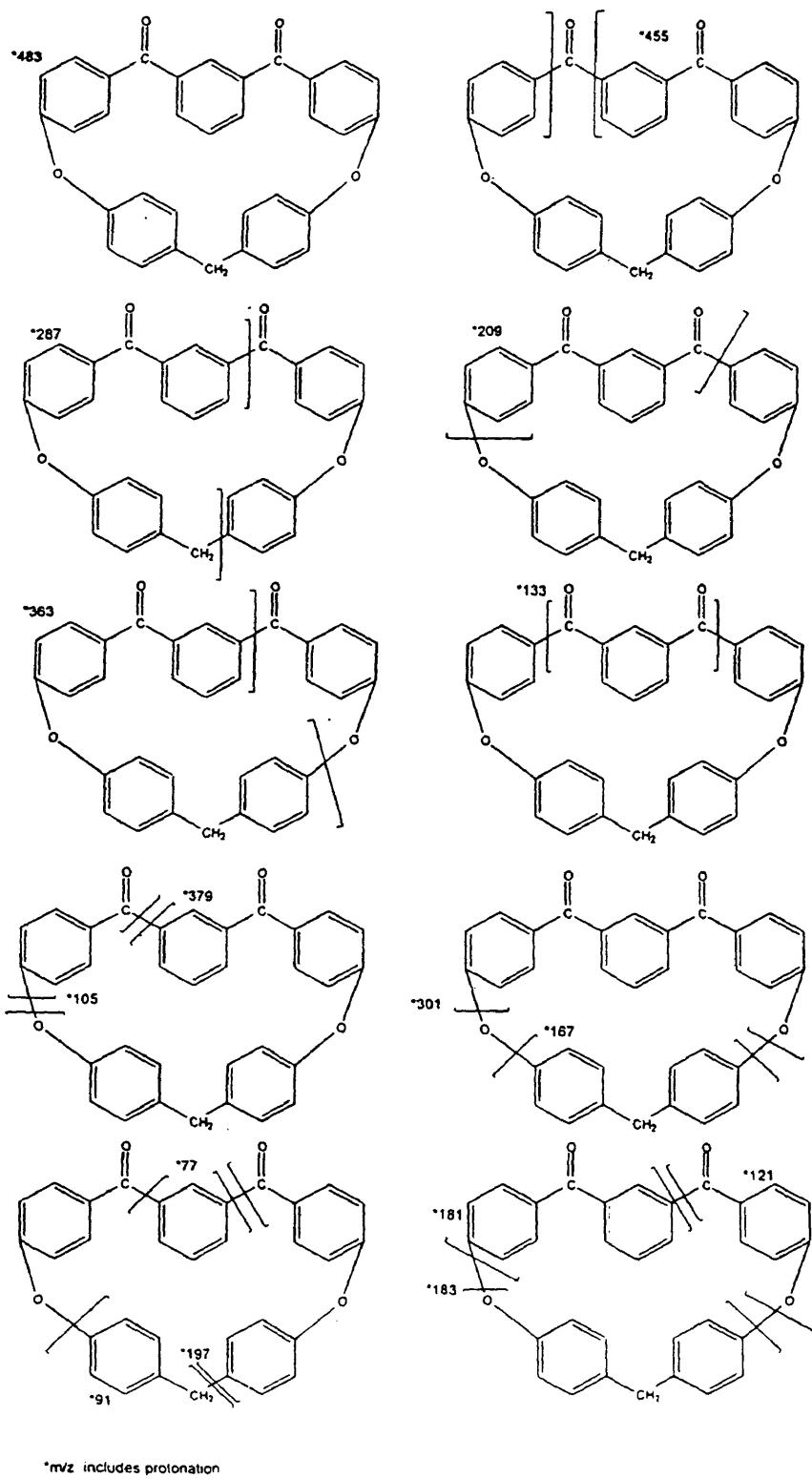


**Figure 49.** Fragments of molecular ion peak 483 (PAE-MP-A).



The precursor ion spectrum of PAE-MP-C (Figure 50) possessed an ion peak at 965, just as in the case of PAE-MM-B. Suspecting that this compound also was a cyclic tetramer, we obtained a product ion spectrum (Figure 51) of the suspected molecular ion peak (shown in Figure 51 as 966). Ion peaks were found that supported the hypothesis (Figure 52). Solvent and unknown ion peaks for these spectra are listed below in Table 16.

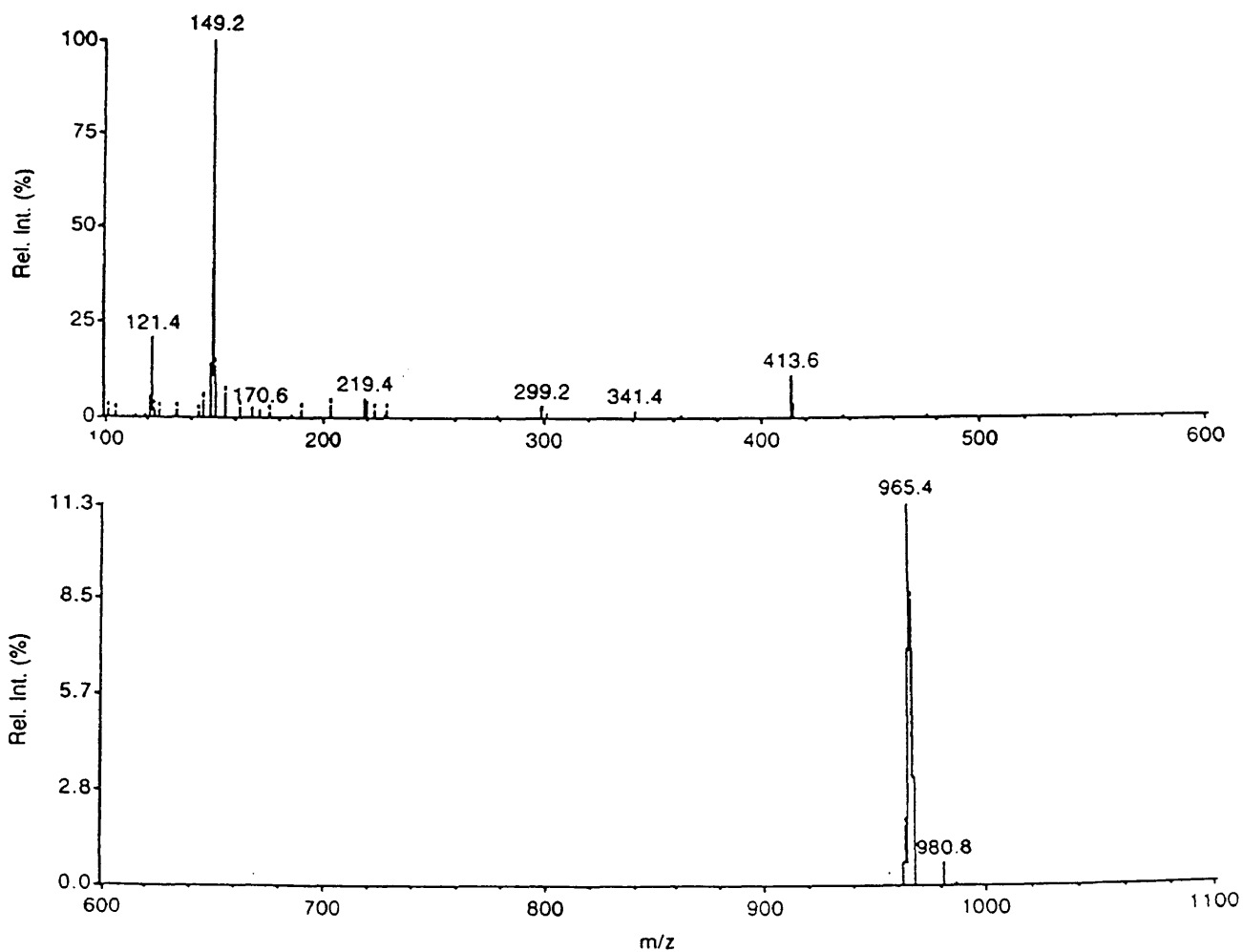


Figure 50. Precursor ion spectrum of PAE-MP-C.

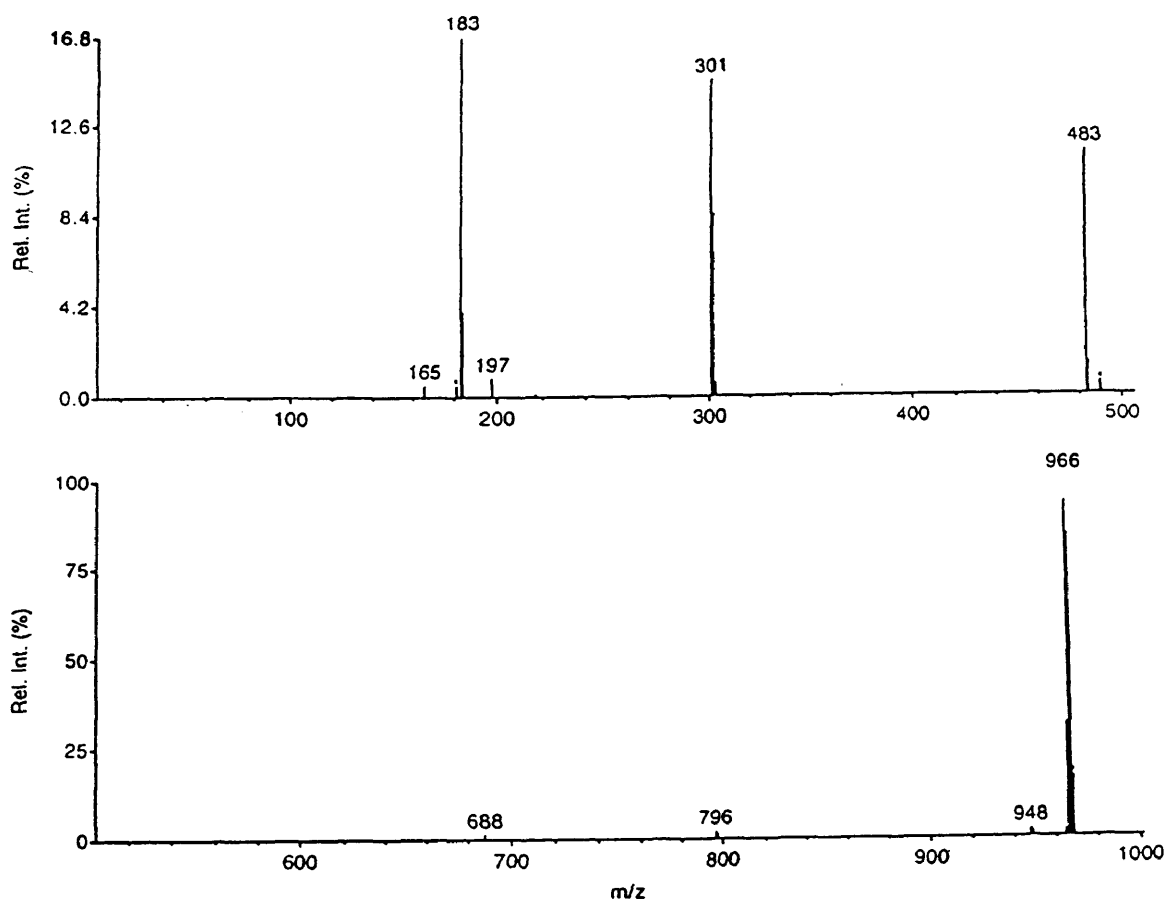


Figure 51. Product ion spectrum of 966 (PAE-MP-C).

Table 16. Unknown and solvent peak ions from mass spectra of PAE-MP-C.

Solvent	Unknown
219.4	170.6
413.6	299.2
	341.4
	980.8
	*165
	*688

\*from product ion spectrum

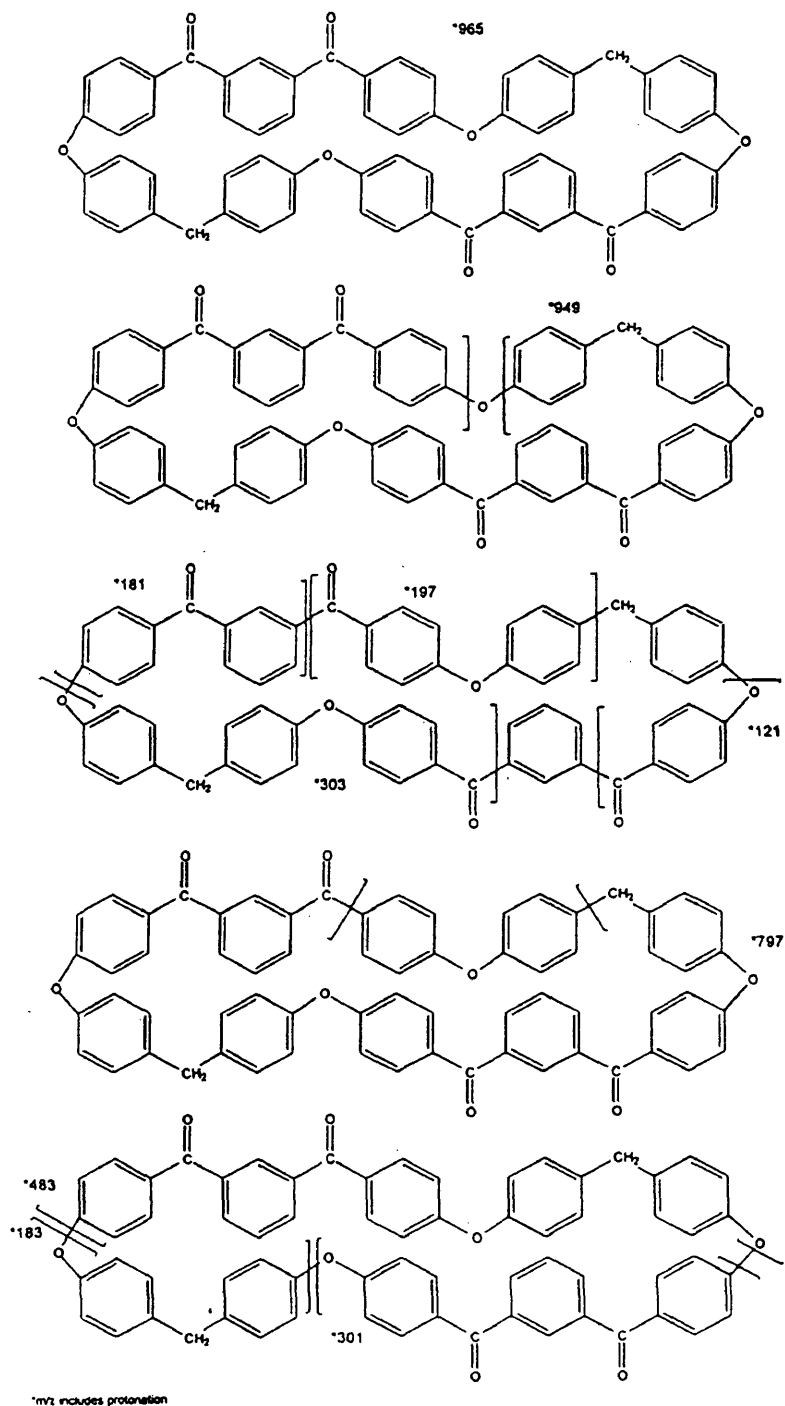
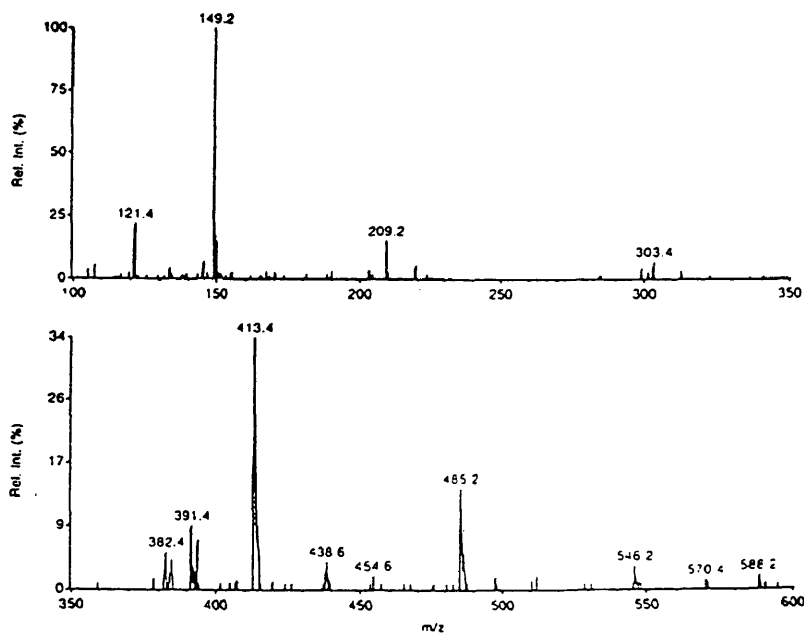


Figure 52. Fragments of molecular ion peak 966 (PAE-MP-C).

*PAE-PM:*

Mass spectra were obtained for PAE-PM-B and PAE-PM-D, but not for E and F. As in the other systems, these two species appear to be the cyclic dimer (B) and cyclic tetramer (D) of their system.

One thing that distinguished PAE-PM-B from the previously suspected dimers was that its probable molecular ion peak was 485 (Figure 53) instead of the usual 483. At this time, this result cannot be explained. Because of this anomaly, product ion spectra of both ion peaks 483 and 485 were taken (Figure 54). These product ion spectra contain many of the same fragments, although (strangely enough) the mass spectrum of 485 contains more fragments expected for the cyclic dimer (Figure 55), while the spectrum of 483 contains more unknown peaks. All the unknown and solvent ion peaks for PAE-PM-B are summarized in Table 17.



**Figure 53.** Precursor ion mass spectrum of PAE-PM-B.

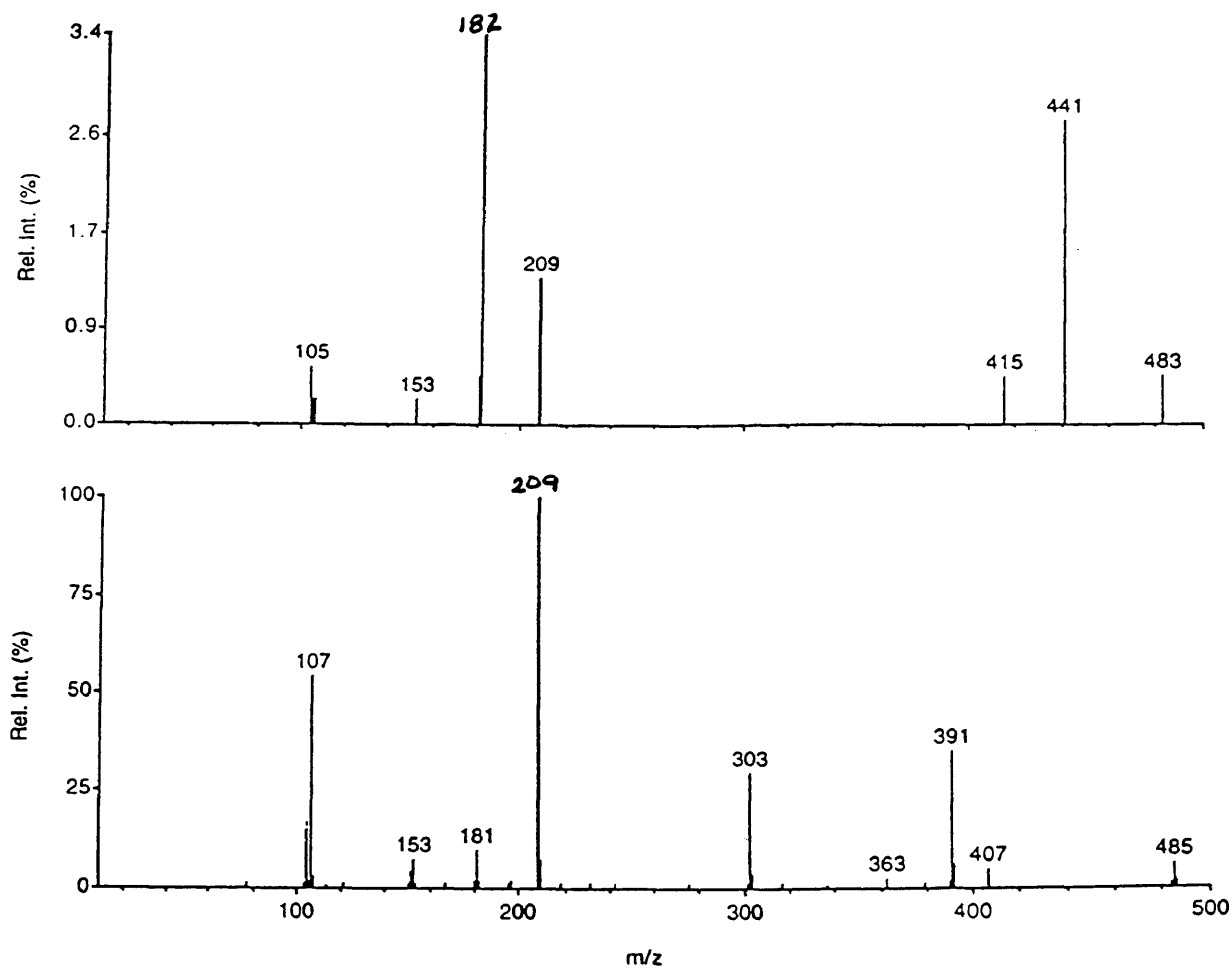


**Figure 54.** Product ion mass spectra of molecular ion peaks 485 and 483 (PAE-PM-B).

**Table 17.** Unknown and solvent ion peaks from the mass spectra of PAE-PM-B.

Solvent	Unknown
149.2	382.4
391.4	438.6
413.4	546.2
454.6	570.4
	588.2
	*153
	*415
	*441

\*from product ion spectrum

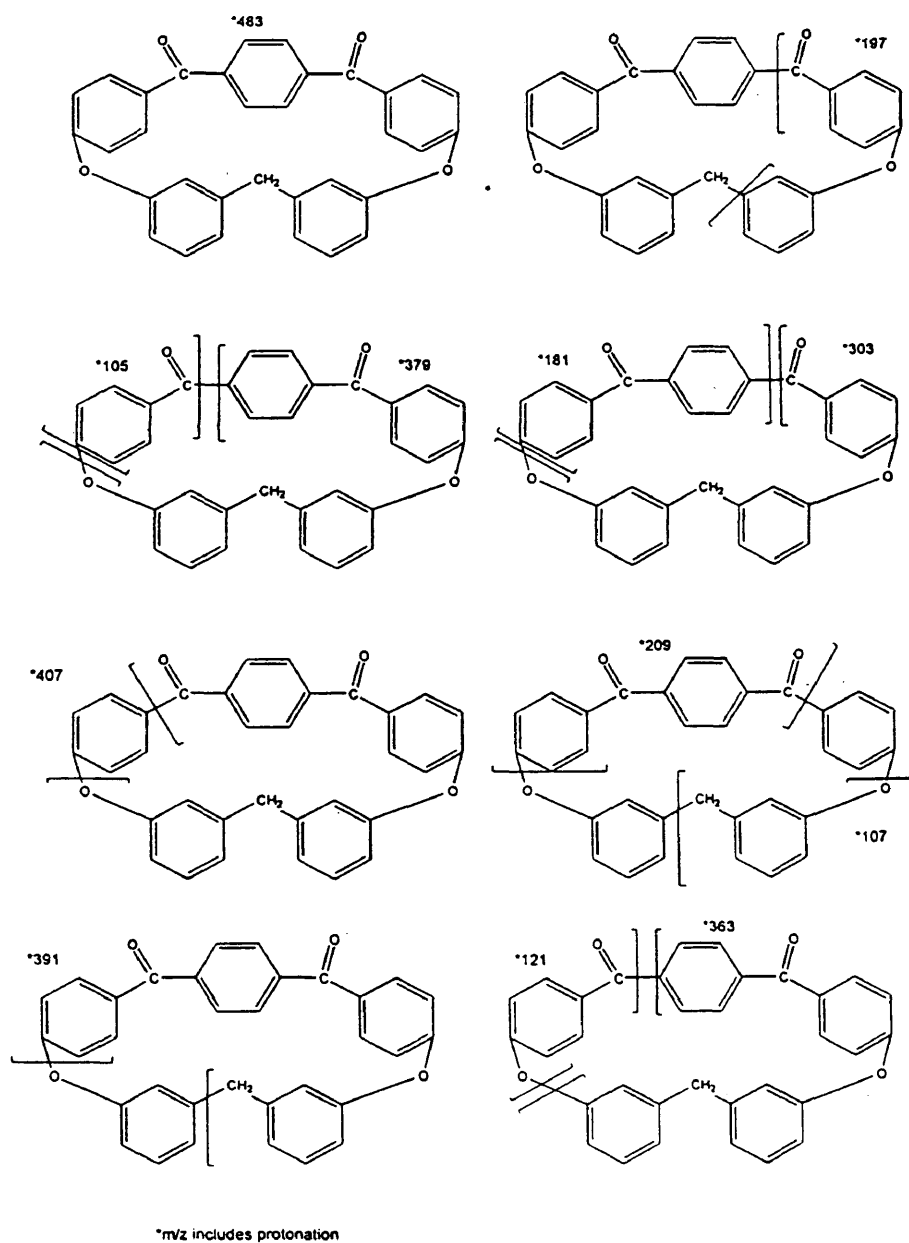


**Figure 55.** Fragments of molecular ion peak 483 and 485 (PAE-PM-B).

The mass spectrum of PAE-PM-D (Figures 56-58; Table 18) seems to indicate that it is a cyclic tetramer. The 965 ion peak is present, and the fragments in its ion product spectrum (some of which are also seen in PAE-MM-B and PAE-MP-C) fit nicely together to form the cyclic tetramer. It should be mentioned again that peak 483, seen in the product ion spectrum (Figure 57), could also be a doubly protonated cyclic tetramer.

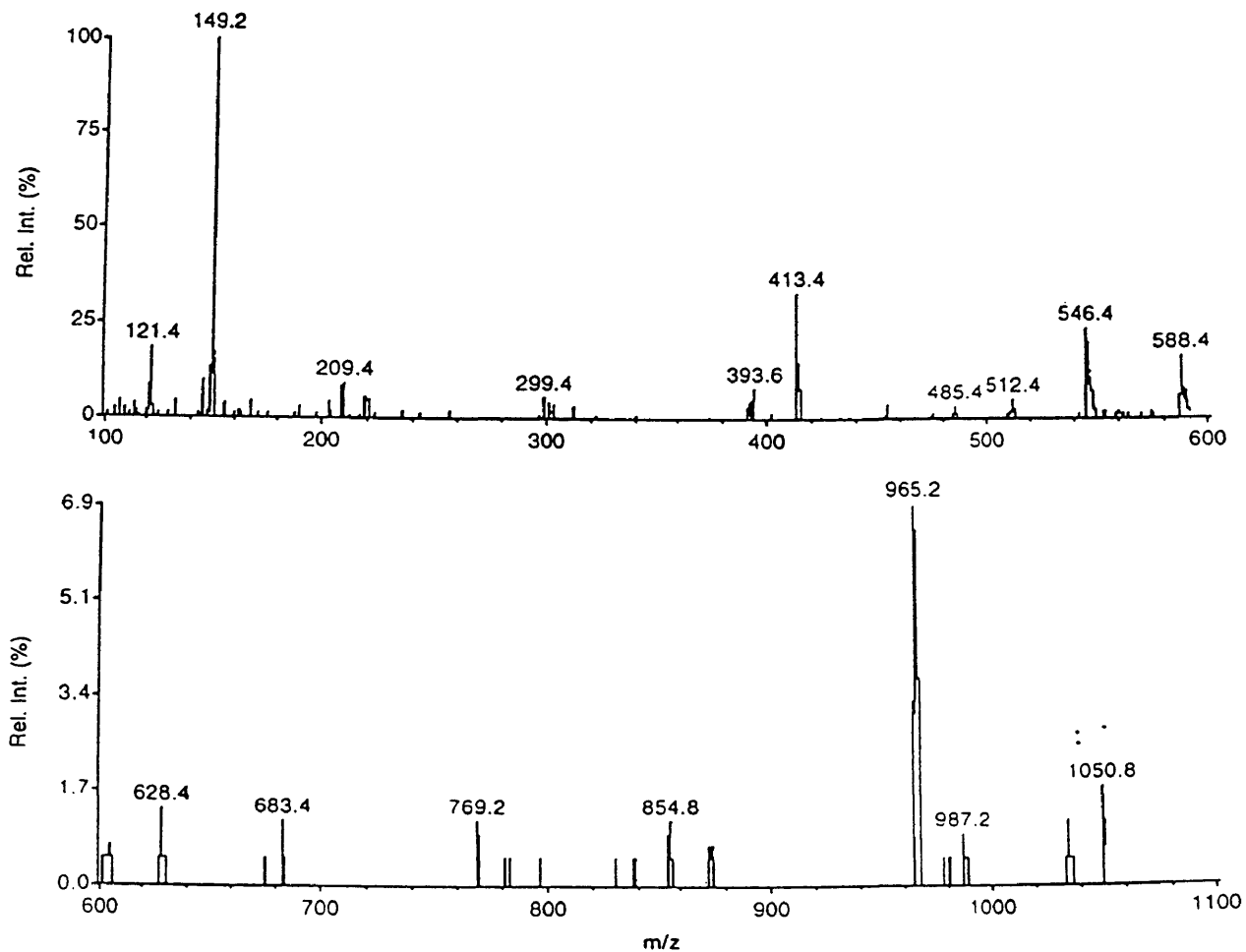


**Figure 56.** Precursor ion mass spectrum of PAE-PM-D.

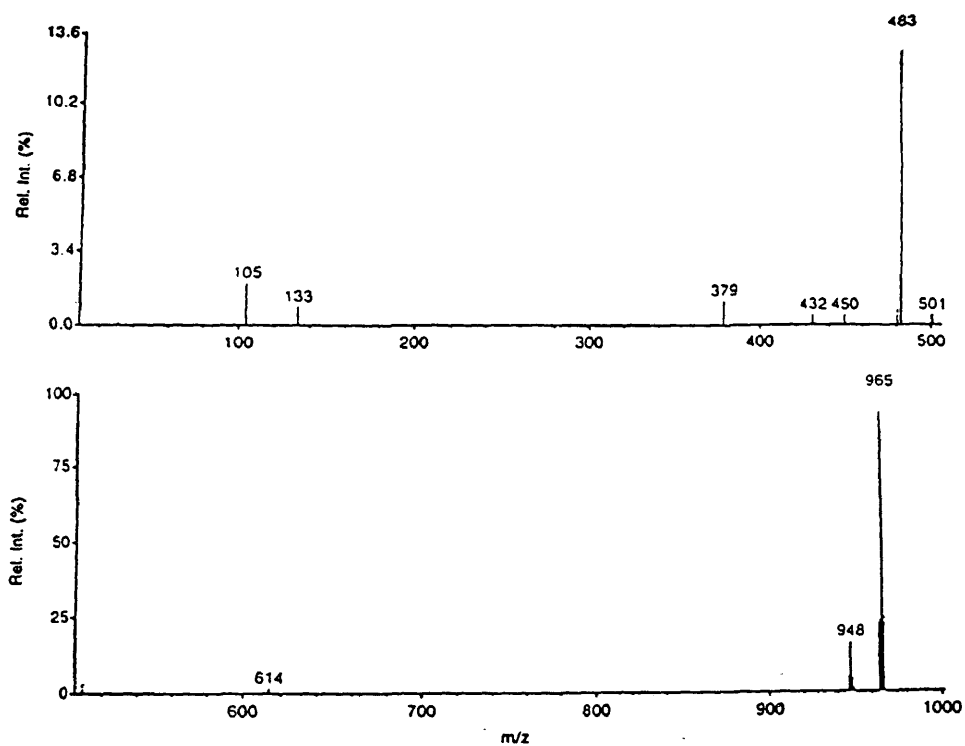


**Figure 57.** Product ion mass spectrum of molecular ion peak 965 (PAE-PM-D)

**Table 18.** Unknown and solvent ion peaks from the mass spectra of PAE-MM-D.

Solvent	Unknown
149.2	299.4
393.6	512.2
413.4	546.4
	588.4
	628.4
	683.4
	854.8
	987.2
	1050.8
	*948
	*614
	*501
	*450
	*432
	*379

\*from product ion spectrum



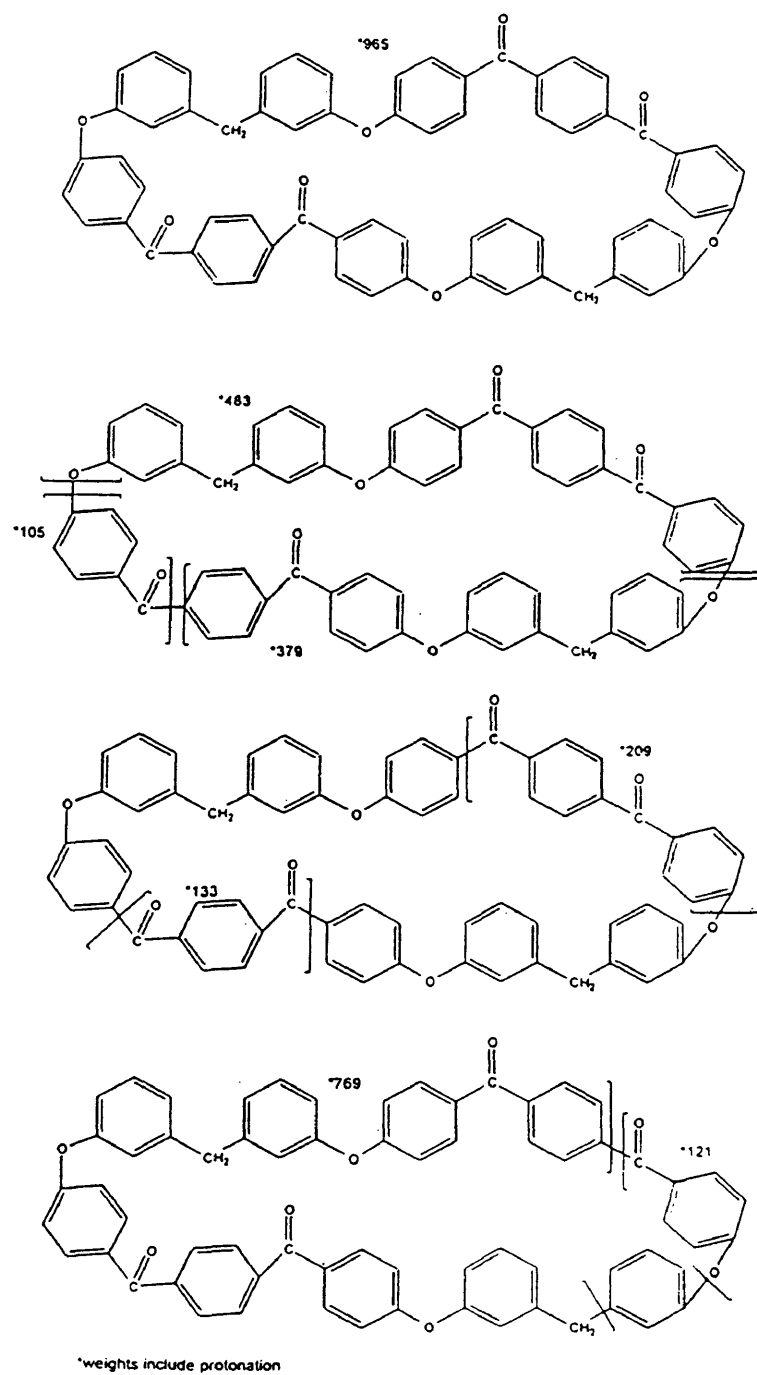


Figure 58. Fragments of molecular ion peak 965 (PAE-PM-D).

**Table 19.** Summary of structures determined by tandem mass spectroscopy.

Cyclic Dimers	Cyclic Tetramers
PAE-MM-A	PAE-MM-B
PAE-MP-A	PAE-MP-C
PAE-PM-B	PAE-PM-D

### **Thin-layer Chromatography**

The data from the mass spectrometer analysis support the hypothesis arising from the analytical GPC work: that there were unknown contaminants, possibly originating from the THF mobile phase, that were mixing together with the PAE samples. As another check, thin-layer chromatography (TLC) was utilized to see if the fractions collected with GPC were pure.

All the fractions for which mass spectra were obtained (the suspected cyclic tetramers and cyclic dimers of PAE-MM, PAE-MP, and PAE-PM) were tested with TLC. When toluene was used as a mobile phase, two components were seen on each plate, except for the PAE-PM cyclic tetramer, which showed a single component. When ethanol was used, again two components were seen in each case, except for the tetramer of PAE-MM, which showed only a single component. Therefore, each species placed on a TLC plate showed two species in at least one case.

Similar results were seen when only THF, both directly from the solvent reservoir and off the column, was examined with TLC. Two components were seen on both occasions when ethanol was used as the mobile phase. The ethanol and toluene were both checked on TLC, and no components were seen upon examination with UV light.

All this evidence suggests that there was at least one impurity forming in the THF reservoir of the GPC apparatus. These impurities seem to form over time and could be one or more different peroxides from THF. The contaminants either remain with the fractions after collection or form again in THF.

## Thermal Analysis

Once mass spectrometry had revealed which species were likely dimers and tetramers, differential scanning calorimetry (DSC) was carried out to determine some of the thermal properties of PAE-MM-A (suspected cyclic dimer) and PAE-MM-B (suspected cyclic tetramer). No other fractionated species were available in a quantity large enough for study. All PAE mixtures also were examined. Melting temperatures were found for each sample analyzed and are summarized at the end of this section in Table 20.

### *PAE-MM:*

We initially ran the PAE-MM mixture (fraction #1) on the DSC instrument from 25°C to 400°C. The results (Figure 59) were quite interesting. First, a large, broad peak was observed that began at about 50°C and ended just short of 100°C. This peak

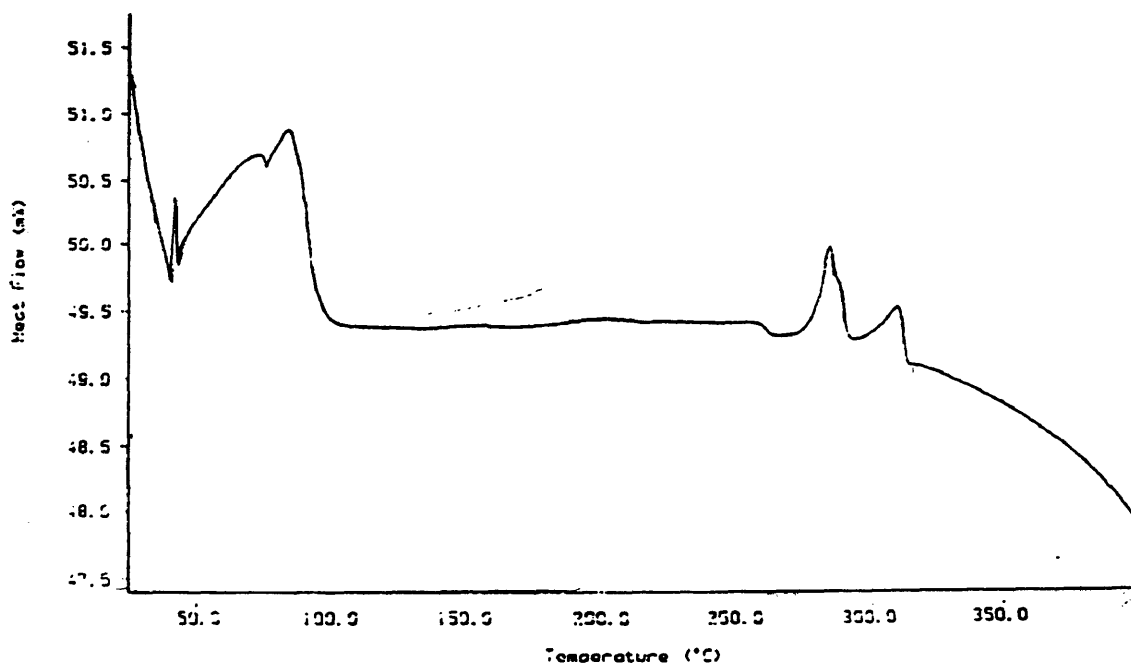


Figure 59. DSC run of PAE-MM.

occurred at a temperature that seemed to be too low to be caused by a first order transition such as melting. Its form also did not suggest a glass transition temperature. Rather, this large, low-temperature peak appeared to be caused by evaporation of solvent still trapped in the PAE-MM mixture. The sample was then oven-dried *in vacuo* overnight at about 170°C, since the highest-boiling solvent to which it had been exposed was DMAc (b.p. 164.5-166°C). This dried sample was run on the DSC. The large peak was still visible although perhaps diminished slightly in magnitude. To test further the hypothesis that this peak was the result of solvent loss, a TGA run (Figure 60) was performed on a portion of PAE-MM by using the same rate of heating and overall temperature range used with the DSC run.

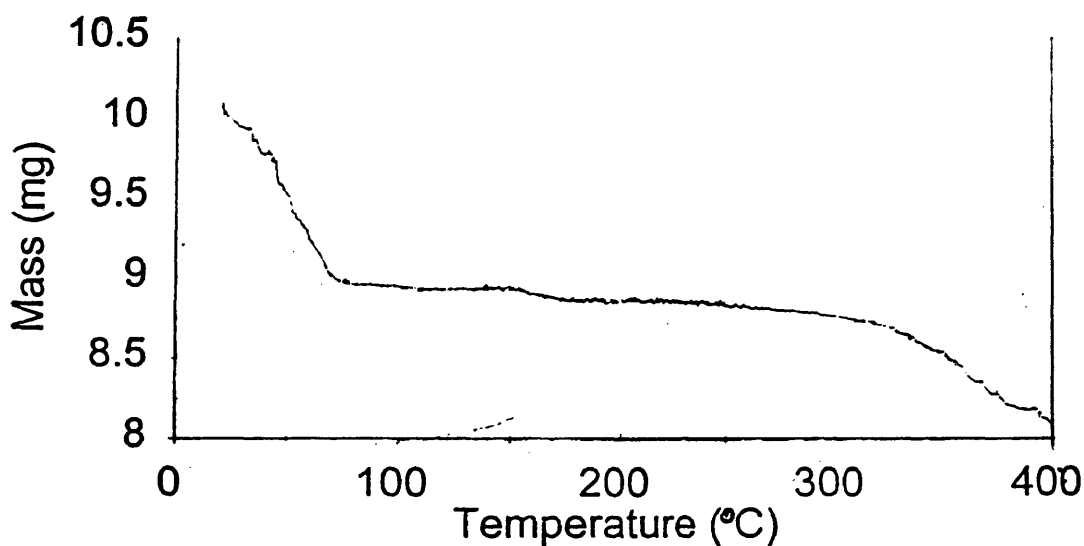


Figure 60. TGA of PAE-MM; heated to 400°C.

Weight loss was found in the TGA data at the same temperatures (1) where the large peak of the DSC trace occurred and (2) where degradation was thought to take

place (about 320°C). Thus it did indeed seem that the large peak corresponded to the loss of solvent. The main questions at this point were what was the solvent and why did it remain with the sample despite thorough vacuum drying. In an attempt to answer these questions, another portion of PAE-MM was dried in an oven overnight at 125°C. This sample was allowed to cool (enough so that it could be easily handled), then examined in the TGA apparatus up to 125°C and held there for twenty minutes. Mass loss still was observed, and the mass stabilized at about 70°C just as before.

With these results, we hypothesized that the PAE-MM was picking up water as soon as it was exposed to the atmosphere. To test this hypothesis, another portion of PAE-MM (with no extra drying) was heated in the TGA furnace up to 125°C and again held there for twenty minutes (Figure 61). This run went no different from the other. As soon

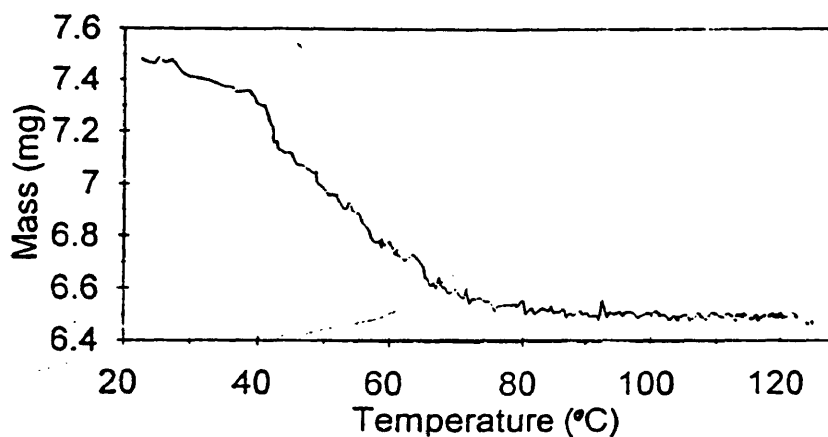
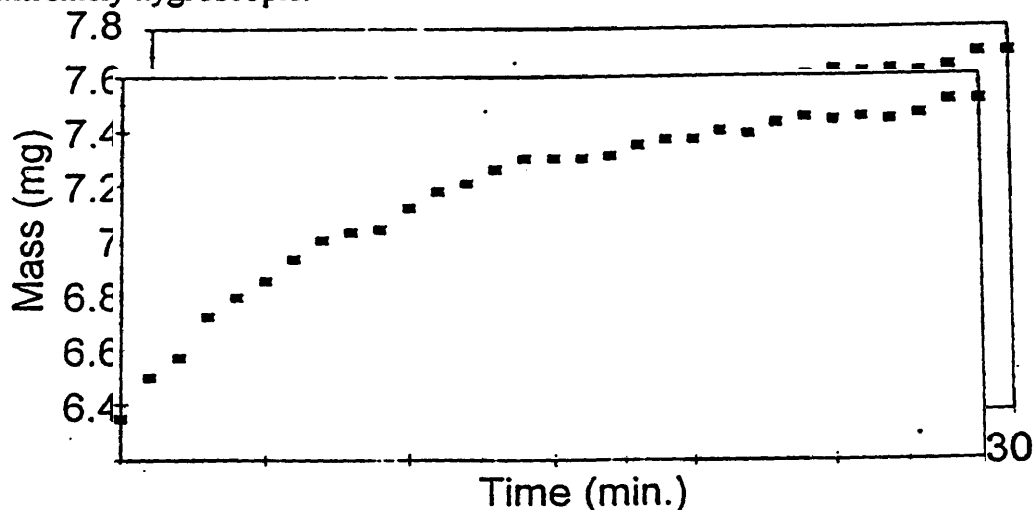


Figure 61. TGA run of PAE-MM; held at 125°C

as the furnace had cooled to room temperature, the mass of the sample was examined over time. As long as the sample was in the furnace and in the presence of dry air, no change in

mass was observed. As soon as the furnace was removed and the sample was held at a temperature range of 19-21°C, the mass of the sample (still in a powdery form) increased to a value slightly higher (Figure 62) than the mass before it was heated. This weight gain was accomplished very quickly: within thirty minutes. It appears that PAE-MM is

extremely hygroscopic.



**Figure 62.** PAE-MM weight gain during exposure to the atmosphere; after heating.

In addition to this first peak, there were two other peaks (apparently first-order transitions) in the DSC run of Figure 59, which were thought to represent melting temperatures. These two lay close to one another (285 and 311°C). It seemed very strange that such a mixture might have two distinct melting points lying so close together. Usually, one expects a simple or binary mixture to begin to melt at the eutectic temperature of the mixture. On further heating, the component in excess continues to melt until no more solid remains. This does not seem to happen with PAE-MM.

Next, a new sample of PAE-MM was subjected to another heat scan (up to 320°C), allowed to cool and then heated again (Figure 63). The first scan was similar to

Figure 59. A small, broad peak (again probably solvent) was seen this time near 170°C. The cooling scan showed no transitions. A second heating displayed similar, but very faint, peaks. It would seem that, in the course of heating solid PAE-MM, some regions of the mixture go from one crystalline structure to another before liquefying. These transitions are not evident on the second heat scan. During cooling, PAE-MM probably does not have time to rearrange itself and reform the original crystalline regions before being supercooled into an amorphous solid.

Examining PAE-MM under a microscope revealed that the mixture turned glassy near 120°C. Two distinct regions, one lighter and clearer than the other, became visible at higher temperatures. No distinct (DSC) transitions were seen at 285 or 311°C.

In an attempt to shed further light on these phase transitions, we did DSC runs of PAE-MM-A and PAE-MM-B (Figures 64 and 65). The PAE-MM-A had a sharp melting transition at about 329°C, and PAE-MM-B had one at 290°C. We have not been able to find any reports of the PAE-MM cyclic dimer and tetramer in the chemical literature and, accordingly, are unable to compare these melting points with previous determinations. These values are similar to the two peaks found for the PAE-MM mixture, but it would be difficult to say for sure whether the two sets of values are identical. Melting enthalpies ( $\Delta H$ ) also were found for PAE-MM-A and PAE-MM-B and are listed at the end of this section in Table 20.



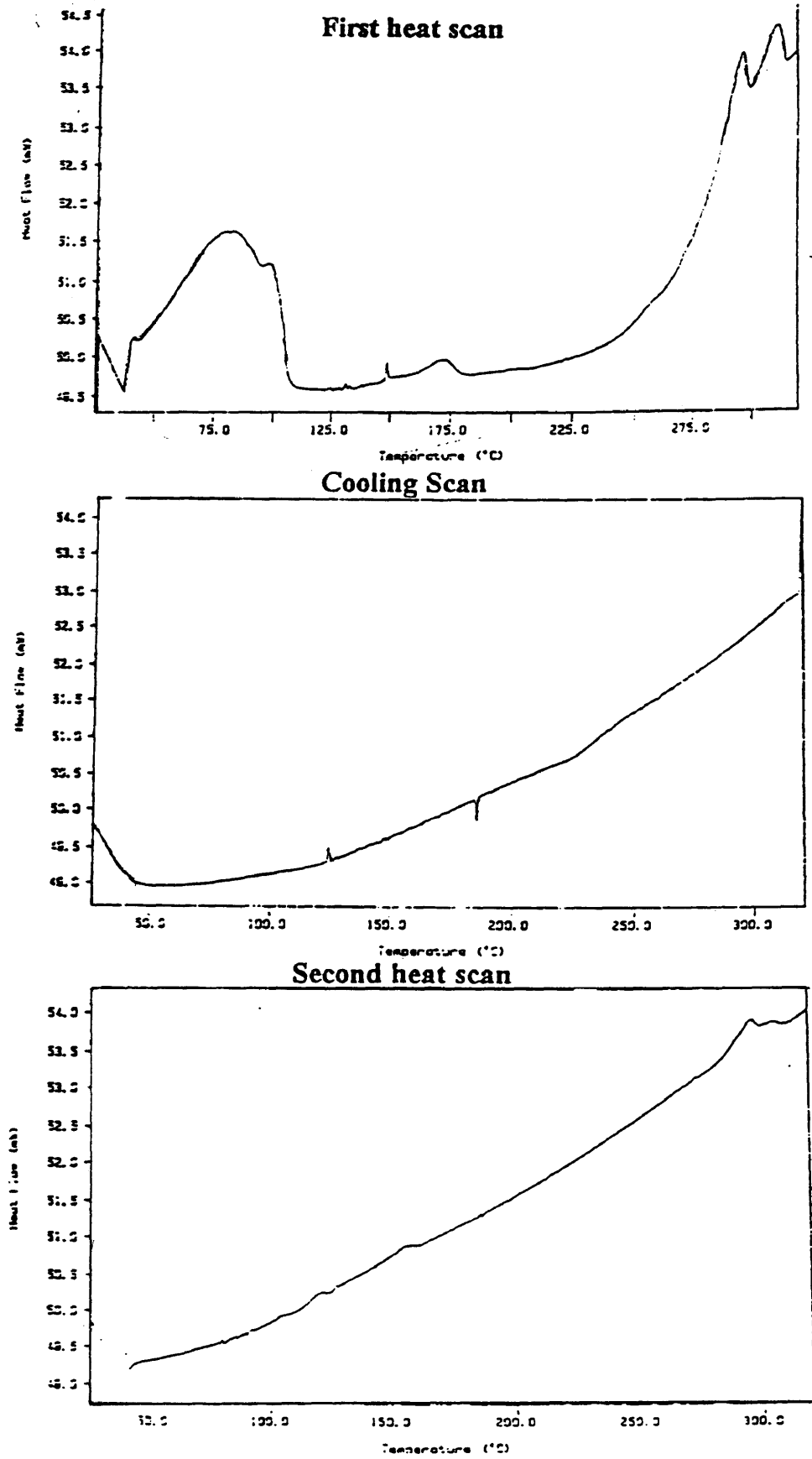


Figure 63. Two DSC heat scans and middle cooling scan of PAE-MM.

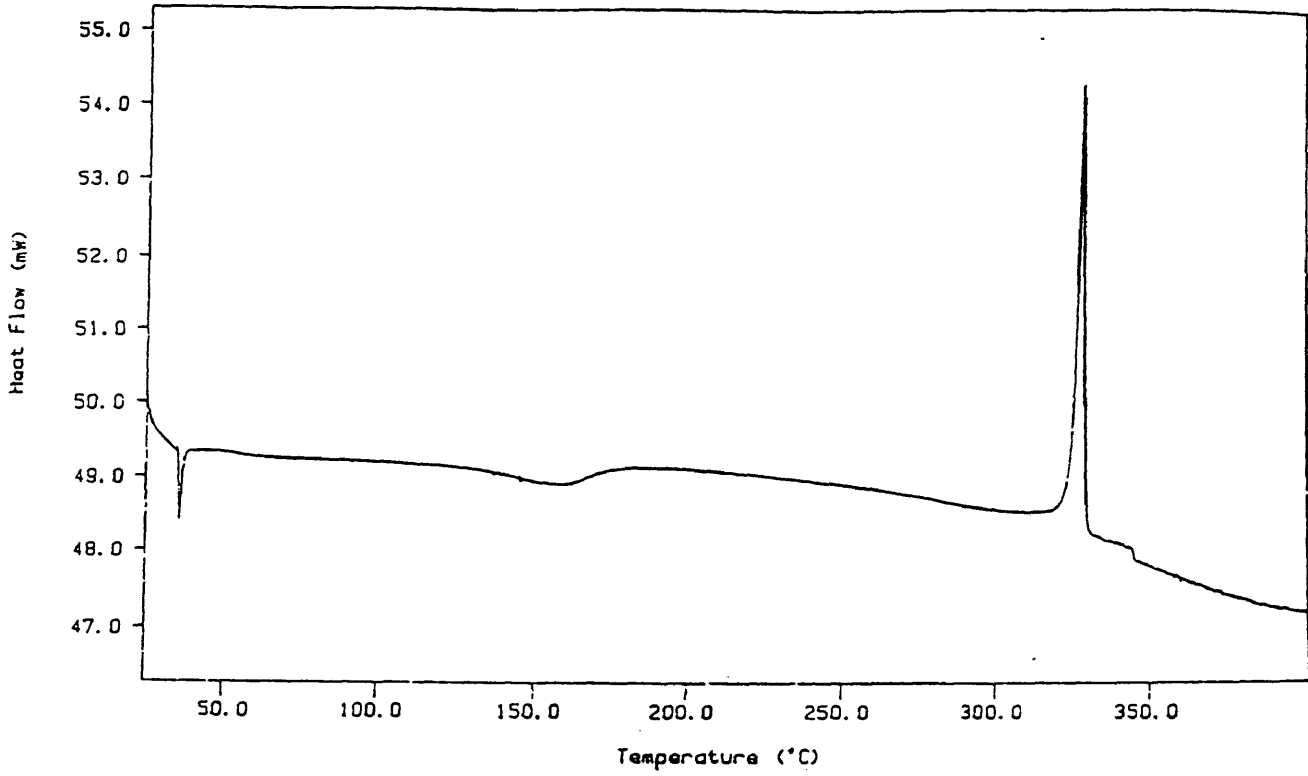


Figure 64. DSC run of PAE-MM-A

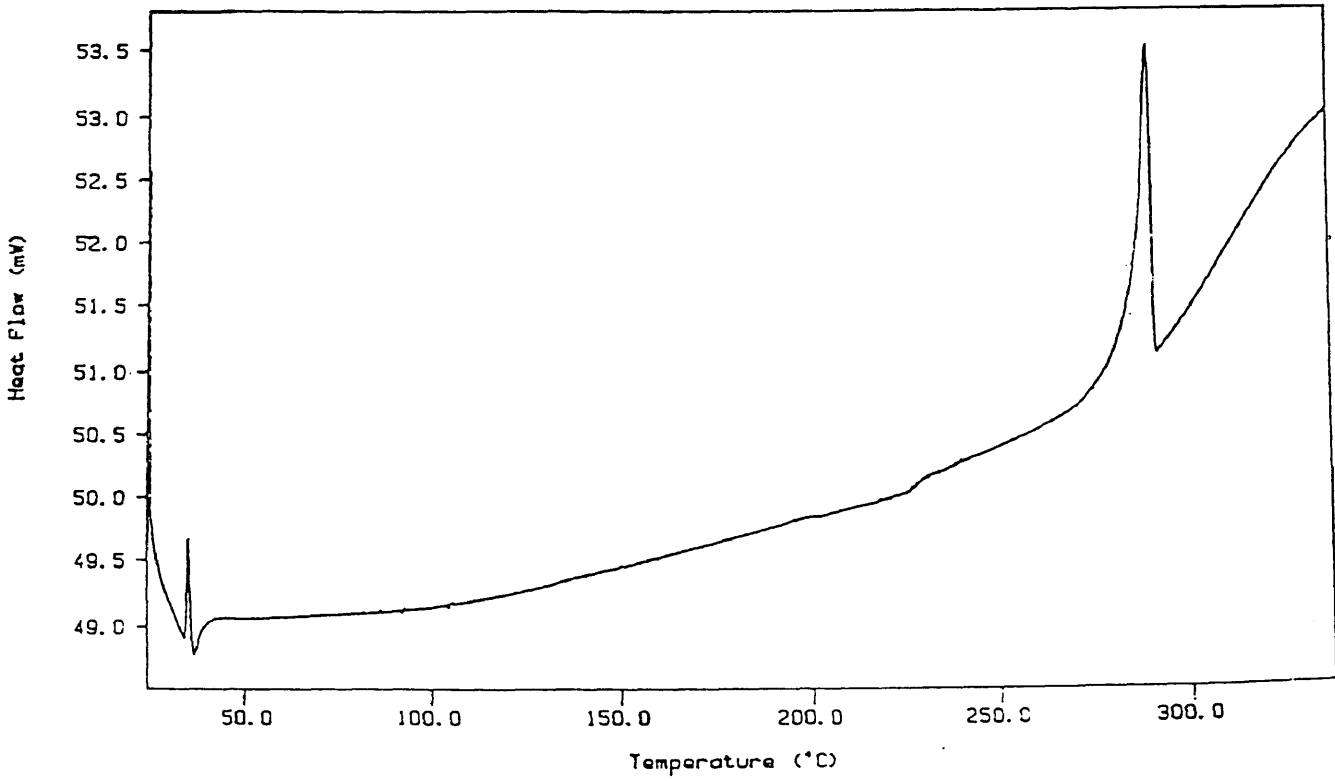


Figure 65. DSC run of PAE-MM-B.

*PAE-PM:*

The unfractionated PAE-PM mixture was run on the DSC instrument (Figure 66) just as PAE-MM had been studied. The only exception was that the maximum temperature was only 350°C for PAE-PM. The maximum temperature, was reduced because previous runs had shown that only degradation probably would occur after this point. As with PAE-MM, a large, broad peak was seen at low temperatures and this peak did not disappear with heating of the sample under vacuum. Also evident was a peak, believed to correspond to the melting temperature, at about 282°C. This peak was broader than the ones obtained earlier for PAE-MM-A and PAE-MM-B, as would be expected for the mixture of species in PAE-PM.

Microscopy of this sample did not reveal a distinct transition at 282°C, however. The sample turned glassy near 80°C and soon separated into two regions much as PAE-MM had done. At around 170°C the sample began to bubble (probably the release of trapped solvent). Periods of sample flow also were evident at this temperature and beyond.

Besides these two peaks, there were several smaller, broad peaks at intermediate temperatures. We hypothesized that these also belonged to solvent, possibly DMAc that was trapped within the sample. A TGA analysis (Figure 67) was done to test this hypothesis. This time the sample was heated up to 300°C (just above the melting temperature). The results were not very definitive. Loss of mass was seen until about 125°C (probably corresponding to the large peak - loss of water) at which point some

stability in mass occurred. However, loss of mass began again at about 175°C and continued through the end of the TGA run. It is possible that in this last stage more solvent was lost.

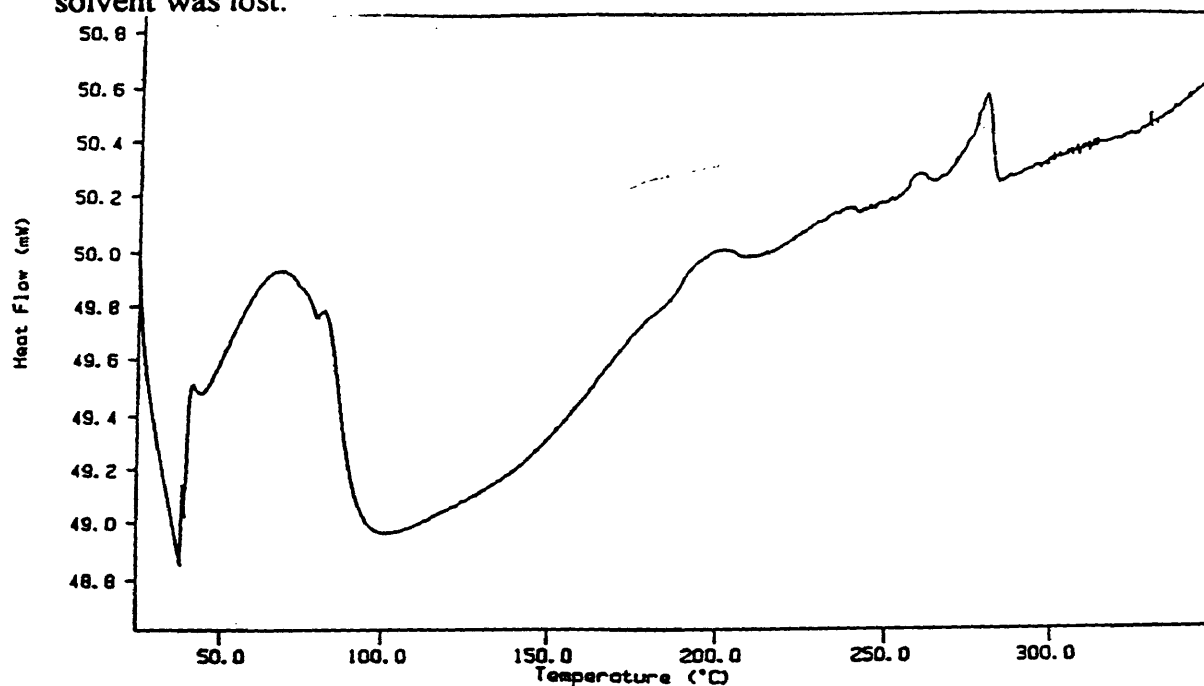


Figure 66. DSC run of PAE-PM.

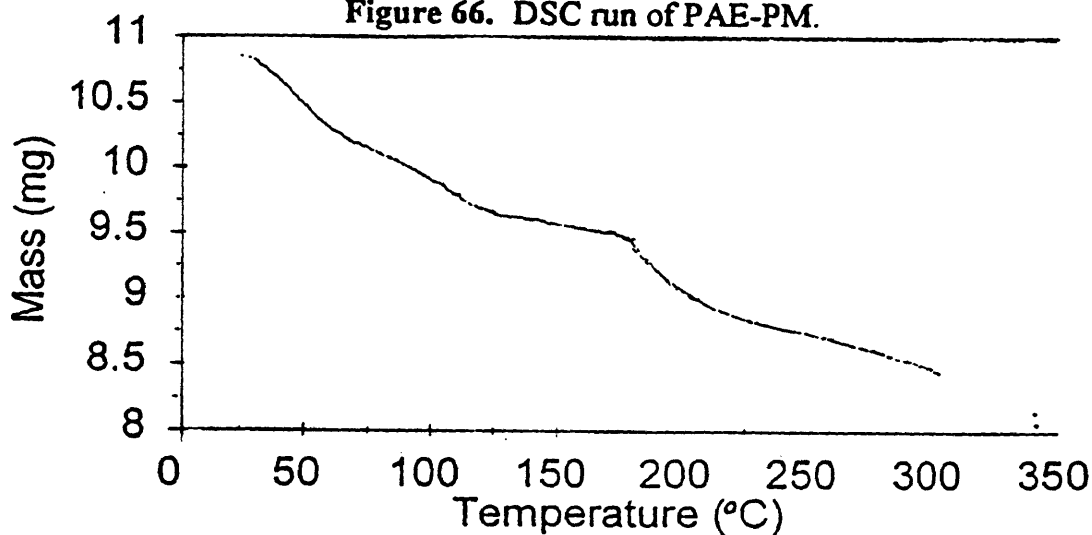


Figure 67. TGA of PAE-PM; heated to 300°C.

A portion of PAE-PM was then examined with the TGA instrument while heating the sample up to 225°C (just after the second stage of weight loss begins). This run

(Figure 68) was very similar to the first TGA run (Figure 67). After this run ended, the sample had the opportunity to cool for thirty minutes outside of the furnace. The sample looked very glassy. A little mass was gained by the sample during this exposure to the atmosphere but not nearly as much as in the case of PAE-MM. The same sample was studied a second time with the TGA while heating again to 225°C (Figure 69). There was again the same initial mass loss. However, during this second run, the mass stabilized at 150°C. Apparently, all solvent was driven off with this second heating.

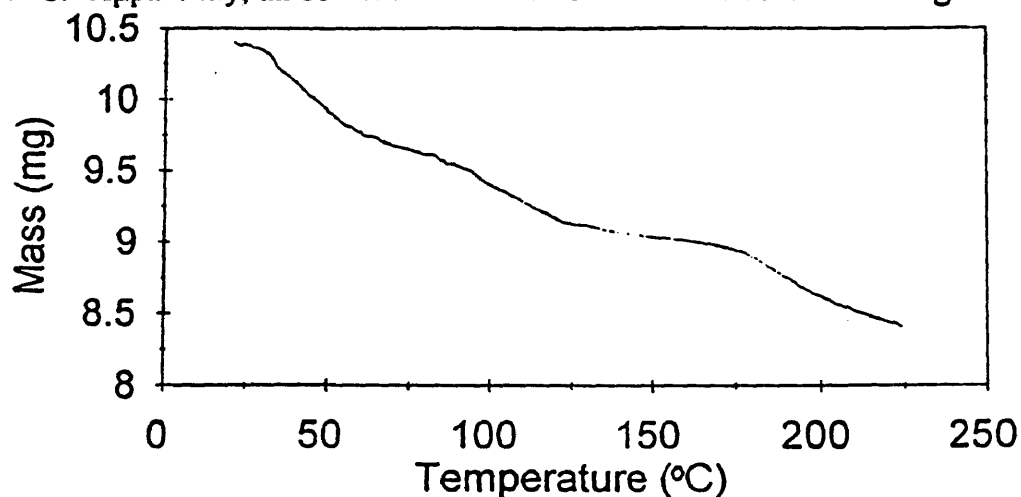


Figure 68. TGA run of PAE-PM; first heating to 225°C.

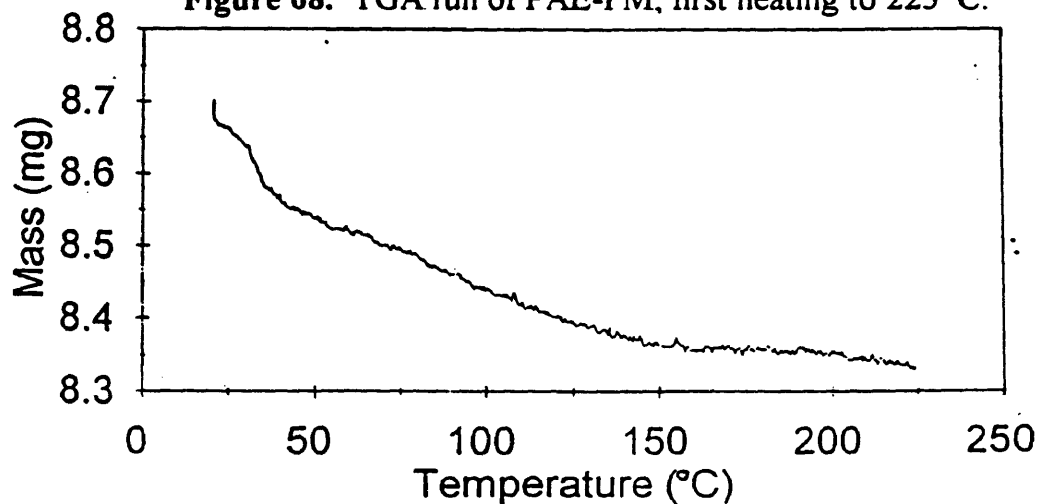
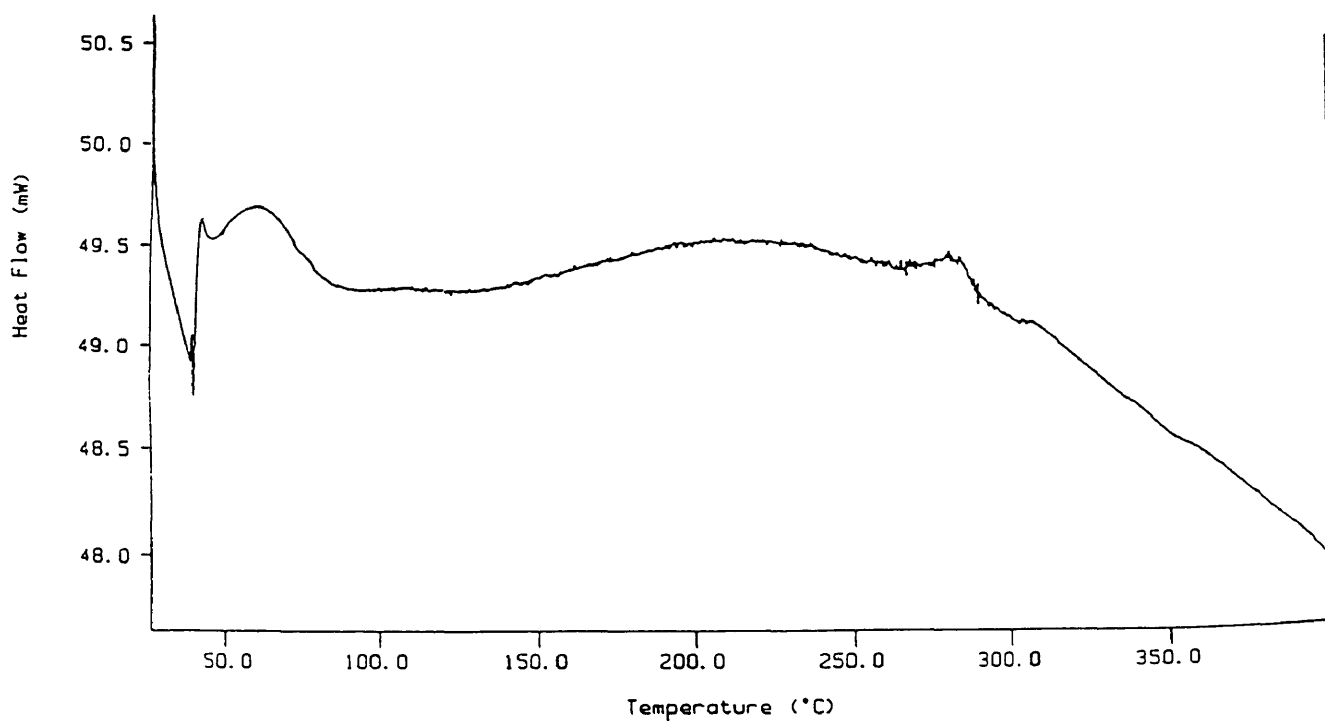


Figure 69. TGA run of PAE-PM; second heating to 225°C.

It seems at least possible then that the smaller, broad peaks found in the DSC of PAE-PM also corresponded to evaporation of solvent. Additional evidence for residual solvent was the clumpy appearance of the sample, despite drying as instructed by Hergenrother *et al.*<sup>1</sup> This sample did not appear to be as hygroscopic as PAE-MM.

*PAE-MP:*

The DSC run of PAE-MP (Figure 70) was also difficult to interpret. The same large, broad peak below 80°C seen in PAE-MM and PAE-PM also was seen with PAE-MP. A faint peak also was seen at 281°C. We believed this peak, though not sharp, to represent melting. In addition, an extremely broad peak was found beginning at 150°C



**Figure 70.** DSC run of PAE-MP.

and ending at about 300°C. This region overlapped the melting peak and made this transition less pronounced. Both of the wide peaks observed were again thought to be caused by the release of trapped solvent.

This compound looked very similar to PAE-PM under the microscope and had two distinct regions. The PAE-MP sample turned glassy earlier (about 55°C). The sample flowed at temperatures exceeding 130°C. Again, no distinct transition was noted at the suspected melting temperature.

A sample of PAE-MP was observed with TGA up to 350°C (past the onset of degradation) in an attempt to explain the broad, middle peak of the DSC scan. The TGA data (Figure 71) looked very similar to those found for PAE-PM (Figure 67). However, these data did not seem to correlate well with the DSC run. Initial mass loss was seen until 150°C, where the second broad peak DSC region begins. However, steady weight loss occurred again at around 200°C (around the peak of the very broad DSC range) and continued through the end of the TGA run. Weight loss occurred during the range of the suspected melting temperature.

Next, another sample of PAE-MP was examined by TGA with two heating runs up to 225°C and cooling in between. This sample showed almost constant weight loss during the first run (Figure 72) with very little of the stability seen before in Figure 71. With cooling and exposure, this sample, appearing glassy as PAE-PM did, gained back very little weight. The second run to 225°C (Figure 73) also showed steady weight loss during the entire run except for a slight pause between 75 and 100°C. These data are difficult to

explain. It seems odd that there would be this much solvent still remaining after two such runs.

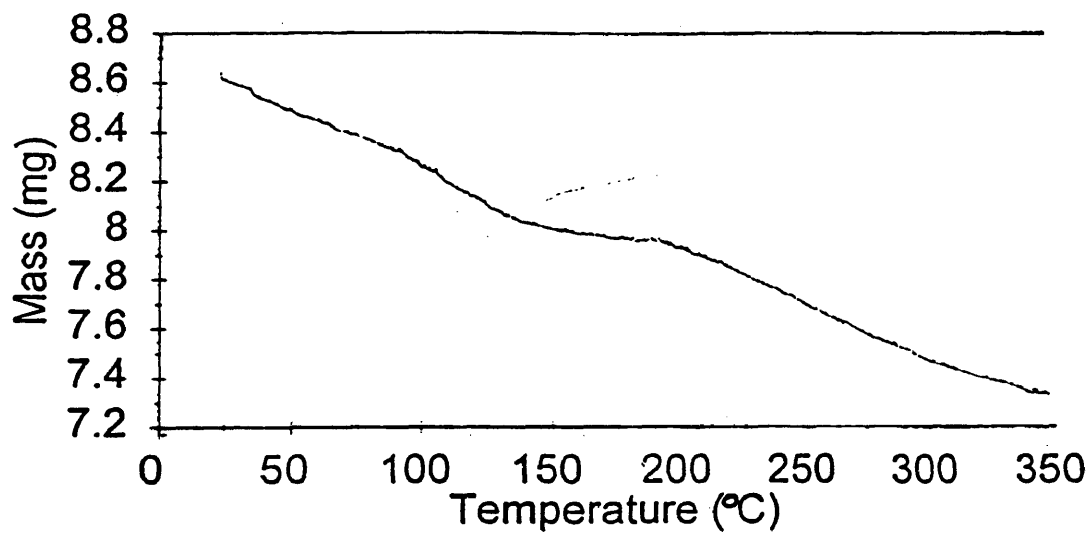


Figure 71. TGA of PAE-MP; heated to 350°C.

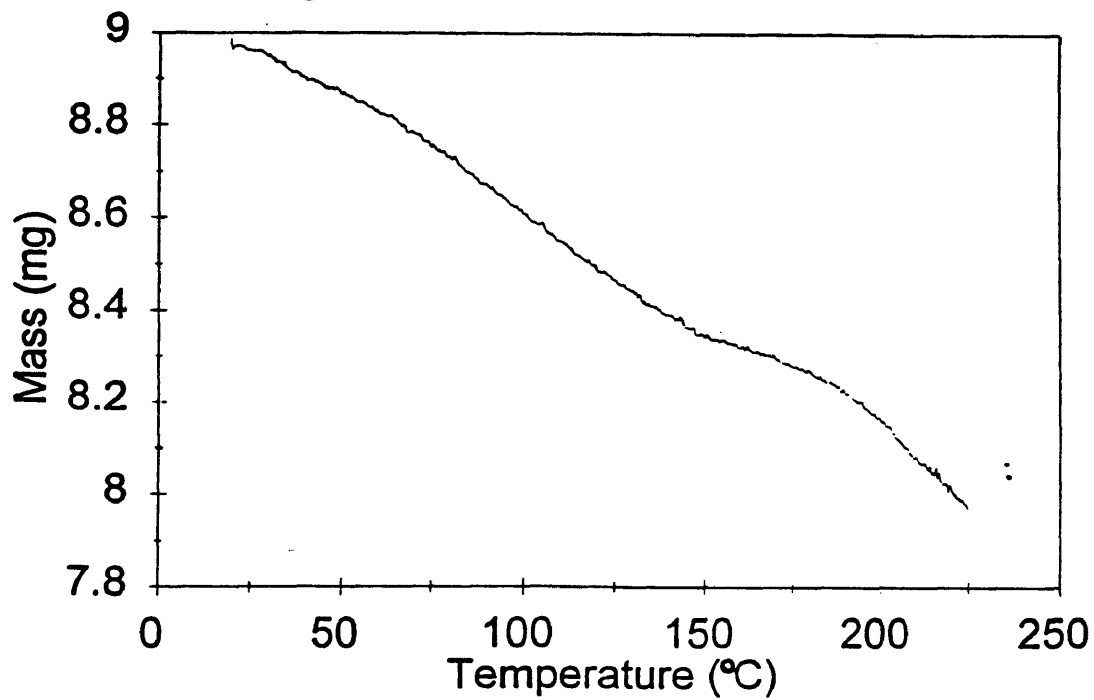
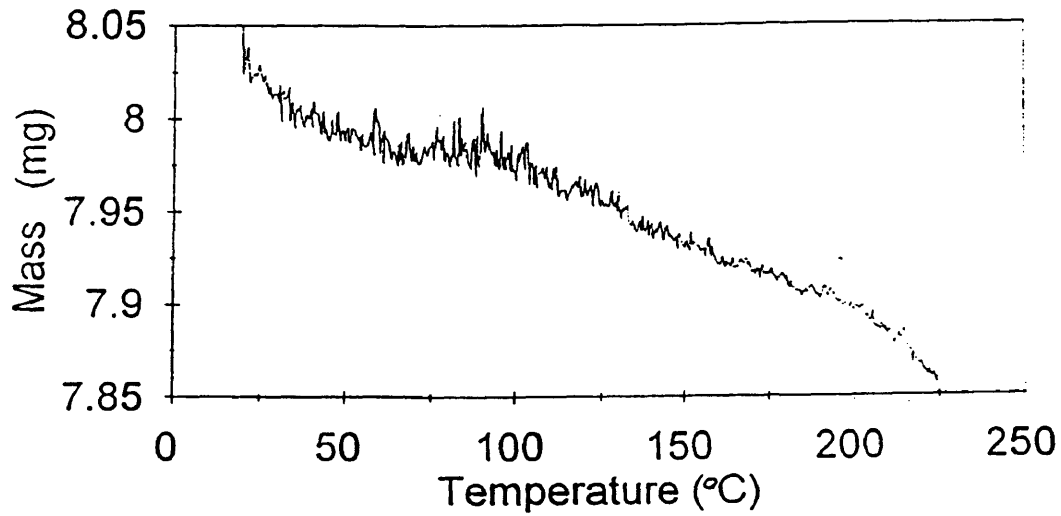


Figure 72. TGA of PAE-MP; first heating to 225°C.





**Figure 73.** TGA of PAE-MP; second heating to 225°C.

Yet another sample of PAE-MP was placed in the TGA (Figure 74) and held at 225°C. This time the compound was held at the temperature for one hour. Significant weight loss did finally seem to end after this length of time. Again it does seem possible that the major peaks in the DSC run (Figure 70) are caused by release of solvent.

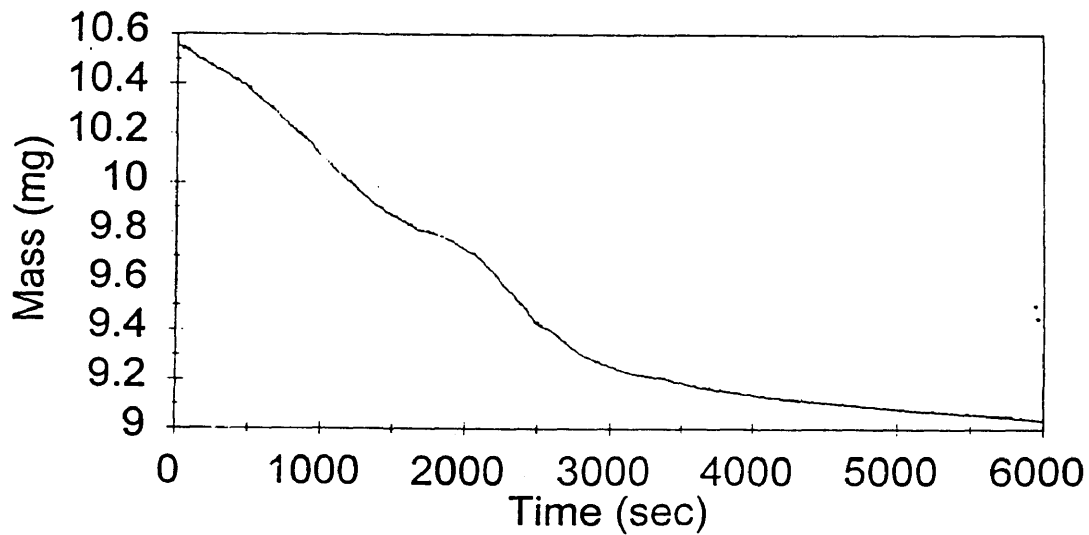


**Figure 74.** TGA of PAE-MP; held at 225°C for one hour.

*PAE-PP:*

The DSC run of this system was not complicated (Figure 75). Only one sharp transition was seen at 283 °C. This peak is thought to correspond to a melting temperature. Under the microscope, the sample turned a darker orange-brown at this temperature. Changes in texture also were observed. The sample went from granular in appearance to a very compressed solid edged with parallel lines. It does appear that some portion of the mixture is melting at 283 °C.

To further examine this transition, two heating cycles (to 320 °C) with a cooling cycle in between were done on the DSC (Figure 76). Strangely enough, on the first heat scan, another transition (never seen in previous DSC runs of PAE-PP) was seen at 312 °C. This is in the same region as the second transition peak found in PAE-MM. Perhaps the PAE-PP mixture is heterogeneous and this particular run had another component. During the cooling and second heat scan, no transitions were observed. This suggests (as in the case of PAE-MM) that the crystalline structure in existence before 283 °C does not have time to reform before it is supercooled into a more amorphous solid.

No broad “solvent” peaks were seen on the DSC. Examination of this sample with TGA (Figure 77) demonstrated that this mixture loses very little mass when heated to 125 °C and held there for half an hour. Apparently, this one isomeric system is not as hygroscopic as the others.

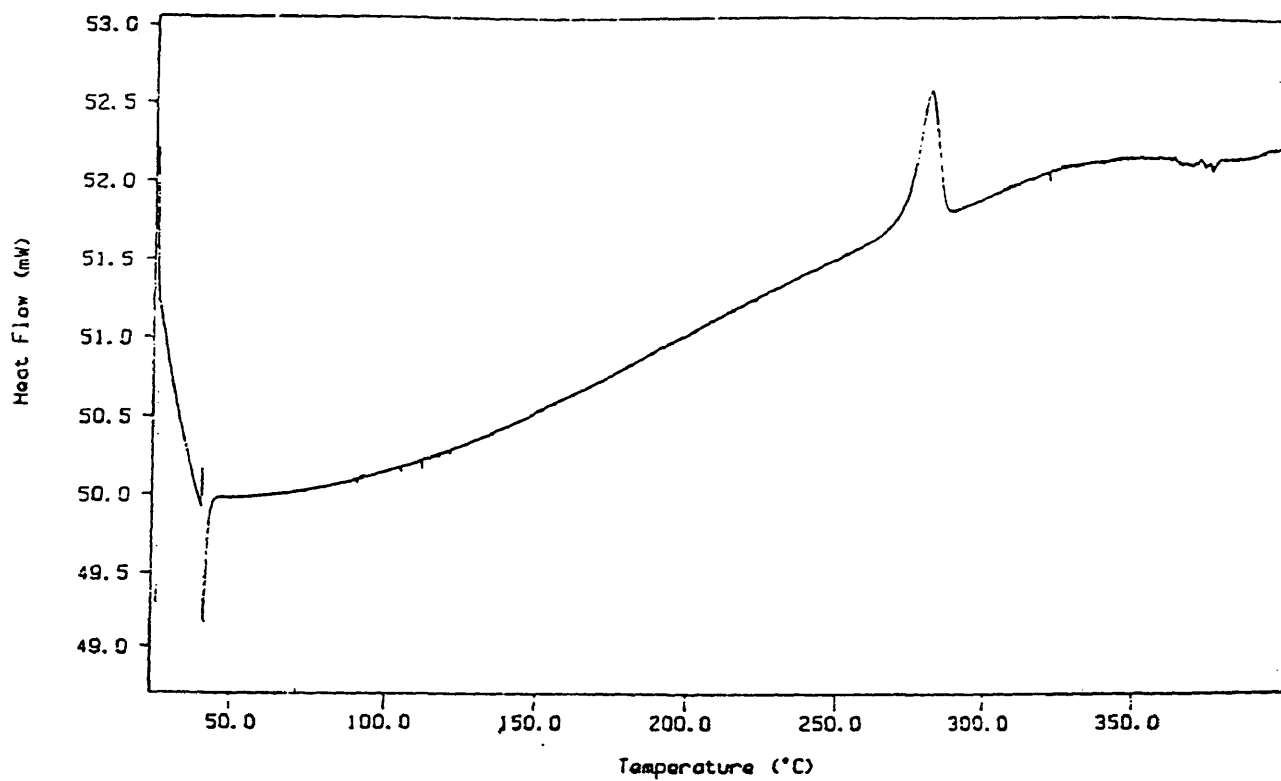
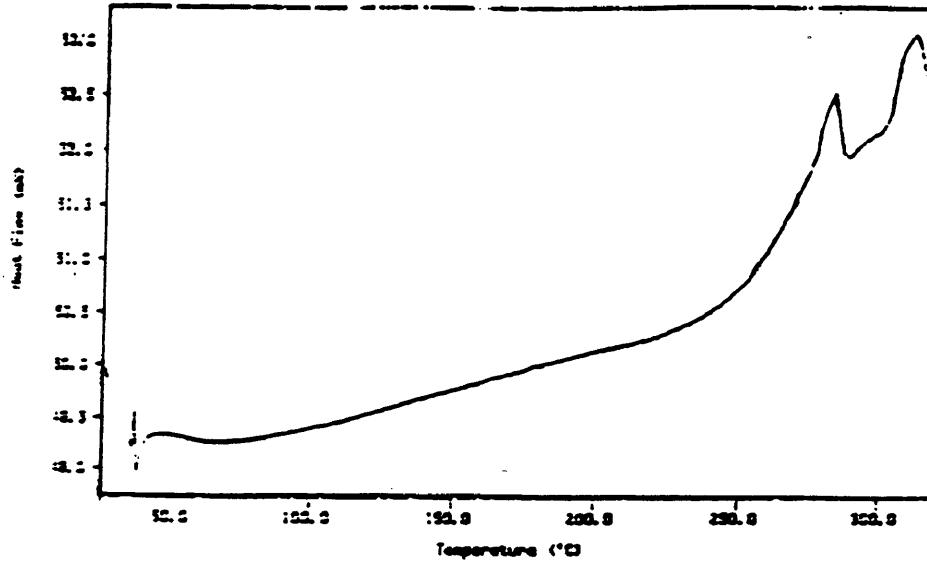
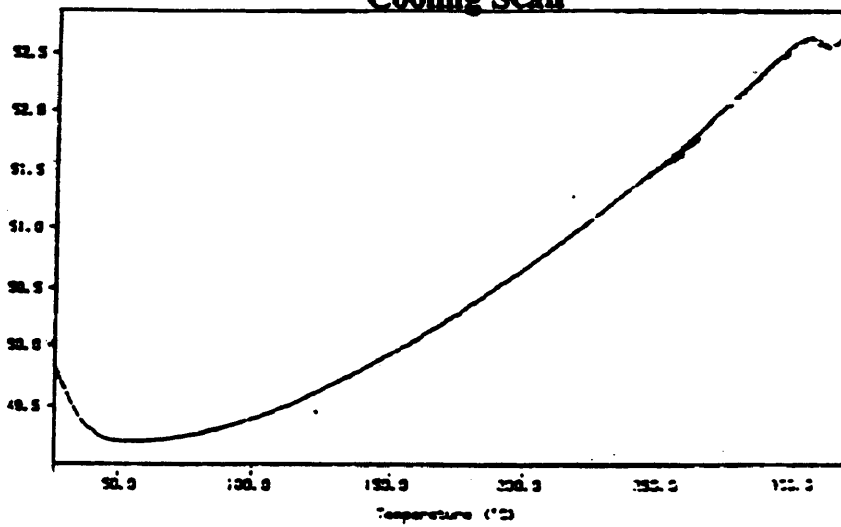


Figure 75. DSC of PAE-PP.

**First heat scan**



**Cooling Scan**



**Second heat scan.**

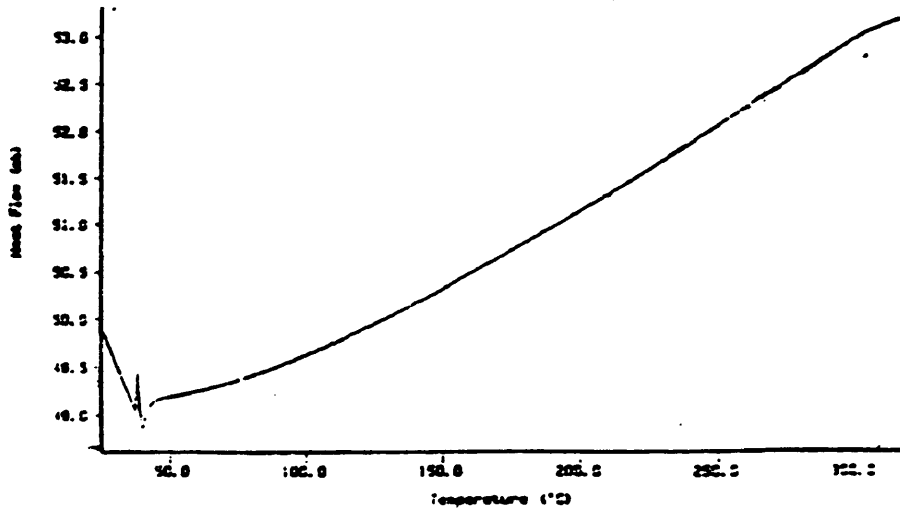


**Figure 76. Two DSC heat scans and middle cooling scan of PAE-PP.**

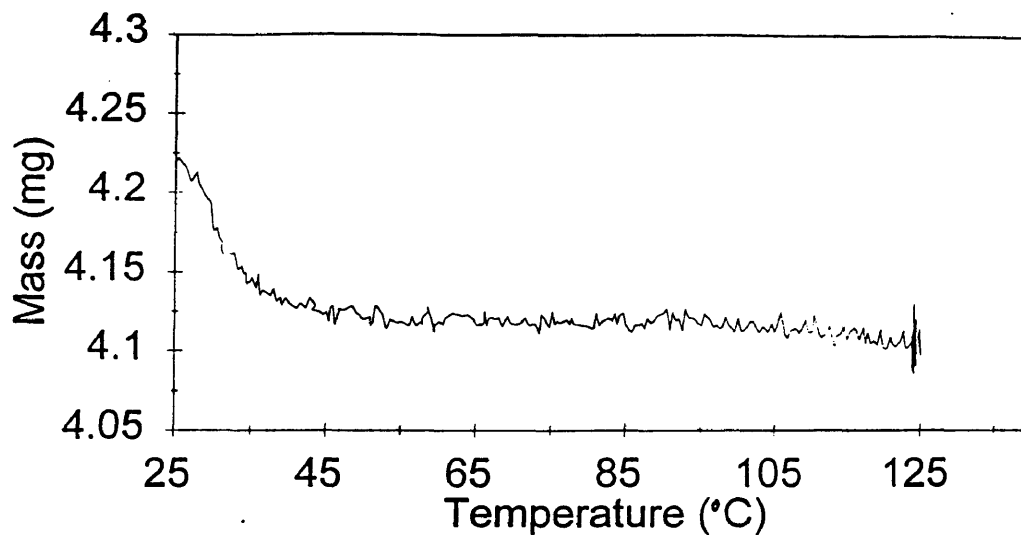


Figure 77. TGA run of PAE-PP; held at 125°C.

Table 20. Summary of thermal analysis data gathered from DSC.

Samples	Melting Temperatures (°C)	$\Delta H$ (J/g)
PAE-MM	311 285	NA
PAE-MM-A	329	96
PAE-MM-B	290	61
PAE-MP	281	NA
PAE-PM	282	NA
PAE-PP	283	NA

## Infrared Spectroscopy

Infrared spectroscopy was conducted to provide structural evidence for the PAE monomers and product mixtures. Both PAE-MM-A and PAE-MM-B also were examined.

The PAE product mixtures and monomers were examined using a mineral oil mull. A major drawback to this choice was that mineral oil (infrared spectrum in Figure 78) absorbs strongly in the same region (about 3000-2800  $\text{cm}^{-1}$ ) as the methylene stretching vibrations of the bisphenol. Both PAE-MM-A and PAE-MM-B readily dissolved in chloroform. Chloroform (Figure 79) also interferes somewhat with the methylene region and absorbs strongly at about 755  $\text{cm}^{-1}$ . Unfortunately, this absorption is near that of the out-of-plane (“oop”) bending of the aryl carbon-hydrogen bonds. Both of these methods, however, did allow the stretching from hydroxyl groups and ketone groups to be clearly seen.

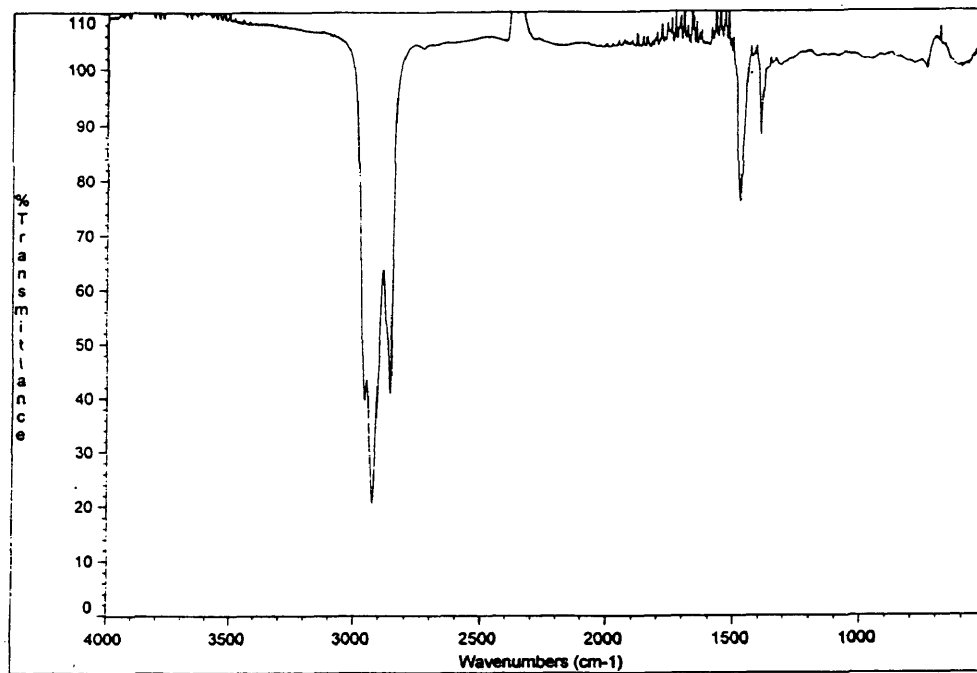


Figure 78. IR spectrum of mineral oil.

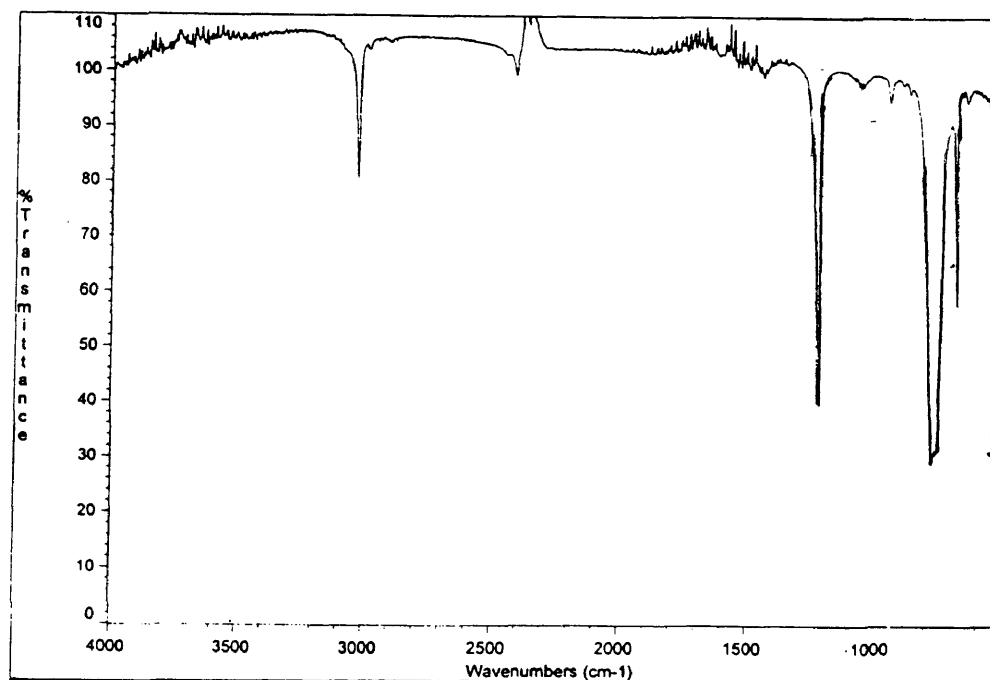


Figure 79. IR spectrum of chloroform.

*Monomers:*

Monomers were examined to identify some characteristic group absorptions that might later be found in their products. Specifically, we looked for frequencies corresponding to O-H stretching, C=O stretching, and aromatic “oop” C-H bending (both *para* and *meta*). In many cases, the suggested aromatic bands were not as strong as expected. The spectrum of each monomer is shown below in Figures 80-83. Frequencies found are summarized below in Table 21.

**Table 21.** Characteristic IR frequencies of monomers.

Monomer	O-H stretch (cm <sup>-1</sup> )	C=O stretch (cm <sup>-1</sup> )	*“oop” bending (cm <sup>-1</sup> )
1,3-FBB	NA	1664.5	851.9 (p) 749.5 (m) 698.4 (m)
3-HPM	3290.0	NA	704.8 (m) 775.1 (m)
1,4-CBB	NA	1658.1	851.9 (p)
4-HPM	3270.8	NA	819.9 (p)

\*p = *para*; m = *meta*



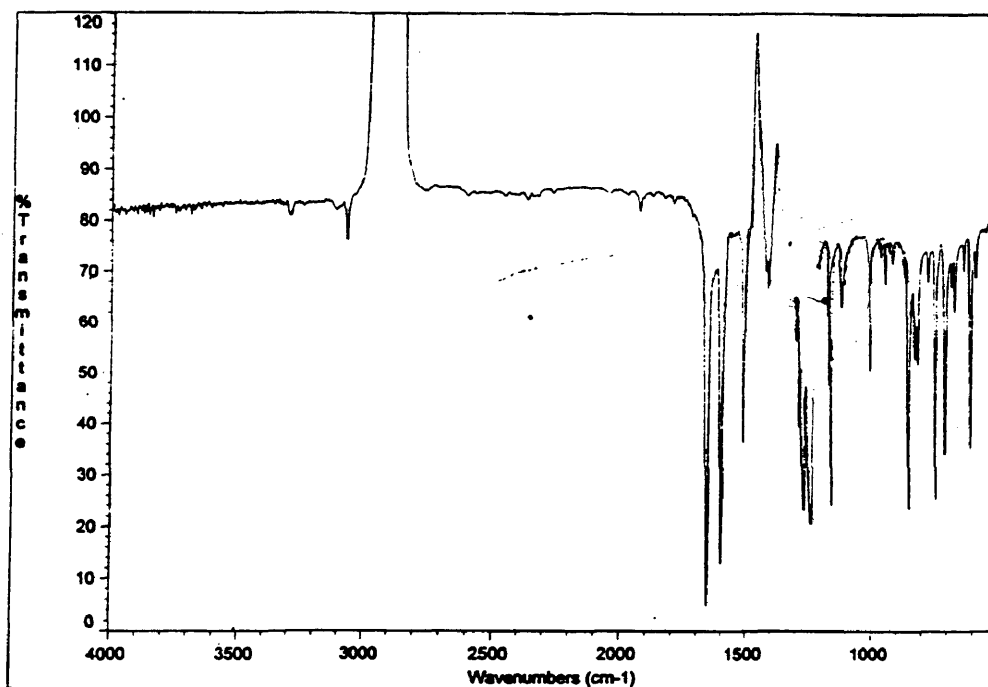


Figure 80. IR spectrum of 1,3-FBB.

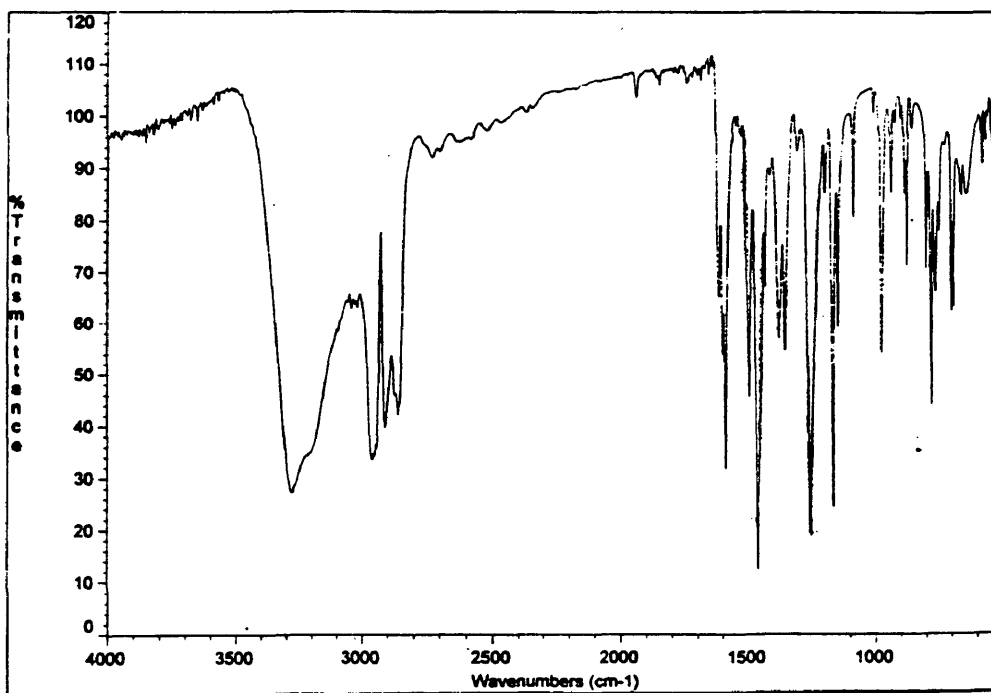


Figure 81. IR spectrum of 3-HPM.

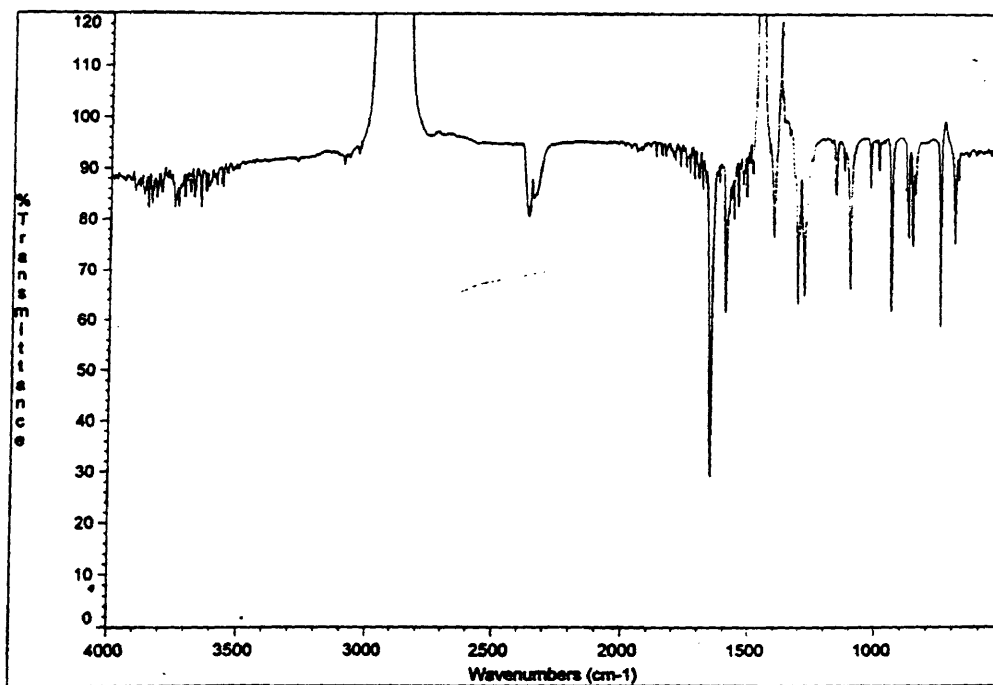


Figure 82. IR spectrum of 1,4-CBB.

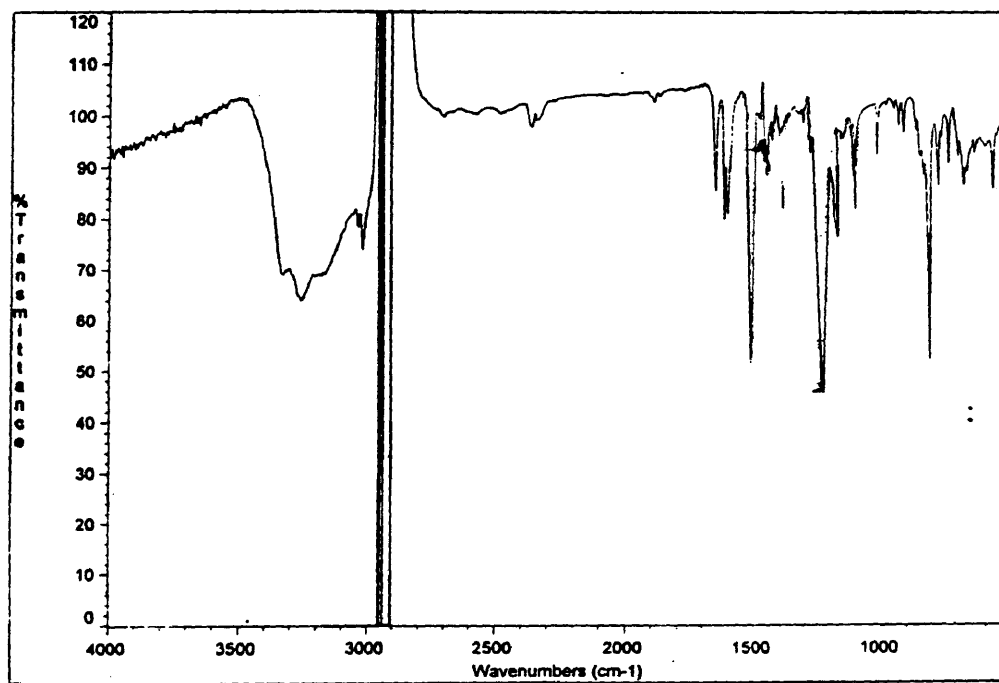


Figure 83. IR spectrum of 4-HPM.

*PAE Product Mixtures:*

Next, the samples of the products were studied with IR (Figures 84-87). A search was made for the regions of absorption already found in the monomers. Generally, similar frequencies were discovered (Table 22). The aromatic bands were again tricky to find. In this area of the spectrum, there was usually more overlapping of peaks than with the monomers. All the mixtures had an hydroxyl stretch. This could be a consequence of residual dihydroxy monomer or linear hydroxy-terminated species. More probably, it may be from absorbed water, evidence for which is presented in the results of the DSC and TGA measurements. More support for this hypothesis arises from the finding that the PAE-PP mixture had an hydroxyl stretch that was less intense than the others. The TGA and DSC results presented above indicated that it is the least hygroscopic isomeric system.

**Table 22.** Characteristic IR frequencies of PAE product mixtures.

Product Mixture	O-H stretch (cm <sup>-1</sup> )	C=O stretch (cm <sup>-1</sup> )	*"oop" bending (cm <sup>-1</sup> )
PAE-MM	3398.5	1658.1	851.9 (p) 762.3 (m) 717.6 (m)
PAE-MP	3296.2	1664.5	851.9 (p) 749.5 (m) 704.8 (m)
PAE-PM	3187.4	1645.3	839.1 (p) 762.3 (m) 698.4 (m)
PAE-PP	3296.2	1651.7	851.9 (p)

\*p = *para*; m = *meta*

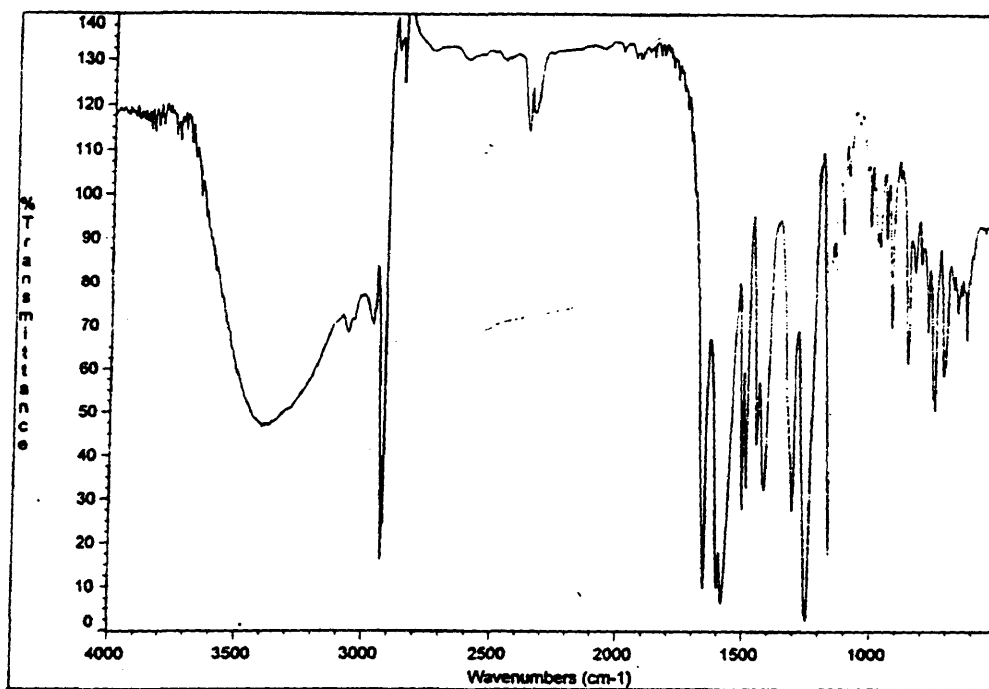


Figure 84. IR spectrum of PAE-MM product mixture.

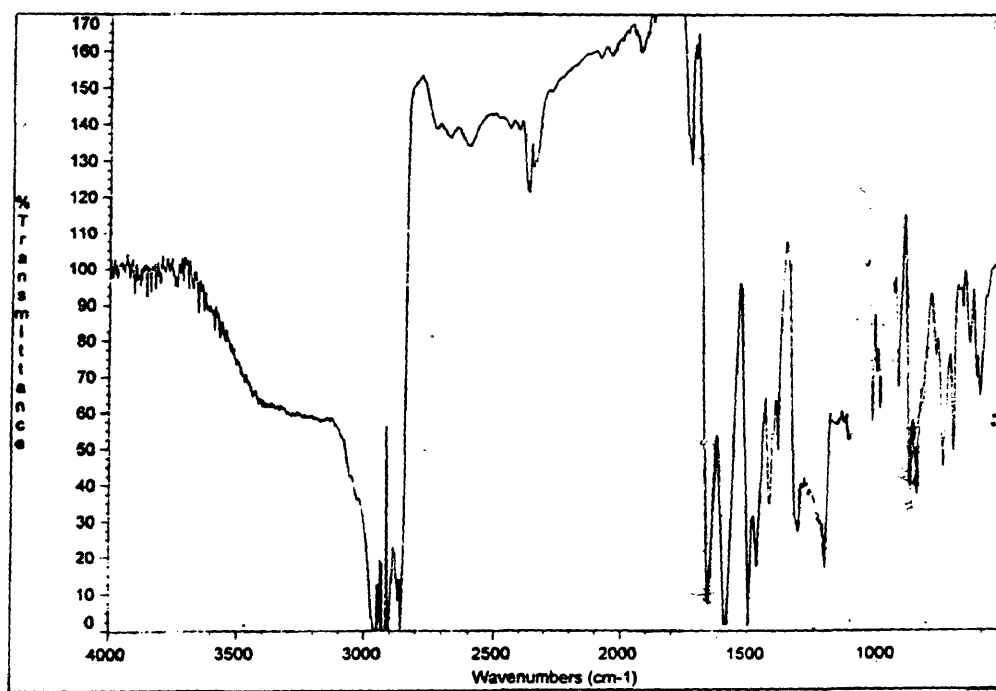


Figure 85. IR spectrum of PAE-MP product mixture.

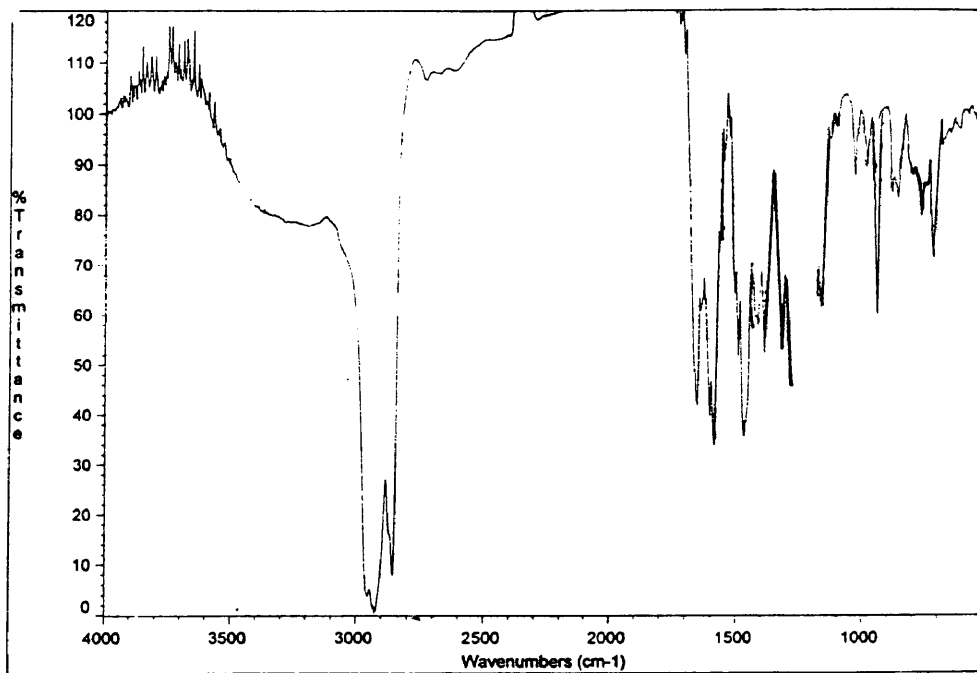


Figure 86. IR spectrum of PAE-PM product mixture.

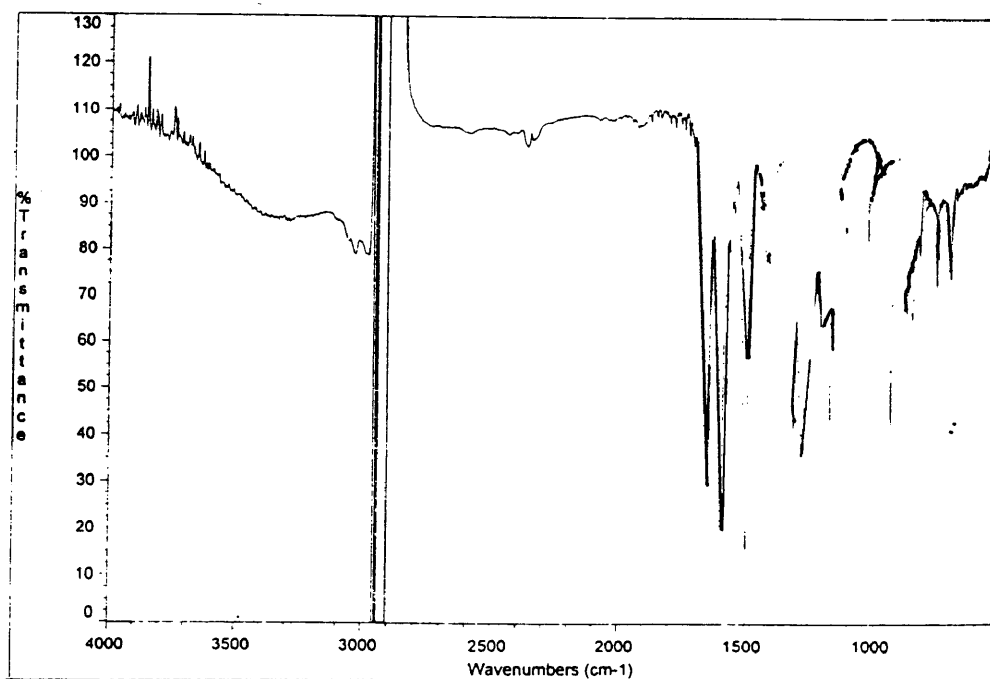


Figure 87. IR spectrum of PAE-PP product mixture.

*Suspected Cyclic Oligomers:*

Samples of PAE-MM-A and PAE-MM-B absorbed weakly in the infrared despite many attempts to increase the concentration of sample solutions. The chloroform signals simply swamped the product signals. PAE-MM-A (cyclic dimer) did exhibit some strong peaks (Figure 88). The chloroform interrupted most of these, but a C=O stretch ( $1651.7\text{ cm}^{-1}$ ) was visible. More important, perhaps, was the absence of evidence of an hydroxyl stretch lending support to the assertion that PAE-MM-A is cyclic. To be linear, a dimer would have to have an hydroxyl end group.

The IR spectra of PAE-MM-B (Figure 89) gave little definite information. However, a very small peak at  $1658.1\text{ cm}^{-1}$  was evident, signaling a C=O stretch. Once again, there is no hydroxyl group. Just as a linear dimer, a linear tetramer would possess such a group.

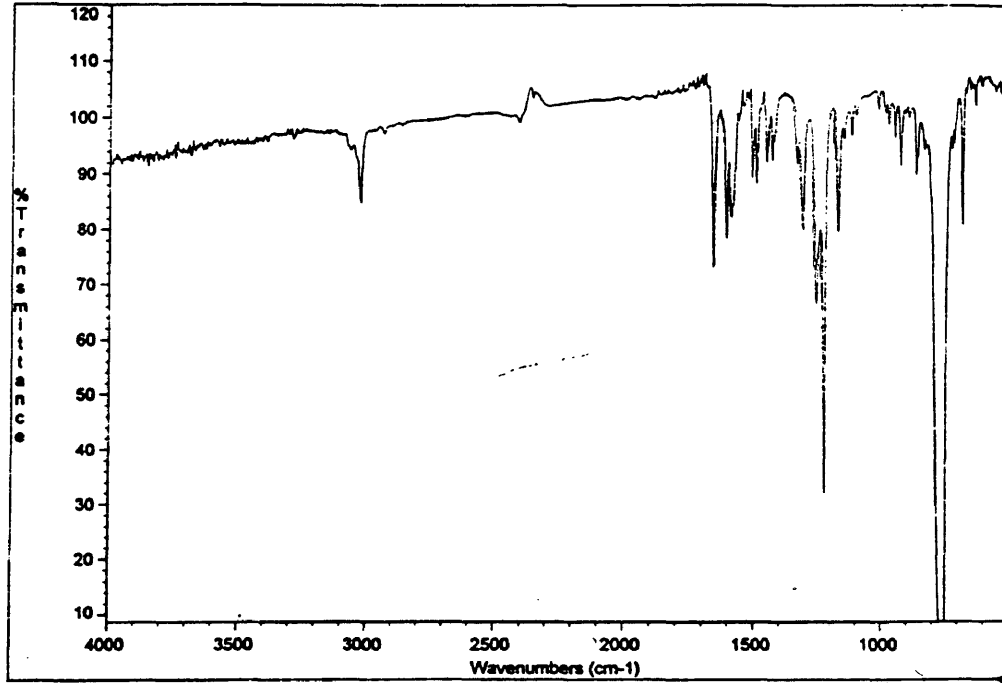


Figure 88. IR spectrum of PAE-MM-A.

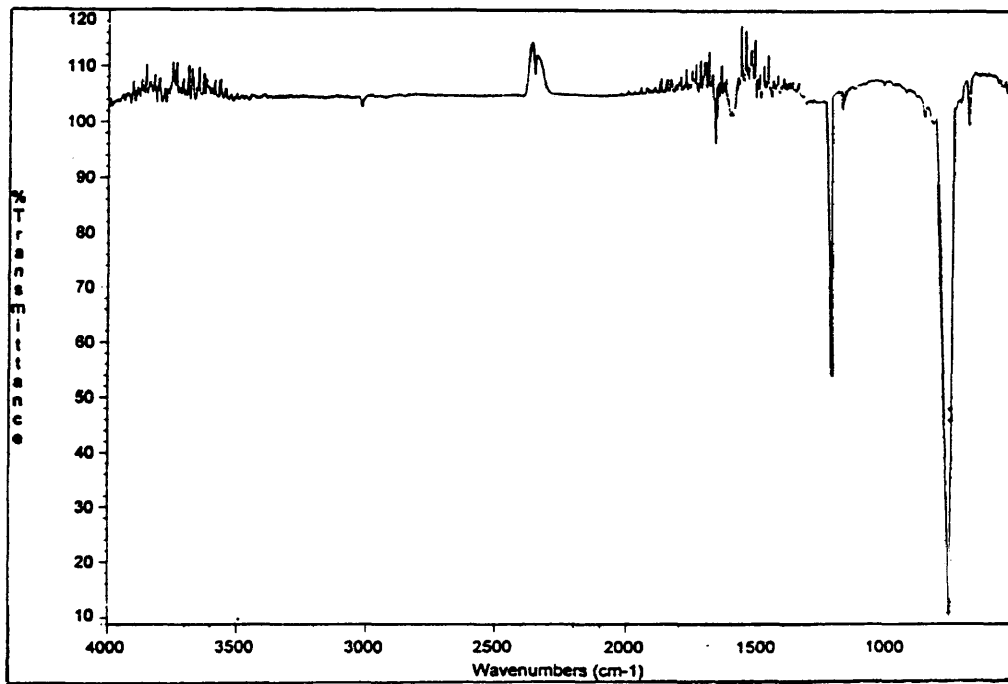


Figure 89. IR spectrum of PAE-MM-B.

## CONCLUSIONS

The condensation reactions between the difunctional monomers, bis(4-halobenzoyl)benzene and bis(hydroxyphenyl)methane, yielded a mixture of products as observed with GPC. Different isomers of the reactants were studied. Fractionation of the reaction products by solubility proved to be a very unreliable technique for identifying the product species. However, cyclic dimers and tetramers in PAE-MM, PAE-MP, and PAE-PM were observed using tandem mass spectrometry. The IR evidence also supported this assertion for the PAE-MM system. Unfortunately, preparative GPC did not yield enough of the PAE-MP and PAE-PM oligomers for further analysis. The PAE-PP may have had cyclic components, but its analysis here was inconclusive without an MS-MS analysis.

Analytical and preparative GPC work indicated that the PAE-MM system produced more of the cyclic dimer and tetramer than the other systems did. The greater number of *meta* linkages in PAE-MM may increase the likelihood that the two ends of its linear dimer and linear tetramer will be close enough to one another to react. For this reason, PAE-MM will be more likely to form a ring than the other systems containing more *para* linkages. The rings with more *meta* linkages may also be more stable. However, we offer no additional evidence to support these conjectures.

The DSC scans of both the PAE-MP product mixtures and the PAE-PM product mixtures suggested that these two systems were amorphous. In PAE-MP no sharp transitions were observed, and with PAE-PM only a very small peak was seen. The PAE-MM product mixture, on the other hand, had two distinct melting transitions. The



individual melting points of the PAE-MM cyclic tetramer and cyclic dimer fall close to these two transitions in the PAE-MM mixture. It seems unlikely that the two cyclic oligomers would not be miscible in one another and produce two distinct melting points. Therefore, it would appear possible that the PAE-MM system formed under our reaction conditions goes through a solid-solid transition before liquefying. The DSC suggests that PAE-PP possesses at least one crystalline phase. One would expect that PAE-PP would be the most crystalline of the four. Its all-*para* bonding would make any of its linear components highly packable.

Solvent trapped in our product (especially in PAE-PM) complicated many of the DSC data gathered. The PAE-MM, PAE-PM, and PAE-MP all seemed to pick up water quickly upon exposure to the atmosphere. This property explains why the DSC, despite thorough heating of all samples beforehand, still showed a large broad peak at low temperatures. The PAE-PP showed a decidedly lower hygroscopic tendency. Both IR and TGA also suggest this. The observation that some of the species in these systems are hygroscopic lends some support to the hypothesis that the behavior of these oligomers may be similar to that of calixarenes. However, this proposal must be made with caution. Neither the DSC scan of PAE-MM-A nor that of PAE-MM-B show the characteristic large, broad peak thought to correspond to water. It seems that some other species in the PAE-MM system are picking up water. Whether the compounds responsible for picking up water are also cyclic oligomers has yet to be determined.

## REFERENCES

1. P.M. Hergenrother, B.J. Jensen, and S.J. Havens, Polymer, 29, 358 (1988).
2. S. Ahmed and R.A. Orwoll, "Separation and Identification of Low Molecular-Weight Polymerization Products: Final Report to Merck Research Laboratories", unpublished report, 1993.
3. T.W.G. Solomons, Organic Chemistry, 5th ed., John Wiley & Sons, New York, 951, 1992.
4. J. March, Advanced Organic Chemistry: Reactions, Mechanisms, and Structure, 4th ed., John Wiley & Sons, New York, 669, 1992.
5. T.W.G Solomons, Organic Chemistry, 5th ed., John Wiley & Sons, 527, 1992.
6. J. March, Advanced Organic Chemistry: Reactions, Mechanisms, and Structure, 4th ed., John Wiley & Sons, 636, 1992.
7. G. Odian, Principles of Polymerization, 2nd ed., McGraw-Hill Book Company, New York, 63, 1970.
8. V. Percec, M. Kawasumi, P.L. Rinaldi, and V.E. Litman, Macromolecules, 25, 3851 (1992).
9. D.J. Brunelle, E.P. Boden, and T.G. Shannon, Journal of the American Chemical Society, 112, 2399 (1990).
10. C.D. Gutsche, Accounts of Chemical Research, 16, 161 (1983).
11. C.D. Gutsche, Calixarenes, The Royal Chemical Society, Cambridge, 27, 1989.
12. C.D. Gutsche, J.S. Rogers, D. Stewart, and K. See, Pure and Applied Chemistry, 62, 485 (1990).

13. C.D. Gutsche, Calixarenes, The Royal Chemical Society, Cambridge, 149, 1989.
14. J.M. Harrowfield, M. Mocerino, B.W. Skelton, C.R. Whitaker, and A.H. White, Australian Journal of Chemistry, 47, 1185 (1994).
15. Elemental analysis performed by Oneida Research Services, Inc.
16. H.R. Allcock, Contemporary Polymer Chemistry, 2nd ed., Prentice Hall, 394, 1990.
17. Viscotek, "Unical GPC Software Version 4.04 Manual," 10, 1991.
18. R.M. Silverstein, G.C. Bassler, and T.C. Morrill, Spectrometric Identification of Organic Compounds, 5th ed., John Wiley & Sons, New York, 158, 1991.
19. J.D. Gilbert, T.F. Greber, J.D. Ellis, A. Baarrish, T.V. Olah, C.Fernandez-Metzler, A.S. Yuan, and C.J. Burke, Journal of Pharmaceutical and Biomedical Analysis, 13, 937 (1995).
20. J.R. Chapman, Practical Organic Mass Spectrometry, 2nd ed., John Wiley & Sons, New York, 240, 1993.
21. G. Pruckmayr and T.K. Wu, Macromolecules, 11, 662 (1978).

## VITA

### David Lewis Eldridge

David Lewis Eldridge was born in Columbus, Ohio, February 1, 1973. He attended Jefferson High School in Shenandoah Junction, West Virginia and graduated from there in June 1991. In May 1995, he earned a Bachelors of Science degree in Chemistry from the College of William and Mary in Williamsburg, Virginia. Afterwards, he enrolled in the Chemistry Graduate Program at the College of William and Mary. He fulfilled his requirements for a Master of Arts degree in Chemistry in August 1996.

In the fall of 1996, the author will begin his M.D. at the Marshall University School of Medicine in Huntington, West Virginia.